Fluoride-salt-cooled High-temperature Reactor (FHR) Annual Report: 2015
MIT, U.C. Berkeley, U. of Wisconsin and U. of New Mexico
For Public Distribution

2015 Annual Report

Fluoride-salt-cooled High-Temperature Reactor (FHR)

Integrated FHR Technology Development: Tritium Management, Materials Testing, Salt Chemistry Control, Thermal Hydraulics and Neutronics with Associated Benchmarking (NEUP14-7476)

Charles Forsberg (Massachusetts Institute of Technology)
Lin-wen Hu (Massachusetts Institute of Technology)
Per F. Peterson (University of California at Berkeley)
Massimiliano Fratoni (University of California at Berkeley)
Kumar Sridharan (University of Wisconsin),
Edward (Blandford University of New Mexico)

January 2016

Fluoride-salt-cooled High-temperature Reactor (FHR) Annual Report: 2015
MIT, U.C. Berkeley, U. of Wisconsin and U. of New Mexico
For Public Distribution

Forward

The U.S. Department of Energy awarded a three year Integrated Research Project (IRP) to a consortium of four universities: the Massachusetts Institute of Technology (MIT), the University of California at Berkeley, the University of Wisconsin and the University of New Mexico. MIT leads the consortium. The long-term goal is to develop a Fluoride-salt-cooled High-temperature Reactor (FHR). This project is to address specific technical challenges in the development of the FHR. This is the first year of the three year project. This IRP is the second IRP grant and thus includes some results from the earlier IRP.

The report describes activities in 2015. It was written as an annual report and the quarterly report for October through December of 2015 and thus provides added information on the last quarter of activities.

We would like to thank the U.S. Department of Energy, Office of Nuclear Energy for their support. We would also like to thank Oak Ridge National Laboratory, Idaho National Laboratory, Westinghouse, and our advisory panel for their assistance.

Fluoride-salt-cooled High-temperature Reactor (FHR) Annual Report: 2015
MIT, U.C. Berkeley, U. of Wisconsin and U. of New Mexico
For Public Distribution

Table of contents

Fluoride-salt-cooled High-temperature Reactor (FHR) Annual Report: 2015
MIT, U.C. Berkeley, U. of Wisconsin and U. of New Mexico
For Public Distribution

Abstract

Integrated FHR Technology Development: Tritium Management, Materials Testing, Salt Chemistry Control, Thermal Hydraulics and Neutronics with Associated Benchmarking

Project Title: Integrated FHR Technology Development: Tritium Management, Materials Testing, Salt Chemistry Control, Thermal Hydraulics, and Neutronics with Associated Benchmarking

Covering Period: Annual Report: 2015 and Quarterly Report: October-December 2015

Date of Report: December 31, 2015

Recipient: Massachusetts Institute of Technology, 77 Massachusetts Ave., Cambridge, MA 02139

Award Number: NEUP14-7476

Principal Investigator: Charles Forsberg, 617-324-4010, cforsber@mit.edu

Co-PI: Lin-wen Hu, lwhu@mit.edu
Per F. Peterson, peterson@nuc.berkeley.edu
Massimiliano Fratoni, maxfratoni@berkeley.edu
Kumar Sridharan, kumar@engr.wisc.edu
Ed Blandford, edb@unm.edu

Project Objectives: The objective of the Integrated Research Project (IRP) is to address major challenges in the development of commercial Fluoride-salt-cooled High-temperature Reactor (FHR) technology: tritium control; fluoride-salt corrosion control and materials selection; thermal-hydraulics and neutronics; and evaluation model benchmarking. This effort will also facilitate work to address other major FHR development challenges, such as high-temperature instrumentation, where this IRP will identify and study the key state parameters that must be monitored by instruments in FHRs to assess safety and reliability, and thus define the key requirements that FHR instrumentation must address. This identification of FHR instrumentation requirements can also support the design of instrumentation systems for FHR integral effects test facilities and test reactors.

Fluoride-salt-cooled High-temperature Reactor (FHR) Annual Report: 2015
MIT, U.C. Berkeley, U. of Wisconsin and U. of New Mexico
For Public Distribution

1. Summary

1.1. Highlights

This annual report covers from January 1, 2015 to December 31, 2015 and includes the activities for the last quarter of the year[1]—October 1, 2015 through December 31, 2015. This IRP is a follow-on to an earlier IRP with some similar activities; thus some of the activities are built upon the earlier work. Papers and other work generated by the earlier IRP are also reported herein when applicable.

- *Tritium workshop.* The *Workshop on Tritium Control and Capture in Salt-Cooled Fission and Fusion Reactors: Experiments, Models, and Benchmarking* was held on October 27-28 in Salt Lake City. The workshop objectives were to bring together researchers involved in experiments, modeling and benchmarking for tritium control at ~700°C in liquid salts and related systems to (1) exchange information and enable the future exchange of information, (2) initiate an effort for benchmarking of experiments and models, and (3) encourage cooperation between different groups working on the same challenges. The salt-cooled, molten-salt (fuel dissolved in salt) and fusion community have common tritium in salt challenges and thus large incentives to work together.
- *Alternative Method to Purify liquid salts (feed materials and on-line).* Chemical redox measurements are made with an electrode that electroplates beryllium from the salt onto to a rod and then follows the electrochemical potential as the beryllium coverts back to a fluoride. Examination of the rod shows many other metal impurities electroplating out and remaining on the rod—a potential method to purify the salt either off-line or on line. The potential to use this process for salt purification is being further investigated.
- *Experimental Thermal Hydraulics Strategy.* Unlike the quarterly reports, the annual report provides a relatively complete picture of the CEIT thermal hydraulics loop activities at UCB. What is noteworthy is that advances in theory (models, computational fluid dynamics, etc.) and experimental techniques (instrumentation, infrared cameras, etc.) now enable validation of computational tools based on such experiments to a level of precision that would not have been possible a decade ago.

Except for the financial/milestone data, this report is shared with the Georgia Tech FHR IRP, other groups working on FHRs, and other interested parties. It is one of several mechanisms we are using to assure integration of work among the different groups working on FHRs.

1.2. Plans for Next Quarter

The next FHR integration workshop will be held in Berkeley, California on April 14-15, 2015. This time and location was chosen because the International Congress on Advanced Nuclear Power Plants (ICAPP 2016) will be in San Francisco on April 17-20, 2015. ICAPP will have a large number of sessions with papers on the FHR. Most groups in the United States and abroad will have people at these meetings. The back-to-back meetings will enable different FHR working groups to meet, compare results, and plan for future activities. Most of the planning for the meetings and workshops will occur in the next three months.

---

[1] This report is both the annual report and the quarterly report for October through December, 2015

Fluoride-salt-cooled High-temperature Reactor (FHR) Annual Report: 2015
MIT, U.C. Berkeley, U. of Wisconsin and U. of New Mexico
For Public Distribution

1.3. Organization of Report and Path Forward

This integrated research plan has 5 coupled tasks.

Task 1: FHR Tritium Control and the Role of Carbon. The objective of this task is to understand the production, transport, control, and recovery of tritium in FHRs and to develop cost effective methods to prevent release of tritium to the environment, minimize exposure to workers, and prevent release of stored tritium during accidents.

Task 2: FHR Corrosion Control with Redox Control, Impurity Control, and Materials Selection. The objective of this task is to develop strategies to assure good long-term FHR materials behavior by selection of appropriate materials and salt purity (redox control and impurity removal). The control of redox and removal of impurities also requires development of instrumentation for experiments that ultimately will be used in future FHRs.

Task 3. FHR Experiments and Modeling for Thermal Hydraulics, Neutronics and Structural Mechanics. The objective of this task is to perform modeling and to provide experimental data for benchmarking of evaluation models for FHR safety and transient response.

Task 4. FHR Evaluation Model Benchmarking and Validation Workshops. The objectives of this task are (1) a set of benchmarking activities to validate design tools using the experimental data collected by this IRP and by collaborators and (2) begin the process of developing an international effort to support evaluation model benchmarking for FHR safety and design.

Task 5. Using Lessons Learned From FHR R&D to Advance All Generation IV Technologies. The objective of this task is to utilize the valuable opportunity provided by FHR technology, to study a novel reactor technology, to identify approaches to create a more technology neutral approach to assessing reactor safety. Quarterly reports will include a section devoted to describing new insights in this area.

There is a growing U.S. and worldwide interest in the FHRs resulting in many more research groups involved in these areas in addition to the Georgia Tech IRP. As a consequence, many of these activities include cooperative activities with the Georgia Tech IRP consortium and other groups.

Fluoride-salt-cooled High-temperature Reactor (FHR) Annual Report: 2015
MIT, U.C. Berkeley, U. of Wisconsin and U. of New Mexico
For Public Distribution

2. Task 1: FHR Tritium Control and the Role of Carbon (MIT and UW)

The objective of this task is to understand the production, transport, control, and recovery of tritium in FHRs and to develop cost effective methods to minimize release of tritium to the environment, minimize exposure to workers, and prevent release of stored tritium during accidents. The work is divided into two components: (1) Task 1.1 experiments at MIT involving tritium and reactor irradiations and (2) Task 1.2 experiments at UW involving hydrogen and deuterium. These are complementary activities where observations at one university will inform work at the other university.

One Task 1 activity is partly coupled to a Task 4 activity. Task 4 (FHR Evaluation Model Benchmarking and Validation Workshops) objectives include (1) a set of benchmarking activities to validate design tools using the experimental data collected by this IRP and by collaborators and (2) begin the process of developing an international effort to support evaluation model benchmarking for FHR safety and design. One of the three major activities is benchmarking materials, corrosion, activation, tritium and transport (MATT). This is reported here (Task 1.1(a)) but is tightly coupled to Task 4 (Section 5).

Task 1.1(a) Tritium modeling

Tritium Workshop

The *Workshop on Tritium Control and Capture in Salt-Cooled Fission and Fusion Reactors: Experiments, Models and Benchmarking* was held on October 27-28, 2015 in Salt Lake City. The workshop objectives were to bring together researchers involved in experiments, modeling and benchmarking for tritium control at ~700°C in liquid salts and related systems to (1) exchange information and enable the future exchange of information, (2) initiate an effort for benchmarking of experiments and models, and (3) encourage cooperation between different groups working on the same challenges.

Three advanced power systems use liquid salt coolants that generate tritium and thus face common challenges. The Fluoride-salt-cooled High-temperature Reactor (FHR) uses the same graphite-matrix coated-particle fuel as high-temperature gas-cooled reactors and fluoride salt coolants. Molten salt reactors (MSRs) dissolve the fuel in a fluoride or chloride salt with release of fission product tritium to the salt. In both systems, the base-line salts contain ^{7}Li. Isotopically separated lithium is used to minimize tritium production. The Chinese Academy of Science plan to start operation of a 10-MWt FHR and a 2-MWt MSR by 2020. High-magnetic field fusion machines propose to use lithium enriched in ^{6}Li to maximize tritium generation—the fuel for a fusion machine. Advances in superconductors that enable higher power densities may require the use of lithium salts as coolants.

The workshop results are summarized herein including: characteristics of salt-cooled fission and fusion machines, the environment for tritium capture, current tritium models, alternative strategies for tritium control, and ongoing experimental work. A workshop proceedings with the various presentations is being prepared. Table 2.1 lists the talks by general area. The workshop was organized so half the time was reserved for discussions.

Fluoride-salt-cooled High-temperature Reactor (FHR) Annual Report: 2015
MIT, U.C. Berkeley, U. of Wisconsin and U. of New Mexico
For Public Distribution

Table 2.1: Workshop Talks by Subject Area

Fission and Fusion Reactor Systems with Salt Cooling and Tritium Challenges

> C. Forsberg (MIT NSE): Fluoride-Salt-Cooled High-Temperature Reactor (FHR)
> B. Sorbom (MIT PSFC): Liquid Immersion Blankets for Fusion Power Plants
> W. Liu (CAS): Thorium Molten Salt Reactor (TMSR) Project in China
> M. Laufer (UCB): Tritium and Chemistry Management for the Mark-1 PB-FHR

Tritium Generation, Corrosion Chemistry and Modeling

> J. Stempien (INL) Tritium Transport and Corrosion Modeling in the Fluoride Salt-Cooled High-Temperature Reactor
> T. Chrobak (UW): FLiBe Electrochemistry and Materials Corrosion Research at UW-Madison

Tritium Control and Carbon

> C. Contescu and T. Burchell (ORNL): Hydrogen – Carbon Interactions: A Brief Literature Survey
> T. Burchell and C. Contescu (ORNL): AGR Fuel Compact Development Program
> H. Wu (UW): Experimental work on tritium transport analysis in Flibe-Graphite system
> S. Lam (MIT NSE): Tritium Control Using Carbon Outside the Core
> H. Wu (UW) Effect of Hydrogen on Tritium Control in Molten Salt System
> D. Carpenter (MIT NRL) Planned FHR IRP-2 Tritium Experiments at the MIT NRL

Tritium Control with Other Technologies

> W. Liu (CAS): Tritium-Control Technologies for TMSR System in CAS (gas sparging)
> F. (UNM): Research on Techniques for Tritium Sequestration and Removal at UNM (gas sparging)
> B. Wallace (UNM): Investigation of Tritium Control and Release Mitigation Options in Double-Wall Twisted-Tube Heat Exchangers (DT-HXRs)
> P. Humrickhouse (INL): Tritium Permeation Control and Extraction – Perspectives from Fusion System Studies
> X. Sun (OSU): Tritium Management in FHRs: Ongoing and Planned Activities in Integrated Research Project Led by Georgia Tech

Tritium Control Experience

> G. Stack (SRNL): An Overview of SRNL Tritium Activities
> M. Shimada (INL): Overview of Tritium and molten salt FLiBe research at Safety and Tritium Applied Research (STAR) facility
> D. Carpenter (MIT NRL): Experience with Tritium Evolution During Irradiation of MSRE Flibe in the MITR
> D. Senor (PNNL): Irradiation Testing in Support of the Tritium Production Enterprise

Fluoride-salt-cooled High-temperature Reactor (FHR) Annual Report: 2015
MIT, U.C. Berkeley, U. of Wisconsin and U. of New Mexico
For Public Distribution

Salt-cooled Fission and Fusion Power Systems

There is a rapidly growing interest in fission and fusion systems that use salt coolants that is driven by (1) separate developments in FHRs, MSRs, and fusion and (2) advances in gas turbines that can couple to salt-cooled reactor systems. Workshop presentations and discussions summarized the multiple basis for interest in developing these three separate technologies.

Salt-Cooled Power Systems

Fluoride-salt-cooled High-temperature Reactors (FHRs). The FHR uses salt coolant and the graphite-matrix coated-particle fuel developed for High-Temperature Gas-cooled Reactors (HTGRs). Advances in the fuel are enabling the development of the FHR. Because this reactor uses a proven fuel and a clean salt coolant, it is the near-term commercialization option for a salt-cooled reactor. Three different fuel designs are proposed by different groups: pebble bed, plate fuel, and fuel inside radial moderator (FIRM). The base-line coolant is a lithium-beryllium-fluoride salt known as flibe ($^{7}Li_2BeF_4$). The characteristics of the flibe as well as other potential salts are listed in Table 2.2. The primary coolant system is a closed loop that operates at atmospheric pressure with nominal core coolant inlet and outlet temperatures of 600°C and 700°C respectively.

Fluoride-salt-cooled High-temperature Reactor (FHR) Annual Report: 2015
MIT, U.C. Berkeley, U. of Wisconsin and U. of New Mexico
For Public Distribution

Table 2.2. FHR Coolant Options

Coolant	T_{melt} (°C)	T_{boil} (°C)	ρ (kg/m^3)	ρC_p (kJ/m^3 °C)
66.7 ^{7}LiF-33.3BeF$_2$	**459**	**1430**	**1940**	**4670**
59.5 NaF-40.5 ZrF$_4$	500	1290	3140	3670
26 ^{7}LiF-37 NaF-37 ZrF$_4$	436		2790	3500
51 ^{7}LiF-49 ZrF$_4$	509		3090	3750
Water (7.5 MPa)	0	290	732	4040

Compositions in mole percent. Salt properties at 700°C and 1 atmosphere. Pressurized water data shown at 290°C for comparison

Molten Salt Reactors (MSRs). Molten salt reactors were first developed as part of the nuclear aircraft propulsion program in the 1950s and then as a thermal-neutron-spectrum breeder reactor using the thorium fuel cycle in the 1960s. The Molten Salt Reactor Experiment (MSRE), an 8-MWt reactor, successfully demonstrated the technology in the late 1960s. This reactor used flibe (^{7}Li$_2$BeF$_4$) salt with fuel and fission products dissolved in the salt. The reactor used bare graphite as the neutron moderator. The program was cancelled in the early 1970s when the United States decided to focus its breeder reactor program on sodium-cooled fast reactors (SFRs). In the last decade there has been a renewed interest in MSR for several reasons

- *Fuel cycle versatility*. MSRs can operate on a variety of fuel cycles including thorium breeder fuel cycles and various cycles that destroy actinides. This capability has been increased by recent work to develop fast spectrum MSRs using chloride salts.
- *Advancing technology*. Many of the technology challenges of the 1960s have been reduced or eliminated thanks to advances in other fields. Better high-temperature carbon composites can provide better materials for reactor internals and may enable high-temperature (>1000°C) distillation to simplify removal of fission products from the liquid fuel salt. The development of high-temperature additive manufacturing enables fabrication of complex components including control rods, distillation columns, and other items out of molybdenum and other salt-compatible high-temperature materials. Advanced carbon and metal absorbers may enable efficient removal of noble metal fission products from the molten salt. Unless removed, these fission-product metals plate out on heat exchanger surfaces, are a major source of short-term decay heat, and cause multiple challenges. Last, advances in metallurgy may enable development of alloys that allow higher temperature operations.

Fluoride-salt-cooled High-temperature Reactor (FHR) Annual Report: 2015
MIT, U.C. Berkeley, U. of Wisconsin and U. of New Mexico
For Public Distribution

- *Safety*. MSRs enable alternative safety strategies relative to solid fuel reactors including the options of (1) dumping the liquid fuel to critically-safe passively cooled tanks under any accident scenario and (2) potentially the option to minimize the inventory of longer lived fission products such as cesium in the reactor that may dominate the accident source term and the potential for land contamination. The second option is enabled by the advancing separation technologies to remove those radionuclides on-line enabled by new materials and material fabrication methods as noted above.

The Chinese Academy of Science plans to build a small 2-MWt MSR by 2020 with an emphasis on the thorium fuel cycle for fuel sustainability. Several large western companies (Terrapower, Hatch) are examining MSRs as are many smaller companies.

High Magnetic-Field Fusion Reactors. Advances in magnetic fusion may drive fusion systems to use liquid salt coolants. The size of magnetic fusion devices for any given fusion power level is determined by the maximum feasible magnetic field with the plasma volume proportional to one over the magnetic field to the fourth power. Practical fusion machines require superconducting wire or tape to generate the magnetic fields to minimize electrical consumption by the magnets. However, standard superconductors lose their superconducting properties in high magnetic fields. In the last five years, methods have been developed to manufacture a new superconductor: Rare-Earth Barium Copper Oxide (REBCO). This new superconductor enables magnetic fields at the coil over 22 Tesla—more than twice the capability of older superconductors. It eliminates magnetic field strength as the primary design constraint in magnetic confinement fusion devices with the new limit being magnetic field induced stress in the coils. The REBCO is in the form of a steel tape that enables addressing the high stresses.

REBCO superconductors may enable doubling the practical peak magnetic field in a fusion machine and thus reduce the volume of fusion systems by an order of magnitude. The radius of a 500 MW plasma fusion system would be about 3 meters—the size of several magnetic fusion devices already built. Figure 2.1 shows JET (an existing fusion experimental device in the United Kingdom) and the proposed high magnetic field fusion system based on REBCO superconductors. It is potentially a revolution in fusion.

Increasing fusion power density by an order of magnitude improves long-term economic viability. However, it imposes major changes in fusion blanket design because of the much higher power densities. Historically proposed blankets have been solid lithium-containing materials for production of tritium fuel ($^6Li + n \rightarrow {}^3H + {}^4He$). The higher power densities will likely require changing to a liquid blanket containing lithium—most likely flibe (66.7^6LiF-$33.3BeF_2$) for several reasons. A liquid blanket is needed for highly efficient neutron shielding with such high plasma fusion power densities. Fusion generates about 17 MeV per fusion of tritium and deuterium—most of this energy is in the form of 14 MeV neutrons. Liquid shielding enables efficient cooling as 14 MeV neutrons slow-down in the salt and deposit their energy as heat in the liquid. The heat transfer challenges in fusion blankets become very difficult at these very high power densities. The coolant choices are (1) fluoride coolant salts—most likely flibe or (2) a liquid metal coolant containing lithium (lithium, lead-lithium, etc.). A low-electrical-conducting liquid salt rather than liquid lithium or a lead-lithium eutectic is preferred to ease magneto hydrodynamic issues such as coolant pumping and plasma control because the magnetic fields produced

Fluoride-salt-cooled High-temperature Reactor (FHR) Annual Report: 2015
MIT, U.C. Berkeley, U. of Wisconsin and U. of New Mexico
For Public Distribution

by external coils more rapidly penetrate through the blanket. These factors may drive magnetic fusion to liquid salt cooling.
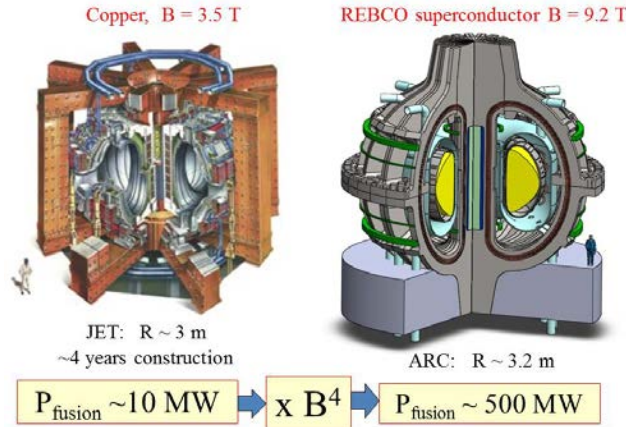

Fig. 2.1. Impact of Higher-Field Superconductors on the Size of Magnetic Fusion System

Nuclear Air Brayton Combined Cycles (NACC)

Salt coolants were originally developed for the Aircraft Nuclear Propulsion Program in the 1950s with the goal of coupling a nuclear reactor to aircraft jet engines. They can transfer heat from the reactor to the power cycle at between 600 and 700°C. Recent advances in utility natural-gas combined-cycle technologies now enable coupling these reactors to a Nuclear Air-Brayton Combined Cycle (NACC) or potentially a Nuclear Helium Combined Cycle (NHCC). NACC can provide base-load electricity with additional variable peak electricity produced by using auxiliary natural gas, biofuels, hydrogen, or stored heat to (1) increase nuclear plant net revenue by 50 to100% relative to base-load nuclear plants and (2) enable a low-carbon nuclear renewable electricity system. These developments create incentives for salt-cooled reactors.

During base-load operation of a NACC, atmospheric air is filtered, the air is compressed, heat is added from the reactor through a coiled-tube heat exchanger (CTHX), the hot compressed air goes through turbines to produce electricity, the warm air exiting the gas turbine goes through a heat recovery steam generator to generate steam that is used to produce added electricity, and the air is exhausted to the stack. This power cycle is very similar to that used in natural gas combined-cycle plants. If coupled to a salt-cooled reactor delivering heat between 600 and 700°C, heat-to-electricity efficiency is 42%. This specific example uses a modified General Electric 7FB gas turbine.

The base-load NACC temperatures, determined by heat-exchanger materials constraints, are far below maximum peak gas turbine temperatures. Thus, there is the option of adding heat after the nuclear heating to further raise compressed gas temperatures before entering a power turbine—a topping cycle. The incremental heat-to-electricity efficiency depends upon the design, ranging from 66 to 70%. This is the most efficient system known to convert heat to electricity based on existing technology.

Fluoride-salt-cooled High-temperature Reactor (FHR) Annual Report: 2015
MIT, U.C. Berkeley, U. of Wisconsin and U. of New Mexico
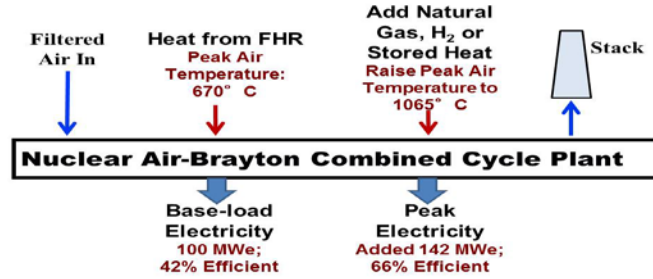For Public Distribution

Fig. 2.2. Nuclear Air-Brayton Combined Cycle (NACC)

An economic analysis was done on the performance of an FHR with NACC in California and Texas using natural gas to produce peak electricity. These states have deregulated electricity markets. The peaking capability increased the plant yearly revenue by about 50% after subtracting the cost of the natural gas compared to a base-load nuclear plant. Because NACC is more efficient than a stand-alone natural-gas combined cycle plant in converting natural gas to electricity (uses less natural gas), its electricity production costs for peak electricity are less than a stand-alone natural gas plant; thus, it earns large profits when electricity prices are set by natural gas plants.

The addition of wind and solar in some electricity grids has resulted in significant hours per year with very low electricity prices—near zero at times of high wind or solar input. In such utility systems it is proposed that a Firebrick Resistance-Heated Energy Storage (FIRES) system replace the use of natural gas for providing heat to produce peak electricity. FIRES consists of high-temperature firebrick heated to high temperatures with electricity at times of low or negative electric prices. For peak electricity production, the compressed air after nuclear heating is sent through the hot firebrick to raise its temperature before going to the turbine. The round-trip storage efficiency from electricity to heat to electricity is ~66%, based on ~100% efficiency in resistance electric conversion of electricity to hot firebrick and 66% efficiency in conversion of incremental heat to electricity within NACC. FIRES enables the reactor to operate at base-load at all times while the station buys electricity from the grid at times of low prices to charge FIRES and sells electricity at times of high prices.
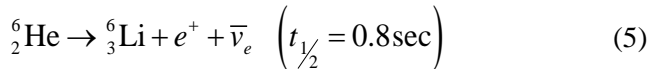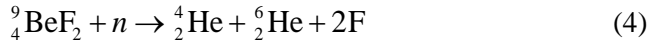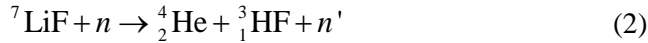
Salt Chemistry and Tritium Generation

Table 2.3 summarizes salt coolant requirements among the different reactor concepts. Carbon in the system can have a large impact on system behavior because carbon can absorb tritium and other impurities in the salt and has other chemical impacts. The choice of salt depends upon neutronic and thermal-hydraulic considerations. Most proposed salts contain lithium because of its ability to lower the melting points of these salts to a few hundred degrees C. Flibe (Li_2BeF_4) has the best overall properties and is the choice in most proposed designs of FHRs and MSRs. For the FHR and MSR, one wants low neutron absorption cross sections with minimum tritium production. If a lithium salt is used, isotopically-separated [7]Li must be used to minimize neutron absorption and tritium production. There are other salt choices for the FHR and MSR with all of the options involve complex tradeoffs. For fusion one wants to maximize tritium production (the fuel) and thus [6]Li is required to maximize tritium production. For fusion systems, flibe is clearly the preferred salt coolant because it maximizes tritium production.

Fluoride-salt-cooled High-temperature Reactor (FHR) Annual Report: 2015
MIT, U.C. Berkeley, U. of Wisconsin and U. of New Mexico
For Public Distribution

Table 2.3. Salt Characteristics of Different Systems

Property	FHR	MSR	Fusion
Salt	Fluoride	Fluoride or Chloride	Fluoride
Impurities	Corrosion impurities	Fission products / actinides	Corrosion impurities
Use lithium salts	Optional	Depends upon goals	Required
Tritium production	Small (^{7}Li in Coolant)	Small (^{7}Li in Coolant)	High (^{6}Li in Coolant)
Tritium value	Waste	Waste	Fuel
Carbon in system	Yes	Depends upon option	No
Redox control	Ce^{+2}/Ce^{+3}, other	U^{+3}/U^{+4}	Ce^{+2}/Ce^{+3}, Be, other

Under neutron irradiation these salts generate tritium by multiple pathways.

$$^6\text{LiF} + n \rightarrow {}^4_2\text{He} + {}^3_1\text{HF} \tag{1}$$

$$^7\text{LiF} + n \rightarrow {}^4_2\text{He} + {}^3_1\text{HF} + n' \tag{2}$$

$$^{19}_9\text{F} + n \rightarrow {}^{17}_8\text{O} + {}^3_1\text{H} \tag{3}$$

$$^9_4\text{BeF}_2 + n \rightarrow {}^4_2\text{He} + {}^6_2\text{He} + 2\text{F} \tag{4}$$

$$^6_2\text{He} \rightarrow {}^6_3\text{Li} + e^+ + \overline{v}_e \quad \left(t_{1/2} = 0.8\,\text{sec}\right) \tag{5}$$

Lithium-7 has a very small neutron cross section and ^{6}Li has a large neutron cross section that maximizes tritium generation rates. With ^{7}Li salts, the residual ^{6}Li will partly burn out but will not go to zero if the salt also contains beryllium. Neutron reactions with beryllium will generate ^{6}Li that is converted into tritium.

The nuclear reactions have important chemical implications. With appropriate materials of construction, clean salts have extremely low corrosion rates. This was demonstrated in the Molten Salt Reactor Experiment, an 8-MWt test reactor built and operated in the late 1960s. The secondary loop used flibe with very low corrosion rates. However, in a reactor LiF is converted to ^{3}HF—hydrogen fluoride. Hydrogen fluoride is corrosive. Corrosion in salt-cooled reactors (fission or fusion) is directly tied to the production of tritium. *Tritium control and corrosion control can't be separated.*

If ^{3}HF is allowed to corrode metals of construction, tritium in its molecular form will be released. To avoid corrosion redox control agents can be added to the coolant that result in converting ^{3}HF to ^{3}H$_2$. The

14

Fluoride-salt-cooled High-temperature Reactor (FHR) Annual Report: 2015
MIT, U.C. Berkeley, U. of Wisconsin and U. of New Mexico
For Public Distribution

redox potential determines the relative amounts ^3HF versus $^3H_2$. While the ^3HF can't escape the system, the $^3H_2$ diffuses through hot metals such as heat exchangers to the environment. Maintenance of long term system integrity by assuring low corrosion rates implies converting ^3HF to $^3H_2$, but $^3H_2$ can escape the system requiring methods for removal of $^3H_2$ and methods for slowing escape of $^3H_2$ from the system. A partial pressure of $^1H_2$ in the cover gas will lead to isotopic exchange with ^3HF, producing ^3H-^1H, thus affecting the tritium transport rates. At the same time, introduction of H_2 in the cover gas may also shift the redox potential of the salt, thus affecting corrosion control.

Tritium generation rates depend not only upon the salt selection and whether the reactor is a FHR, MSR, or fusion machine but also on the specific design features. This is most evident in the design of FHRs where there are large variations in the fraction of the core that is salt with a significantly higher salt fraction in a pebble-bed reactor than one with a FIRM core design. For one design of pebble-bed FHR, it was estimated that ~0.03% of the tritium produced could be allowed to escape in order to stay below the tritium emission rates of the current fleet of pressurized water reactors (2.2 Ci/GWe/d), or 810 Ci/GWe/y.

Stempien has built a model for FHRs that accounts for tritium production, corrosion, transport that can predict behavior and calculate the impact of different methods to limit tritium loses or capture tritium. The model has been validated with the limited experimental data that is available. More experimental data is required to validate results. The model features are shown in Figure 2.3.
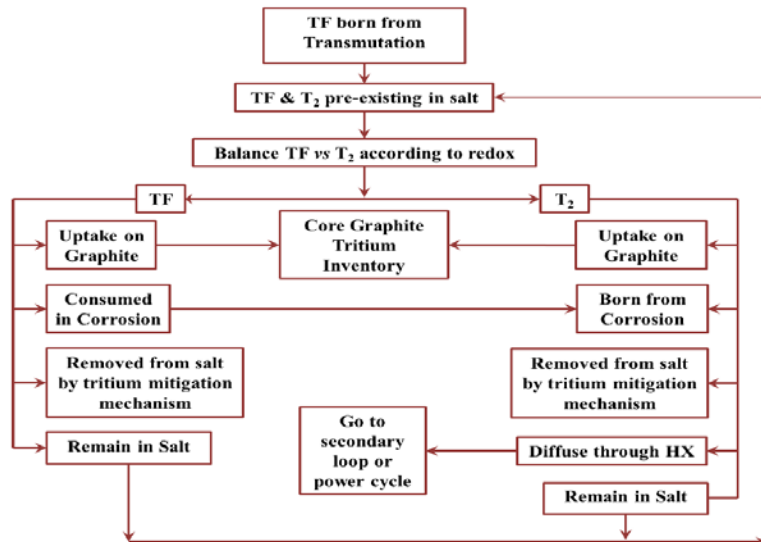

Figure 2.3. TRIDENT: Tritium Diffusion EvolutioN and Transport

TRIDENT has been used to model an FHR with a carbon bed for tritium removal as $^3H_2$. The model results are shown for one case (pebble bed FHR) in Table 2.4. In this case the carbon bed is designed to enable sufficient tritium removal to limit tritium releases to acceptable levels.

There are several observations from such modeling. The allowable tritium gas pressure in the primary system with metallic heat exchangers is on the order of magnitude of 0.05 Pa. If the tritium gas pressure is greater than this, the concentration gradients of tritium through hot heat exchangers may allow tritium to

Fluoride-salt-cooled High-temperature Reactor (FHR) Annual Report: 2015
MIT, U.C. Berkeley, U. of Wisconsin and U. of New Mexico
For Public Distribution

escape during operations in excess of releases from LWRs. The same limit would apply to a MSR or a fusion machine. The difference with a fusion machine is that the starting concentration of tritium in the salt is three orders of magnitude larger than in an FHR, and tritium is recovered from the salt for subsequent use as fuel. The calculated partial pressure of ^3HF is also given but HF can't diffuse through hot metal. Graphite absorbs both $^3H_2$ and ^3HF.

The requirements in Table 2.4 for allowable levels of tritium in the salt are strongly dependent upon permeation rates of tritium through hot heat exchanges to the environment. If high-performance coatings are incorporated into the heat exchangers to slow migration of tritium, much higher concentrations of tritium can remain in the salt. Consequently there is a tradeoff between high-efficiency removal of tritium from the salt and highly effective barriers to slow tritium transport through the heat exchangers. The CAS has a major effort to measure and develop better tritium barriers. The INL STAR facility for the fusion program has also had a major effort in measuring permeation rates through various materials.

Table 2.4. TRIDENT Output for FHR with Tritium Carbon Absorber Bed

Temperatures*	
Coolant Freezing	$459^{o}C$ (FliBe)
Operating Core Outlet	$700^{o}C$
ATWS	$<800^{o}C$
Coolant Boiling	$1400^{o}C$ (FliBe)
Pressures (primary loop) *TRIDENT Simulation	
p_{T2} Unmitigated	3.3-20 Pa
p_{T2} with Graphite Capture	**0.03-0.08 Pa** (Peak release 7.5 Ci/GW/d)
p_{TF} Unmitigated	0.03-0.075 Pa
p_{TF} with Graphite Capture	**0.27-0.45** (Peak release 7.5 Ci/GW/d)

Tritium Control and Carbon

The largest fraction of the workshop was devoted to carbon and tritium in salt-cooled systems. Carbon absorbs tritium and is chemically compatible with high-temperature salts. It is important in these systems in three different contexts.

Carbon in Reactor Cores. The FHR fuel is made of carbon and thermal spectrum MSRs use bare graphite. Tritium holdup in the carbon is significant. In the pebble-bed FHR with on-line refueling, there

Fluoride-salt-cooled High-temperature Reactor (FHR) Annual Report: 2015
MIT, U.C. Berkeley, U. of Wisconsin and U. of New Mexico
For Public Distribution

is the potential to use the pebbles as the main tritium capture system. In a pebble-bed reactor the pebbles circulate through the core typically once a month. There is the option of heating pebbles as they are circulated out of the core to remove the tritium before recirculating the pebbles back to the reactor core. This is not viable for other fuel forms because the carbon capability to pick up tritium will saturate due to the longer times between refuelings.

Tritium on carbon components is important in one other context. If carbon components in the nuclear system pick up a large inventory of tritium over time, this inventory could be partly released in a reactor over-temperature transient event. The equilibrium quantities of tritium in the core depend upon the average tritium levels in the coolant. The reactor core tritium inventories can be minimized by maintaining low levels of tritium in the coolant because there is an equilibrium between these tritium reservoirs.

Tritium uptake on carbon depends not only upon the carbon form but also on radiation damage in the graphite and potentially radiation flux levels. The MIT activities are primarily associated with experimental activities to understand these behaviors in 700°C salt in the MIT reactor. UW activities are investigating absorption onto previously-irradiated fuel matrix graphite.

Out-of-Core Tritium Removal with Carbon. Initial modeling indicated that a carbon bed out-of-core should be able to remove tritium from the clean salt in FHRs. The TRIDENT modeling used the limited tritium absorption data available on nuclear grade graphite for this analysis. However, non-nuclear-grade carbon forms have surface areas per unit of mass up to 1000 times larger than nuclear grade graphite—and potentially hydrogen sorption capacities a 1000 times larger. Nuclear grade graphite undergoes very high-temperature processing to produce a graphite with dimensional stability under high neutron radiation—a requirement that does not exist for any carbon absorber outside the reactor core. An out-of-core carbon bed can have the carbon and the bed optimized for tritium removal. This suggests the potential for relatively small carbon beds to efficiently remove tritium to very low concentrations. MIT is investigating this option.

In the design of the MSRE great efforts were undertaken to avoid uptake of xenon and krypton in the graphite moderator because they are neutron absorbers. However, some uptake of xenon and krypton was observed. It is believed that these inert gases diffused into void spaces that do not fill with salt because of liquid surface tension. It is unknown at this time whether efficient carbon absorbers could be developed for MSRs to simultaneously remove tritium, krypton, and xenon—or potentially removal of the fission-product noble metals from the salt. Fission product noble metals that are generated insitu migrate to liquid-gas and liquid-solid surfaces because of the very low solubility in salts. Metals can be plated onto carbon. What is unknown is whether a practical system can be developed to efficiently remove noble metals from the salt and what type of surface treatment of carbon may be required. That will require good methods to generate noble metals in salts or a MSR test loop to test different carbon absorbers for noble metals.

Carbon and Corrosion. The presence of carbon in a salt system alters corrosion rates. Experiments at MIT and Wisconsin are underway to understand the various mechanisms and testing different materials with and without carbon in the system.

Other Options for Tritium Removal from Salt

Fluoride-salt-cooled High-temperature Reactor (FHR) Annual Report: 2015
MIT, U.C. Berkeley, U. of Wisconsin and U. of New Mexico
For Public Distribution

Gas Sparging. Tritium can be removed from high-temperature salt using gas sparging where an inert gas such as helium or argon is mixed with the liquid salt and tritium in different forms preferentially transfers to the gas phase and then to the off-gas system. The Chinese Academy of Science (CAS) has an ongoing experimental program to develop such a system is initially using water analogs to be followed by testing in salt systems. The CAS plans to complete by 2020 a 10 MWt FHR and a 2 MWt MSR. In a MSR, the off-gas system must remove tritium but also remove much larger quantities of fission product xenon and krypton. This creates an incentive for a common system to remove all volatile gases—a capability of a gas sparging system.

New Mexico is initiating a program using ultrasonic gas sparging. Ultrasonics can potentially create smaller gas bubbles with higher surface area and thus more efficient mass transfer of tritium to the inert gas phase. While ultrasonic gas dispersion has been used in a variety of systems, it has not been applied to very high temperature systems.

There is the option of using a spray tower or equivalent where the salt is in droplets or flowing over a high-surface area media and the purge gas is the continuous media—reverse of gas sparging. It is an option originally examined by LLNL for fusion machines. The complication with this strategy is the larger size of equipment when the purge gas is the continuous phase.

This option may be particularly attractive for one class of advanced MSR designs that is being developed by Hatch of Canada where the liquid salt flows downward through the reactor core through constrictions to critically-safe passively-cooled dump tanks under the reactor core—a type of spray tower. The liquid salt is pumped from these tanks through the heat exchangers back to the reactor core. Any failure, including loss-of-power, results in the salt draining to a safe configuration. This upside-down configuration may allow tritium, xenon, and krypton removal options not available with other designs. The salt can be dispersed as droplets or flow over a metal mesh—both providing a high surface area for the liquid salt to allow the dissolved gases to diffuse over short distances from the liquid salt phase into the gas phase.

If a high-surface-area metal mesh is used, one would expect the noble metals to plate out on the surface of the mesh—addressing another salt cleanup challenge of MSRs. Alternatively the metal mesh could be salt pool at the bottom of the system for criticality control and noble metal plate out.

Permeators. Tritium can be removed by metallic permeators. Permeators are tubes designed for high rates of hydrogen transfer through the tube where salt would be on one side of the tube and a vacuum or hydrogen getter would be on the other side of the tube to provide a large hydrogen gradient to maximize hydrogen transport. Permeators are used in the laboratory and some process operations for tritium separation and isotopic separation of different hydrogen isotopes. Investigations are underway at Ohio State for tritium separation in salt-cooled systems using permeators.

Double-Wall Heat Exchangers. Double wall heat exchangers are used in the chemical industry where there are two fluids where violent reactions would occur if there was a tube failure. They have also been developed for sodium-cooled fast reactors for sodium water heat exchangers. Such heat exchangers can be used to block tritium transport by three mechanisms: (1) vacuum between the tubes to capture tritium, (2) solid hydrogen getter between the tubes to sorb the tritium or (3) flowing fluid such as lithium that acts as a getter. The disadvantages of double wall heat exchangers is cost and added temperature drop

Fluoride-salt-cooled High-temperature Reactor (FHR) Annual Report: 2015
MIT, U.C. Berkeley, U. of Wisconsin and U. of New Mexico
For Public Distribution

across the heat exchanger. Oak Ridge National Laboratory and Ohio State are investigating this option for liquid salt systems.

Tritium Control Experience

There is a massive experience base in tritium separations and control from national security, heavy water reactor, high-temperature gas-cooled reactor, fusion, and research programs. This experience provides the basis for research going forward and provides many of the required research tools. It also provides proven methods to handle tritium once captured for disposal as a waste or recycle as a fuel (fusion).

In the United States there are three organizations with much of this experience. Savannah River National Laboratory has the national security tritium handling facilities. Pacific Northwest National Laboratory has been responsible for targets to produce tritium in the Watts Bar Nuclear Power Plant. Last, Idaho National Laboratory has facilities that conduct research on tritium for the fusion community. Oak Ridge National Laboratory has the expertise in carbon and done much of the work on hydrogen absorption on carbon. MIT laboratories using the MIT reactor are investigating tritium behavior in 700°C salt under neutron irradiation with the University of Wisconsin conducting similar work in a laboratory environment (no irradiation).

Workshop Conclusions

A confluence of events in three power technologies (FHR, MSR, and Fusion) in the last several years has created the need for control and removal of tritium from high-temperature coolant salts. While there is massive experience in tritium capture and control under many different environments, that experience has not been in 700°C salt where the tritium is in the forms of $^3H_2$ and ^3HF at partial pressures of fractions of a Pa. A first workshop has been held as a starting point for a larger international cooperative effort to develop the required technologies for tritium control. A basic understanding of requirements and options has been developed but there is a large need for experimental data to develop models and engineered systems.

Tritium Modelling

FliBe (Li_2BeF_4) is an attractive choice for primary coolant as it provides excellent thermal and neutronic properties. One challenge with using FliBe however, is the production of radioactive tritium (^3H) in the reactor core. In FliBe, tritium is produced predominately due to thermal neutron reaction with Li-6. In the MK-1 FHR [1], the molten salt initially contains 0.005 wt %, which is consumed in early reactor life. However, Li-6 is continuously regenerated by the beryllium neutron transmutation of Be-9. In the molten salt, tritium exists as either T_2 or TF, dependent on the redox state of the solution. In the molecular form T_2, tritium can diffuse through metals and release to the atmosphere. As TF, tritium is highly oxidizing and will corrode stainless steel in piping and heat exchangers. Thus, tritium inventory in the FHR will need to be properly managed.

In 2015, a Tritium Diffusion Evolution and Transport code (TRIDENT) was developed at MIT [2] to model tritium in an FHR. TRIDENT is a time-dependent model accounting for generation, system absorption and diffusion, speciation between T_2 and TF, and pipe corrosion. The model overview in Fig.

Fluoride-salt-cooled High-temperature Reactor (FHR) Annual Report: 2015
MIT, U.C. Berkeley, U. of Wisconsin and U. of New Mexico
For Public Distribution

2.3 illustrates the relationship between various coupled effects, which dictate tritium evolution in the FHR [3].

TRIDENT calculates that the 236 MWt Mk1 PB-FHR with 99.995% Lithium-7 enrichment would produce approximately 2931 Ci/GWt/d (1.3 mg H-3/GWt/d) at equilibrium. This is orders of magnitude higher than a typical PWR, which produces only 12.3 Ci/GWt/d (304.8 mg/GWt/d). TRIDENT calculates that the peak tritium release for the baseline 236 MW$_{th}$ FHR without engineered mitigation is nearly 2410 Ci/EFPD (250.6mg/ EFPD) [3]. In comparison, the total tritium release in a PWR is only 0.74 Ci/GWt/d (0.1 mg/GWt/d) in a PWR and 20.07 (2.1 mg/GWt/d) in a HWR. [4].

The TRIDENT code was used to evaluate 3 different options for treatment of tritium: a permeation window, a stripping column and a continuous counter-current graphite absorber bed. Of these three, only the graphite absorber was able to lower release rates to a similar magnitude of current commercial reactors. For an absorber bed consisting of ISO-88 graphite operating at1 full regeneration per 30 days, the peak tritium release rates reduced from 2410 to 7.5 Ci/EFPD. Further, this technology shows promise as the performance and economics may be greatly enhanced through use of other highly absorptive carbons, which would be suitable outside of the reactor core. [5] The absorber tower was modeled in the primary loop downstream of the core before the primary heat exchanger. In concept, the tower will consist of a carbon bed running counter current the flow of salt shown in figure 2. One option of regenerating carbon is shown via off-gassing at high temperatures above 1000K.

In addition to a potential carbon absorber bed, an FHR also contain large volumes of graphite in the pebble fuel and core reflectors, which will significantly affect tritium inventory and release during transients and accidents. Currently, significant uncertainties are present in the tritium release rates and graphite absorption quantities due to lack of experimental data at FHR operating conditions.

Research characterizing hydrogen behavior on carbon has been primarily focused on collecting data at near-ambient temperatures and pressures for storage or for relatively large quantity applications such as for hydrogen storage

Figure 2.4: Carbon Bed Concept Drawing [7]

on porous carbon (eg. 0.8 wt.% at 25°C and 2MPa) [6]. In contrast, tritium quantities expected in the FHR are very low as TRIDENT estimates baseline tritium saturation at 0.00024 wt.% of core graphite. This equates to a steady-state T$_2$ partial pressure of 20 Pa (0.0002 atm) without mitigation and 0.08 Pa (7.9*10^{-7} atm) if a continuously regenerated carbon absorber bed is used.

In order to reduce uncertainty and the demonstrate feasibility of carbon absorber bed, MIT is experimentally investigating tritium absorption on carbon and graphite at the high operating temperature of 700°C and sub-atmospheric tritium pressures (below). [5] In parallel, we are now planning to conduct non-radioactive hydrogen absorption experiments on various carbon forms at pressures (~1 Pa) and temperatures expected in an FHR and in the tritium handling system. New data will allow the
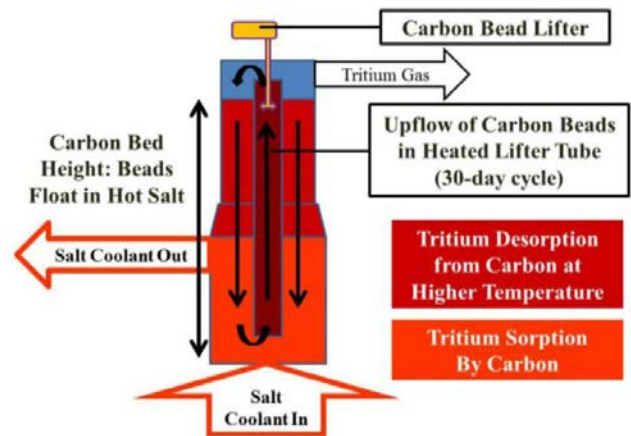
Fluoride-salt-cooled High-temperature Reactor (FHR) Annual Report: 2015
MIT, U.C. Berkeley, U. of Wisconsin and U. of New Mexico
For Public Distribution

improvement of existing simulations and development of new models for better prediction of tritium behavior in the FHR.

[1]   C. Andreadas, A. Cisneros, J. K. Choi, A. Chong, M. Fratoni, S. Hong, L. Huddar, K. Huff, D. Krumwiede, L. Michael, M. Munk, R. Scarlat, N. Zweibaum, E. Greenspan and P. Peterson, "Technical Description of the "Mark 1" Pebble-Bed Fluoride-Salt-Cooled High-Temperature Reactor (PB-FHR) Power Plant," University of California, Berkeley, Berkeley, 2014.

[2]   J. Stempien, "Tritium Transport, Corrosion, and Fuel Performance Modeling in the Fluoride Salt-Cooled High-Temperature Reactor," Ph.D. Thesis MIT, Cambridge, 2015.

[3]   J. Stempien, "A Model of Tritium Transport and Corrosion in Salt-Cooled Reactors," in *Proceedings of the 2015 American Nuclear Society Winter Meeting,* Washington D.C., November 2015.

[4]   IAEA, "Management of Waste Containing Tritium and Carbon-14," IAEA, 2014.

[5]   S. T. T. Lam, "Tritium Control Using Carbon Outside of Core," in *Workshop on Tritium Control and Capture in Salt-Cooled Fission and Fusion Reactors Session 5*, Salt Lake City, 2015.

[6]   V. B. Bhat and C. I. Contescu, "A Typical Hydrogen Uptake on Chemically-Activated Ultrmicroporous Carbon,: *Carbon*, **48** (*5*), 1331-1340, 2010.

[7]   J. Stempien, "Tritium Control from Salt-Cooled Reactors Using Carbon," Paper 15199, *Proc. 2015 American Nuclear Society Annual Meeting*, Washington D.C., November 2015

Task 1.1(b, c) Irradiation Experiments

Measurement of Tritium in Irradiated Graphite

The two salt irradiations that were conducted by first Integrated Research Project at MIT observed that there was very little release of tritium from the capsules relative the quantities that were generated. These capsules contained 700°C salt in graphite containers, various types of carbon, and surrogate coated-particle fuel. Work is underway to measure the tritium content of the different components from those irradiations to collect data on tritium uptake under realistic FHR conditions.

The MIT NRL is identifying and training students to assist with the measurement of tritium, and in particular the thermal release of tritium from irradiated specimens and components. They will be responsible for the final assembly, testing, and calibration of the high-temperature tritium furnace and capture system at the NRL. This system will bake out various irradiated samples to drive off the tritium and obtain quantitative measurements of tritium uptake.

The main part of the graphite holder from the first set of irradiation experiments has been transferred out of the hot box facility (radiation levels are elevated due to the presence of a thermocouple) to a filtered hood for sectioning. A special saw mount has been prepared by the MIT Central Machine Shop that will be used to guide a series of diamond blade cuts through the holder. Once sectioned, the pieces will be transferred into an inerted glove box and used to expose areas on a β-sensitive imaging plate

Fluoride-salt-cooled High-temperature Reactor (FHR) Annual Report: 2015
MIT, U.C. Berkeley, U. of Wisconsin and U. of New Mexico
For Public Distribution

provided by Prof. Raluca Scarlat at UW-Madison. These experiments will help determine the tritium distribution versus depth in the graphite.

Tritium Focus Group Meeting

FHR researchers from the MIT NRL attended the 2015 DOE Tritium Focus Group meeting at Los Alamos National Laboratory (November 3-5). This meeting is organized to promote communication and enhance safe tritium handling and operations. This was an opportunity to introduce the tritium management challenges of the fluoride slat-cooled reactor concept to the larger DOE tritium user community, familiarize them with the accomplishments and plans of the current FHR IRP research program, and solicit input and collaboration from this knowledgeable community. Presenters included researchers working with tritium from Los Alamos, Savannah River, and Pacific Northwest National Laboratories, as well as the University of Rochester Laboratory for Laser Energetics. This group provided substantial and useful feedback about the plans for tritium measurement for this IRP, as well as practical advice on experimental protocols. There are plans to further this collaboration, including a site visit to SRNL during the TRITIUM 2016 conference early next year.

Tasks 1.2(a), 1.2(b), and 1.2(c) (Understanding Tritium Absorption in Graphite):

These tasks deal with tritium absorption in graphite which University of Wisconsin performing in collaboration with MIT. In addition we are taking the opportunity to understand another important issue pertaining to graphite, namely intrusion of molten FLiBe salt into the graphite which deteriorate the properties of graphite. Nuclear graphite grade IG-110 and the matrix graphite grade A3-3 are being used in these studies. To understand the two aforementioned effects, it is critically that the graphite structure be thoroughly characterized at macro- to micro- to nano-length scales. To this end we are investigating methods to measure pore size distribution both at the surface in the bulk using techniques such as mercury porosimetry. Grain size and crystallite size and the degree of graphitization are being studied using techniques such as x-ray diffraction, and Raman spectroscopy. FliBe intrusion analysis is being performed using by glow discharge mass spectroscopy (GDMS). We are designing and constructing an equipment to study tritium absorption – initial experiments with this equipment will be performed using hydrogen as a surrogate for tritium.   Finally, we are presently working with MIT on measurements of tritium in irradiated graphite crucible, FLiBe salt, and metals with a commercially procured imaging plate. We are also in discussions with Dr. Cristian Contescu, an internationally recognized expert in the area of graphite testing and characterization at Oak Ridge National Laboratory to host one of our graduate students at ORNL to enhance our knowledge of graphite characterization techniques.

Graphite Characterization

Investigation of various methods to characterize nuclear graphite and matrix graphite are underway. The parameters of interest include porosity, surface area, graphitization, grain size or crystal size (L_a, L_b, L_c), and the lattice parameter (a_o).

Porosity and Surface Area:

We are investigating *Brunauer–Emmett–Teller* (BET) and mercury porosimetry (MP) methods to measure porosity and surface area using the services of the company, Quantachrome Instrumentation (QI). The first set of data from the MP method was obtained using a pressure range of 0.2 psi to 59510.738 psi. For IG-110 nuclear grade graphite, these measurements yielded a total intruded volume of

Fluoride-salt-cooled High-temperature Reactor (FHR) Annual Report: 2015
MIT, U.C. Berkeley, U. of Wisconsin and U. of New Mexico
For Public Distribution

0.1185 cc/g and a total surface area 18.9163 m^3/g. Pore size distribution measurements showed a predominant peak at about 3.5 µm and a smaller peak at 0.01 µm. The value of total surface area measured overestimates the data reported in literature by a factor of over 20. This may be because the MP technique measures the largest entrance towards the pore and not actual inner size of a pore. Second, due to the pressure range capabilities of MP, it may not provide the required accuracies for the small pore sizes in IG-110. Therefore the BET measurement technique will be pursued. Figure 2.5 shows the results of mercury porosimetry results of the two types of graphites. The results of microscopic examination and porosimetry are reasonably consistent.

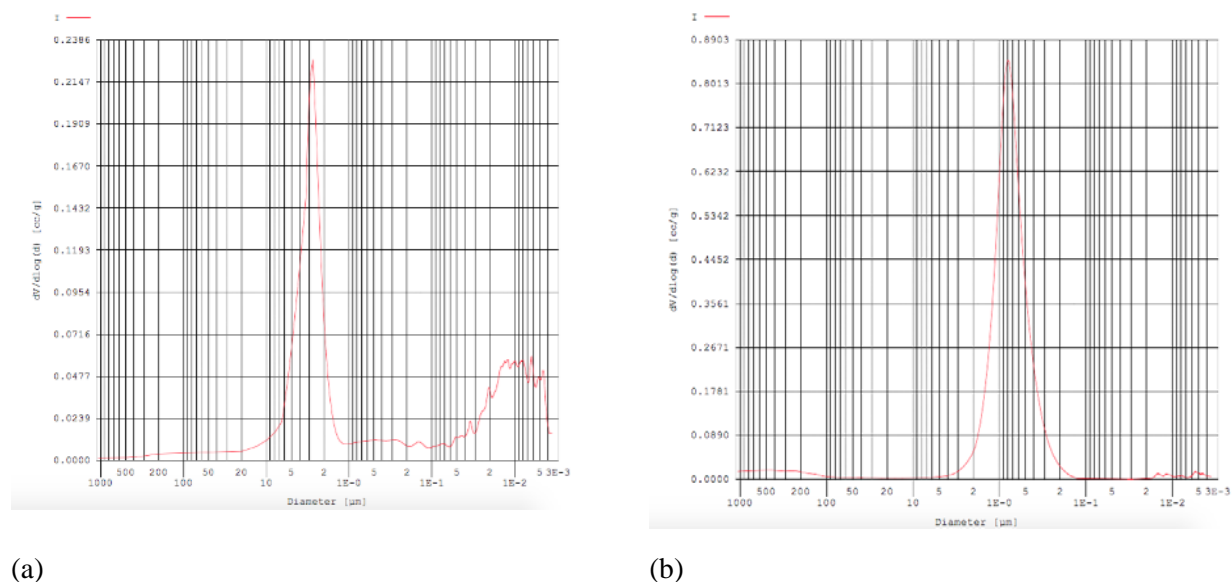(a)   (b)

Figure 2.5. Results of pore size distribution obtained by mercury porosimetry for (a) IG-110 nuclear graphite and (b) A-3 matrix graphite.

For A-3 matrix graphite, a significant fraction of the pore size is in the 0.1 um to 5 um range and there are almost no pores smaller than 0.1um. For or IG-110 nuclear graphite, the pore size distribution is mainly between 1 um to 10 um and smaller than 0.1 um.

Microstructure:

Graphitization will affect tritium trapping sites in graphite, as indicated by a tritium transport model. One of the major differences between nuclear graphite and matrix graphite is the degree of graphitization – matrix graphite has lower degree of graphitization. The degree of graphitization can be calculated with the knowledge of lattice parameter d$_{002}$, which can be determined by x-ray diffraction (XRD). XRD measurements are therefore being performed to obtain different lattice parameters in order to calculate the degree of graphitization. These XRD results will be supported by Raman spectroscopy. One consideration in these studies is that the nuclear grade graphite IG-110 is much more homogeneous than the matrix graphite A3-3.

Filler grain or binder size or Crystal size:

Scanning electron microscopy (SEM) and optical microscopy (OM) of graphites have been initiated for imaging and measurements of filler grains, binder, cracks, and grain size. Pore size distribution analysis

23

Fluoride-salt-cooled High-temperature Reactor (FHR) Annual Report: 2015
MIT, U.C. Berkeley, U. of Wisconsin and U. of New Mexico
For Public Distribution

is being performed using by Matlab. Figure 2.6 shows examples of such measurements for IG-110. Subsequently we will compare these results with those obtained by BET analysis
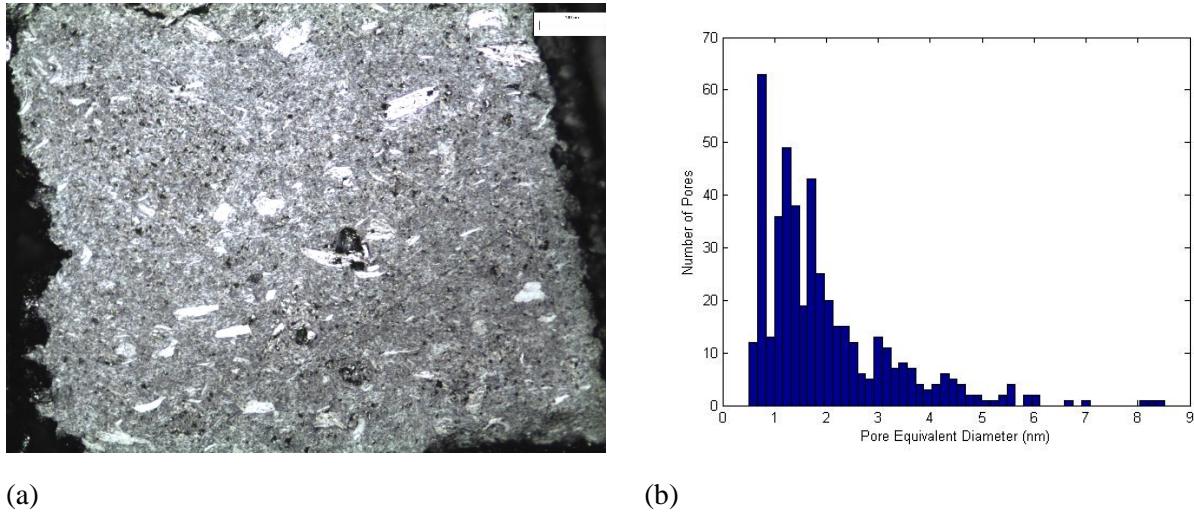

(a)   (b)

Figure 2.6. (a) Optical microscopy mage for nuclear grade graphite IG-110 and (b) pore size distribution.

Research has continued in the area of characterization of microstructure of two types of graphite, IG-110 (nuclear graphite) and A-3 (matrix graphite from ORNL). Such microstructural characterization is important for understanding FLiBe infiltration and tritium capture by the graphite. At present optical and scanning electron microscopy are being used for the visual microstructural examination of graphite for features such as grain size, porosity, and phases. Figure 2.7 shows the microstructures of graphites IG-110 and A3, respectively.
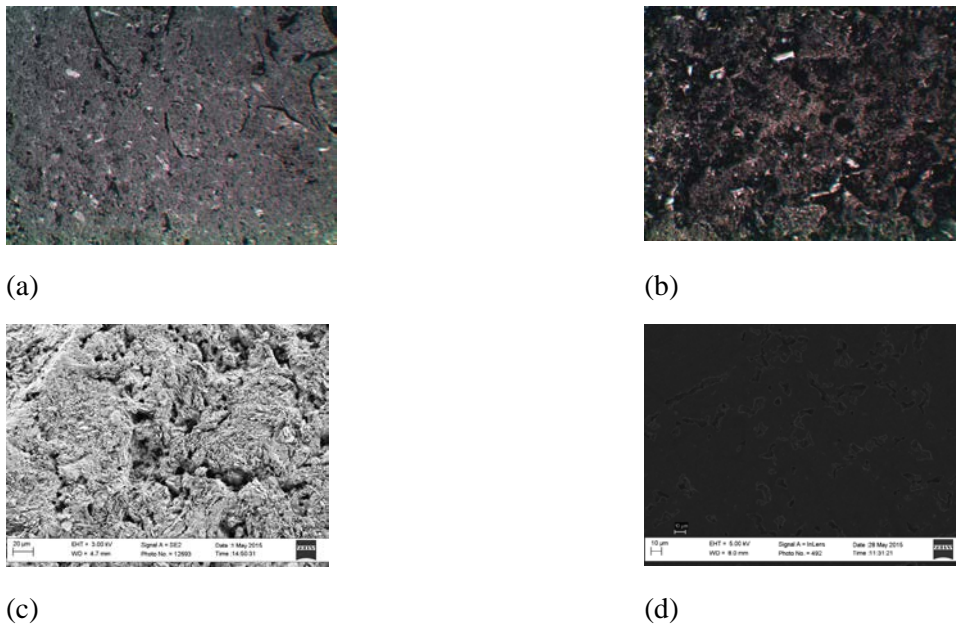

(a)   (b)

(c)   (d)

Figure 2.7. (a) and (b) Low magnification (10X) optical microscopy images of IG-110 nuclear graphite and A3 matrix graphite, respectively, (c) and (b) scanning electron microscopy surface images of IG-110 nuclear graphite and A3 matrix graphite, respectively.

24

Fluoride-salt-cooled High-temperature Reactor (FHR) Annual Report: 2015
MIT, U.C. Berkeley, U. of Wisconsin and U. of New Mexico
For Public Distribution

Crystallite Size

Lattice parameters are being measured by x-ray diffraction while Raman spectroscopy is being used for determining chemical bonding information. Preliminary studies have been initiated in using Raman spectroscopy for determining the crystallite size in the two types of graphites. Raman spectroscopy is based on Raman scattering, which is a form of inelastic scattering. The output of this technique is the Raman shift, which is the frequency difference between the incident laser and the Raman scattered radiation. From Raman shift, we can potentially calculate the lattice parameter-crystalline size using the expression, $2.4*10^{-10}*\lambda laser^4*(Ig/Id)$, where Ig and Id is the intensity of G-band and D-band from Raman shift. Preliminarily analysis shows that IG-110 nuclear graphite has a slightly smaller crystallite size compared to A-3 nuclear graphite.

(a)   (b)
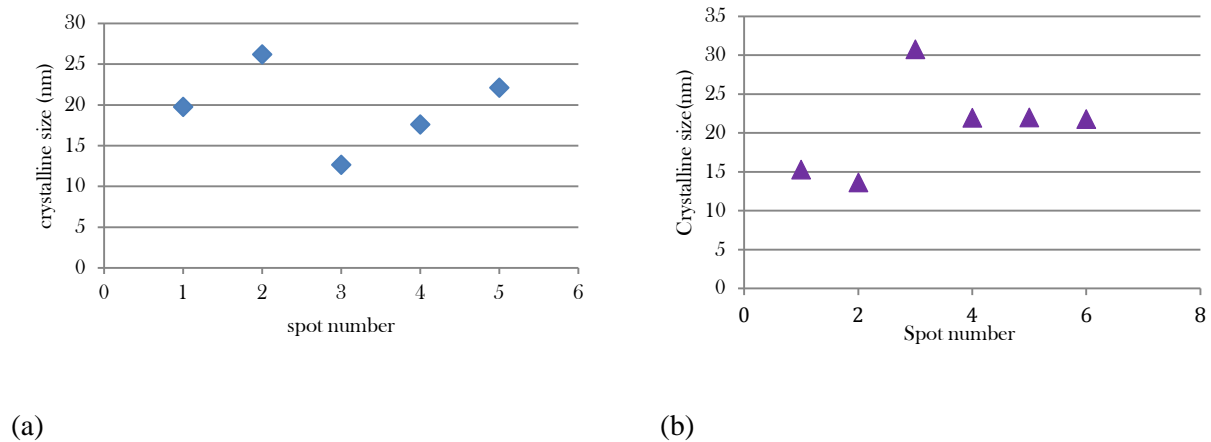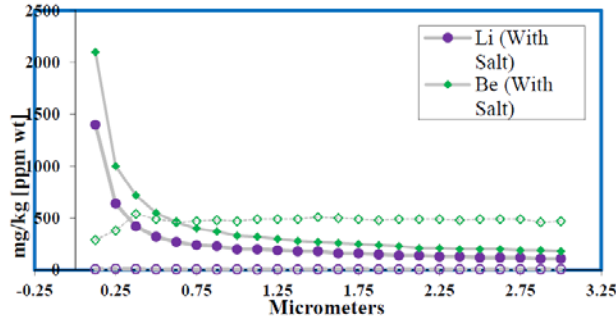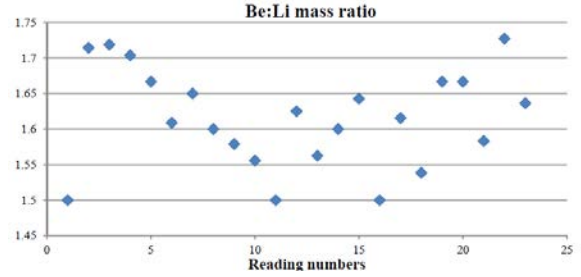
Figure 2.8. Application of Raman spectroscopy for determination of crystallite size in the two types of graphites: (a) IG-110 nuclear graphite and (b) A-3 nuclear graphite.

FliBe Intrusion Analysis by Glow Discharge Mass Spectroscopy (GDMS)

A key area of importance in FHR, related to graphite is the intrusion (or permeation) of the primary salt FLiBe into graphite. To investigate this, we sectioned graphite samples from our prior corrosion test crucibles and sent them for analysis to EAG Laboratories for Glow Discharge Mass Spectroscopy (GDMS) evaluations. A control graphite sample not exposed to FLiBe was also submitted for analysis. The primary features of interest here were the depth (*vs.* concentration) profiles of beryllium and lithium concentrations in the graphite. Figure 2.9 shows the results of these analyses. These data indicate a higher beryllium to lithium ratio (average is about 1.61) in the graphite than would be expected of FLiBe stoichiometry (ratio should be 0.649) and could be potentially attributed to the deposition of a few monolayers of beryllium dust on the graphite samples.

25

Fluoride-salt-cooled High-temperature Reactor (FHR) Annual Report: 2015
MIT, U.C. Berkeley, U. of Wisconsin and U. of New Mexico
For Public Distribution

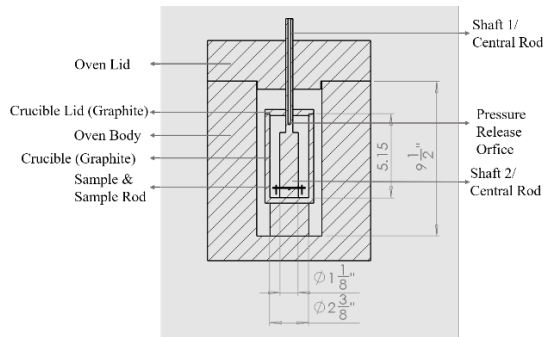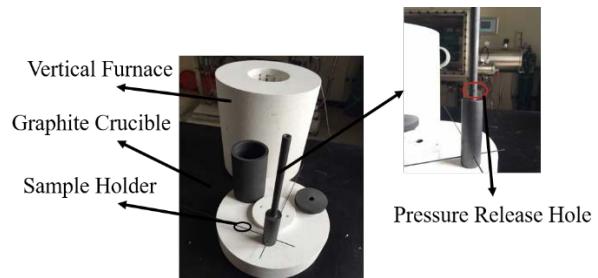(a)   (b)

Figure 2.9. (a) depth profile for Be and Li for graphite exposed to FLiBe and control graphite (not in contact with FLiBe) samples and (b) Be to Li mass ratio measured over the 25 data points.

Flibe Intrusion-Related Experiment

We are designing FLibe intrusion experiment in order to study FLiBe intrusion into IG-110 and A-3 (Fig. 2.10.

(a)   (b)

Figure 2.10. (a) Experimental setup for salt intrusion experiments and (b) components for FliBe intrusion experiment

Square graphite samples of 1mm thickness will be suspended in the molten FLiBe salt with sample holder rods such that both sides of the samples are exposed to the salt. The holders will prevent the graphite samples from float in the molten salt. The crucible and sample holders will be made of high purity graphite to prevent introduction of metallic impurities or metal alloy corrosion products in the salt. The entire experimental apparatus, including the graphite crucible will be placed inside a vertical furnace that can operate up to 1200ºC. The experiment is performed inside a glove box with argon atmosphere, with $O_2 <$ 1ppm and $H_2O <$ 1 ppm.

The variables in this study will be:

1. Salt type

Fluoride-salt-cooled High-temperature Reactor (FHR) Annual Report: 2015
MIT, U.C. Berkeley, U. of Wisconsin and U. of New Mexico
For Public Distribution

2. Graphite type

3. Sample surface preparation

4. Exposure time

5. Degassing treatment of the graphite

The measurement we will performed by:

1. Sample weight change

2. Graphite microstructural analysis before and after exposure to salt (mercury pycnometer, X-ray diffraction, SEM, Raman)

3. Contact angle

4. Mass spectroscopy depth profile on the sample fractional surface

The first experiment will be conducted with two samples of nuclear graphite, IG-110. The size of the sample is about 12mm x 12mm x 0.35 mm. The first sample will have different surface treatments on the two sides –one side will be ground with 1200 grit SiC paper and cleaned with DI water, while the other side is just as-machined. For the second sample both sides have the same treatment (1200 grit hand polishing and cleaned with DI water). After we established the experimental procedure and post-exposre measurements, we will include include A-3 graphite samples as well in the tests, and then compare the results of FLiBe intrusion for IG-110 and A-3 graphites.

Tritium-related Work

Tritium-Related Experiment

Besides FLiBe intrusion experiment, we are designing the following two sets of experiments aimed at tritium diffusion into graphite: (a) tritium diffusion in graphite, and (c) tritium diffusion in graphite-FLiBe system. In these experiments, our goal will be to investigate tritium diffusion mechanisms in matrix graphite and to study how features of graphite microstructure such as grain size, pore size, and degree of graphitization, affect tritium diffusion. Prior to the above tritium diffusion experiments, we will perform experiments using hydrogen (as surrogate from tritium). Figure 2.11 shows the experimental setup of the "constant volume method" we are going to use to start the hydrogen-graphite experiment.

Fluoride-salt-cooled High-temperature Reactor (FHR) Annual Report: 2015
MIT, U.C. Berkeley, U. of Wisconsin and U. of New Mexico
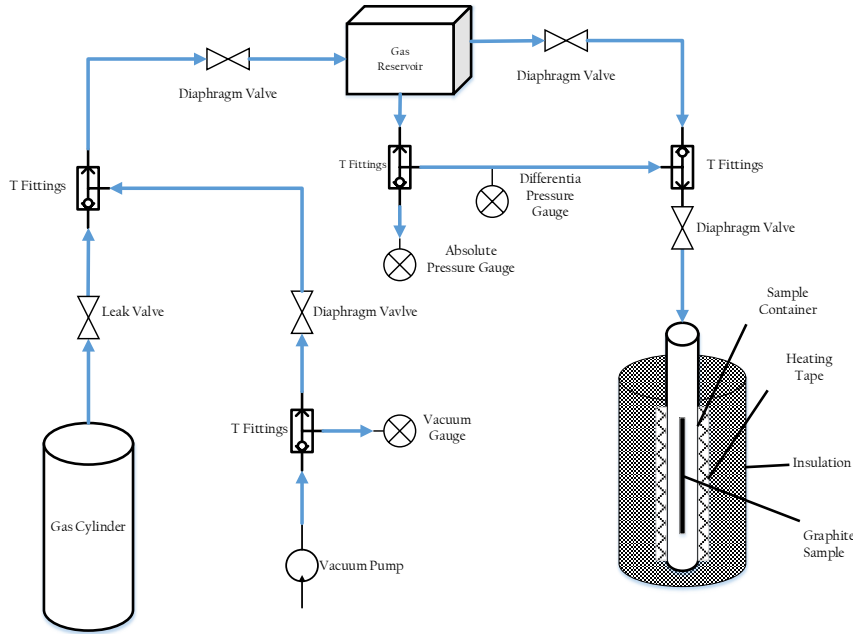For Public Distribution

Figure 2.11. Schematic illustration of the hydrogen-graphite experiment.

Tritium Mapping with Imaging Plates

Besides the H-G experiment, we are presently working with MIT on measurements of tritium in irradiated graphite crucible, FLiBe salt, and metals with an Imaging Plate. The sensitivity of imaging plate is 100dpm/mm^2/hr, and based on beta travel length in graphite 3.5um (from SRIM). H-3 detection limit is 0.74 wppb, which is significantly lower than calculated H-3 concentration in FS-1 graphite crucible which is 346.7 wppb, assuming all H-3 is in graphite. Presently, we are working on a methodology to differentiate beta particle from H-3 (5.7 keV (Ave.)) and C-14 (49 keV (Ave.)).

Fluoride-salt-cooled High-temperature Reactor (FHR) Annual Report: 2015
MIT, U.C. Berkeley, U. of Wisconsin and U. of New Mexico
For Public Distribution

3. Task 2: FHR Corrosion Control with Redox Control, Impurity Control, and Materials Selection (UW and MIT)

The task focuses FLiBe salt preparation and purification, electrochemistry, static corrosion, and construction of a FLiBe salt flow loop to study flow-assisted corrosion, transport of beryllium redox transport in molten salt, and temperature gradient induced corrosion. The loop of course could be used for other engineering aspects of FHR such as measuring thermodynamic properties and testing instrumentation. We are working with two types of FLiBe salts, namely [7]Li enriched MSRE FLiBe and in-house prepared FLiBe prepared by mixing LiF and BeF_2. Both salts have been prepared in tens of kg quantities. It has been well-established in booth MSRE and our own experiments that impurities in salt can dramatically accelerate corrosion. To this end we have worked extensively on salt purification protocols that include hydrofluorination, beryllium reduction, and filtration steps. Using these approaches we are able to prepare FLiBe salts with varying corrosivities (or redox potential) for controlled fundamental experimentation.

In the area of electrochemistry we have developed a beryllium-probe. This probe, partly based on an earlier Russian design, is capable of measuring the molten FLiBe salts' redox potential that determines whether the salt is oxidizing or reducing. The lower the redox potential the lower the corrosivity, generally speaking, but very low redox potentials can lead to formation of carbides which is undesirable. We have tested the robustness of this probe in regards to accuracy and reproducibilty by making measurements in salts that have been purified to varying degrees and have had deliberately different levels of impurities added to the purified salt.

Corrosion studies of 316 stainless steel and Hastelloy N have been tested in graphite crucibles and metal-lined graphite crucibles. The FHR uses graphite-based fuel. Graphite has been show to increase corrosion attack and form carbides in the near-surface regions of the alloy. Other potential structural alloys including Mo-Hf-C and W-ZrC, and SiC-SiC$_f$ and C-C$_f$ composites will be corrosion tested in the coming quarters at different redox potentials.

Last, the design and construction of a natural circulation FLiBe flow loop (3/4" diameter flow tube) has commenced and should be completed in the next two quarters.

Two PhD degrees (one in the area of salt chemistry and purification and the other on corrosion) and one Master's degree (on electrochemistry) were awarded this year. Three publications in journals have accrued from this work in 2015 and preparation of three other manuscripts is underway. Three presentations on this work have been made at national conferences in 2015. A work-shop focusing on *Materials and Salts* was held at the University of Wisconsin on September 25th, 2015 with members of the Georgia Tech-led IRP and Oak Ridge National Laboratory. A report on the proceedings of this work-shop has been prepared and is available for circulation.

Task 2.1(a) - FLiBe Salt Purification:

All [7]Li enriched MSRE FLiBe was re-purified in December of 2014. The present IRP project involves the construction of natural circulation loops to be used for corrosion tests which simulate reactor environments more closely and would allow us to study thermal gradient driven corrosion by having hot and cold legs in the loop. These experiments do not require [7]Li enriched FLiBe. To avoid the use of large quantities of [7]Li enriched MSRE coolant salt, new non-enriched FLiBe was produced for these and other out-of-reactor experiments. To support our-of-core corrosion and electrochemistry research, a batch purification of FLiBe prepared from raw materials was carried out at the University of Wisconsin in March 2015. Lithium-fluoride of 99.8% purity was procured from Noah Technologies and 98.8% pure beryllium-fluoride was obtained from Materion.

Fluoride-salt-cooled High-temperature Reactor (FHR) Annual Report: 2015
MIT, U.C. Berkeley, U. of Wisconsin and U. of New Mexico
For Public Distribution

Lithium fluoride and BeF_2 were loaded into the purifier in twenty-eight additions, in seven layers, over the course of nine hours spread between two days. Salt components were layered in order to accelerate melting by providing many melting interfaces. Since the eutectic of $LiF-BeF_2$ melts at about 363°C, these layers would start to mix at that time. Each addition was weighed on a 1 g accuracy weighing balance and then added to the purifier through its charging port. Beryllium fluoride chips used had a large variance in size. During the initial loading, a nickel pipe with identical inner diameter to the charging port was kept next to the high accuracy scale. Each beryllium fluoride chip was dropped through this pipe to ensure that it was of proper size. If a chip was too big, it was discarded into a separate bag. After sorting 15 kg of beryllium fluoride it was found that roughly half of the chips had to be discarded. These discarded chips were placed inside of an inflatable glove box which contained a large stainless steel pot. Using a hammer, the chips were broken to manageable size in the pot and then loaded into the weighing boat. This method proved to be satisfactory, although it produced considerable beryllium fluoride powder within the inflatable glove box. After breaking, chips were loaded with tongs, one by one, into the charging port. Any small powder was then poured through the funnel. The weight change after the addition was recorded by the scale for the purifier, which had an accuracy of 10 g.

Once all FLiBe was loaded the charging port and stainless steel vessel flanges were reattached with a new gasket and O-ring. Vacuum was pulled on the stainless steel vessel to around -10 to -15 mm Hg several times. After each pump down, the space was refilled with argon to 3 psi. This was done before the previous purifications and seemed to prevent excessive oxidation in the head space which reaches a maximum temperature of 90°C during the purification. Container pressures were monitored during each pump down and refilling to assure good seals.

The purification vessel was then heated up to 50°C and then incrementally increased to 110°C. While heating up, the purification vessel was purged with argon. Water was seen to escape after the salt temperature reached 100°C. The vessel was kept at 110°C for 20 hours, after which no water was observed in the effluent. At this point, the salt was heated up to 200°C, 300°C, and then set to 500°C to melt. Water was observed in the effluent stream at all of these temperatures. Melting took about ten hours and was made obvious by decreasing temperatures with constant heater power input, shown in Figure 3.1. The temperature was briefly increased to 520°C to melt any remaining components. After melting, the salt was sparged with alternating hydrogen and argon for 48 hours at flow rates varying from 0.5 L/m to brief peaks of 2.25 L/m to reduce the salt and force water and hydrogen fluoride out. Average flow rates were 0.83 L/m.
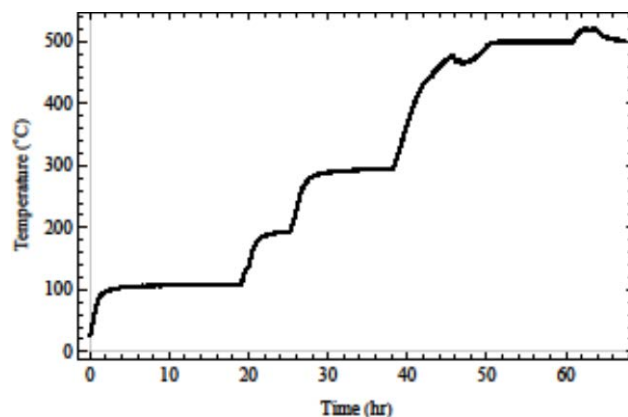

Figure 3.1: Melting FLiBe from raw components. The large depression at roughly 48 hours and 460°C is caused by the latent heat of melting $LiF-BeF_2$.

The hydrofluorination of natural lithium FLiBe used parameters similar to those used for purifying the MSRE coolant salt. A total flow rate of 2.5 L/m was selected with a 1:10 $HF:H_2$ ratio. Hydrofluorination was performed at 597°C for about 80 hours. Accounting for gas trips, the total

Fluoride-salt-cooled High-temperature Reactor (FHR) Annual Report: 2015
MIT, U.C. Berkeley, U. of Wisconsin and U. of New Mexico
For Public Distribution

purification time was 72 hours. As compared to the second batch purification, the hydrogen fluoride cylinder was left at room temperature, about 23°C. Previously, cylinder temperatures of 34°C were used but were found to overload the hydrogen mass flow controller. By reducing the temperature, the pressure was reduced, producing a smooth flow of hydrogen fluoride. Figure 3.2 shows the salt temperature overlaid with the flow rates of both hydrogen and hydrogen fluoride for the first purification of FLiBe from raw materials.
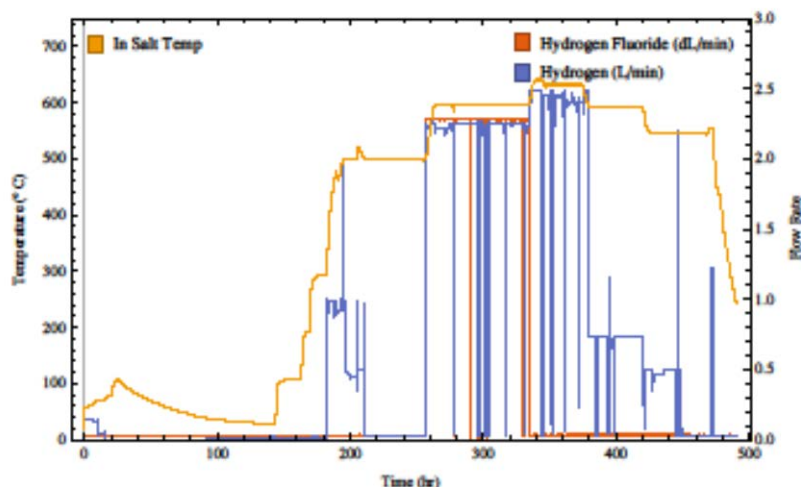

Figure 3.2: Salt temperature overlayed with the flow rates of both hydrogen and hydrogen fluoride for the first purification of FLiBe from raw materials.

A total batch size of 38.7 kg was purified – a sample of the resulting salt is shown in Figure 3.3. The frozen salt had a slight green tint, which is likely caused by metal fluoride impurities. The composition of the purified FLiBe was measured with ICP-OES and ICP-MS techniques. These results are shown in

Table 3.1. Elements in bold are considered to be the most stable impurity fluorides, so their effect on redox potential or corrosion can be profound. A total of 3.5 kilograms of the salt will be used for electrochemistry and static corrosion tests, with the majority of salt being saved for a natural convection flow loop.

Fluoride-salt-cooled High-temperature Reactor (FHR) Annual Report: 2015
MIT, U.C. Berkeley, U. of Wisconsin and U. of New Mexico
For Public Distribution

Figure 3.3: Purified FLiBe prepared from raw materials, lithium-fluoride and beryllium-fluoride.

Table 3.1: Composition of raw materials FLiBe measured using ICP-OES and ICP-MS.

Analyte	Result [mg kg^{-1}]	Analyte	Result [mg kg^{-1}]
Lithium	135000	**Chromium**	53.3
Beryllium	88200	Aluminum	28
Potassium	544	**Nickel**	10.7
Sodium	469	Thallium	10.6
Magnesium	139	Barium	9.51
Calcium	132	Strontium	3.7

Approximately 2.2 kg portion of this FLiBe was transferred into the glovebox using the nickel transfer vessel shown in Figure 3.4. A Ni transfer tube was bent, trace heated, and thoroughly insulated before being attached to the vessel for salt extraction. A pressure of about 1-2 psi above atmosphere was sufficient to pour at an acceptable rate.

Fluoride-salt-cooled High-temperature Reactor (FHR) Annual Report: 2015
MIT, U.C. Berkeley, U. of Wisconsin and U. of New Mexico
For Public Distribution

Figure 3.4: Nickel transfer vessel in glovebox (left) without insulation showing trace heating of transfer tube and (right) insulated with gas inlet to control pour rate secured.

Figure 3.5 shows the transfer apparatus and UW-made FLiBe as a fluid liquid salt in Ni tray. Once solidified, this FLiBe was broken up into large pieces as well as powdered and granulated particles. FLiBe was additionally poured into Ni crucibles and stored for future electrochemical experiments.

Fluoride-salt-cooled High-temperature Reactor (FHR) Annual Report: 2015
MIT, U.C. Berkeley, U. of Wisconsin and U. of New Mexico
For Public Distribution

Figure 3.5: Complete transfer apparatus on left. Liquid FLiBe in Ni tray on right is completely translucent and flows fluidly. Provided adequate trace heating, salt can be poured by controlling Ar gas pressure through valves.

The total inventory of 2.2 kg of FLiBe transferred into the glovebox is shown in Figure 3.6. Ni crucibles are filled with FLiBe and stored in glass jars. Approximately 150g of salt is required per crucible in corrosion test. Granulated salt before and after Be reduction will be ground to a homogeneous consistency to facilitate loading into crucibles.

Figure 3.6: Total of 2.2 kg of UW-made FLiBe currently stored in glass jars. Four nickel crucibles are all fully filled with FLiBe. Approximately 250 g of granulated salt was separated for one crucible in corrosion test.

Fluoride-salt-cooled High-temperature Reactor (FHR) Annual Report: 2015
MIT, U.C. Berkeley, U. of Wisconsin and U. of New Mexico
For Public Distribution

An example of the purification, H_2/HF sparging and beryllium reduction of MSRE salt is shown in Figure 3.7. The two stages of reduction outlined in the figure are analogous to the stages of reduction of UW-made FLiBe to be compared in corrosion tests. It has been established that an addition of Be metal is required to fully reduce impurities, specifically Ni, Fe, and Cr, dissolved in the salt as fluoride compounds.

Neutron Activation Analysis Results

	Pure	Green	Grey
Ni	0.21 ppm	10.2 ppm	0.38 ppm
Fe	<4.3 ppm	31.3 ppm	144 ppm
Cr	0.37 ppm	32 ppm	46 ppm
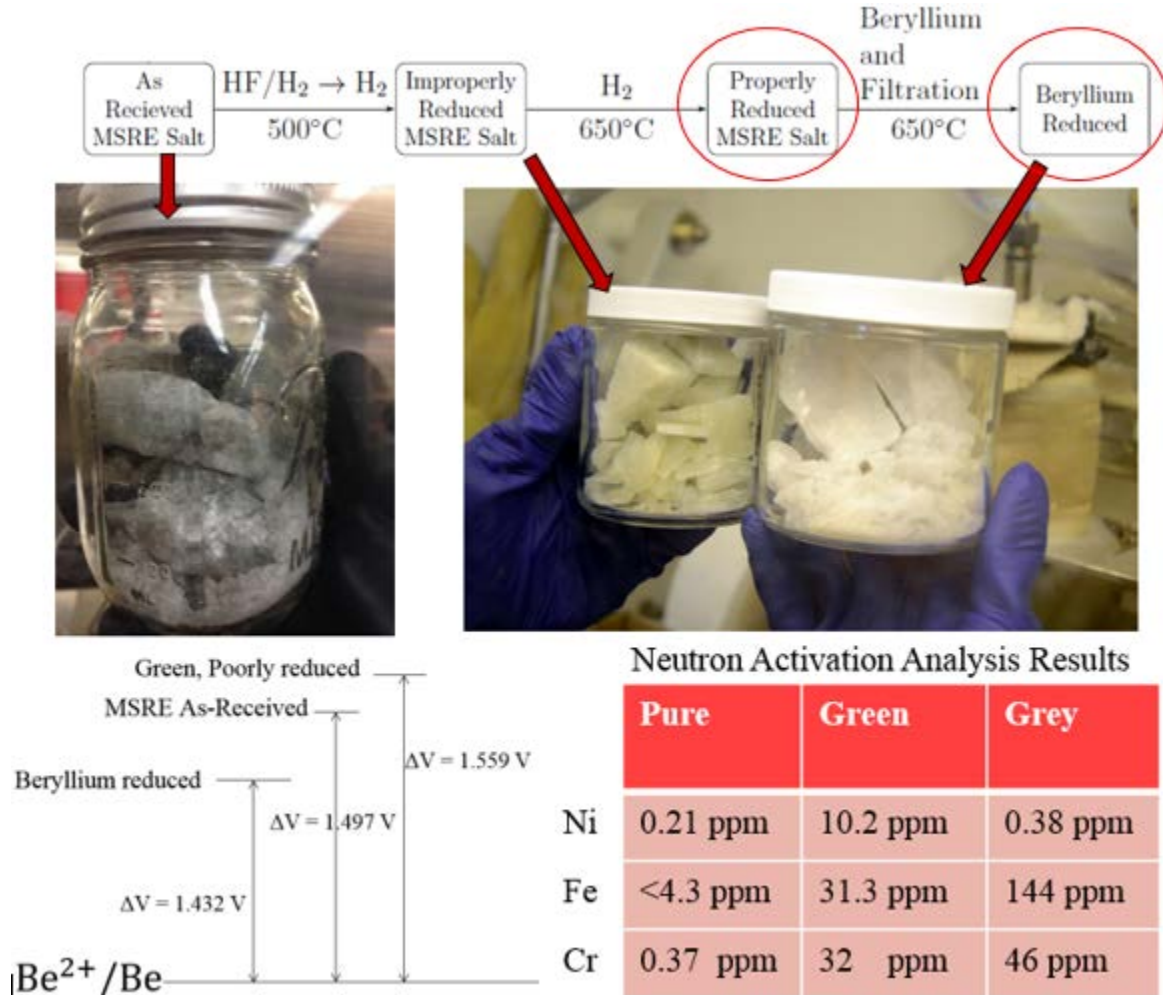
Figure 3.7: MSRE FLiBe at different stages of reduction. Red circles signify equivalent reduction stages of UW-made FLiBe to be used in future corrosion tests. Redox potentials estimated to be -1.7V and -1.4V, respectively.

The un-reduced UW-made FLiBe with a redox potential of -1.70V will be Be reduced to -1.40V, and subsequently filtered prior to loading of crucibles in the corrosion test shown in Figure 3.29. Filtration of salt through a mesh filter to capture metals reduced from fluoride states in FLiBe will be required to yield a pure and fully-reduced salt avoid contamination in later studies.

Based on ppm amounts of Cr, Ni and Fe in UW raw materials FLiBe measured with Neutron Activation Analysis (NAA) shown in Figure 3.8, an estimated .0681mg of Be per 50g batch of FLiBe would sufficiently reduce impurities, assuming that they are fluorides. Further work in FLiBe purification will be the development of a batch-wise Be-reduction procedure to prepare reduced salt for comparison to un-reduced salt in corrosion test.

Fluoride-salt-cooled High-temperature Reactor (FHR) Annual Report: 2015
MIT, U.C. Berkeley, U. of Wisconsin and U. of New Mexico
For Public Distribution

Element	MSRE Metal Standards (ppm)	ORNL as Received (ppm)	UW Raw Materials (ppm)	ORNL Poorly Reduced (ppm)	ORNL Properly Reduced (ppm)	ORNL Beryllium Reduced (ppm)
Ni	25	0.38 ± 0.32	63.6 ± 10.1	10.2 ± 1.2	0.73 ± 0.24	0.21 ± 0.08
Fe	100	144 ± 13	12.7 ± 1.4	31.3 ± 2.1	< 9.7	< 4.3
Cr	25	46 ± 1	2.42 ± 0.12	32 ± 1	31.5 ± 0.9	0.37 ± 0.02

Figure 3.8: Comparison of impurity content of various FLiBe salts measured via NAA at MIT. A total of 78.7 mg/kg was added to 50g of FLiBe to fully reduce impurities.

Task 2.1(b) - FLiBe Electrochemistry Measurements:

Work is ongoing at the University of Wisconsin using electrochemical measurements in molten FLiBe salt in order to better understand salt chemistry and predict corrosion behavior. This is being done by measuring the redox potential of the salt, which is an intrinsic chemical potential energy of the melt that determines which reduction or oxidation reactions will occur. In these experiments, the redox potential is measured directly as a voltage using an electrochemical probe immersed in the salt. The UW FLiBe electrochemistry probe is unique in that it uses the dynamic beryllium reference electrode described by Afonichkin et al.[2] as opposed to a traditional stationary electrode design. A dynamic reference electrode is well suited for FHR applications because it can be fully submerged in a static or flow environment while producing stable, repeatable measurements for long periods of time.

Operation of the probe begins by applying a voltage between a submerged glassy carbon anode and a molybdenum cathode, causing beryllium ions from the salt to be plated onto the molybdenum electrode's surface. The voltage is then disconnected, and the plated beryllium is allowed to re-dissolve back into the salt. As the plated beryllium recombines with displaced fluorine atoms, a distinct voltage signature is created which can then be compared to the voltage at an isolated molybdenum indicator electrode in order to measure the redox potential of the salt. The positive lead in the voltage measurement is connected to the cathode, which is in an electronegative state once the beryllium is plated. After the beryllium dissolves, the voltage between the molybdenum cathode and indicator electrodes relaxes to zero. The beryllium reaction is assumed to always take place at a fixed voltage, whereas the voltage at the indicator electrode will vary depending on the redox potential. Therefore, a voltage measurement closer to zero indicates a more reducing salt because the potential of the salt is closer to the lower, beryllium reaction voltage.

---

1) V. K. Afonichkin, A. L. Bovet, V. V. Ignatiev, A. V. Panov, V. G. Subbotin, A. I. Surenkov, A. D. Toropov, A. L. Zherebtsov, Dynamic reference electrode for investigation of fluoride melts containing beryllium difluoride, Journal of Fluorine Chemistry 130 (1) (2009) 83 – 88.

Fluoride-salt-cooled High-temperature Reactor (FHR) Annual Report: 2015
MIT, U.C. Berkeley, U. of Wisconsin and U. of New Mexico
For Public Distribution

Table 3.2: Redox potential of FLiBe salt under various conditions of purity.

Impurity (ppm)	Poorly Reduced MSRE FLiBe	Properly Reduced MSRE FLiBe	Beryllium Reduced MSRE FLiBe	Purified UW Raw Materials FLiBe
Nickel	10.2 ± 1.2	0.73 ± 0.24	0.21 ± 0.08	10.7
Iron	31.3 ± 2.1	<9.7	<4.3	12.7 ± 1.4
Chromium	32 ± 1	31.5 ± 0.9	0.37 ± 0.02	53.3
Redox Measurement:	**-1.56 V**	**-1.45 V**	**-1.43 V**	**-1.71 V**

Redox measurements of salt at various chemical conditions have been taken using the described electrochemical method. The main source of differences between salt states is the level of dissolved impurities, which usually come from corrosion. Another area of research at UW is in the purification of FLiBe salt in order to remove impurities such as these.

Table 3.2 shows neutron activation analysis results, performed by MIT, for Ni, Fe, and Cr impurities in three different batches of salt. Also in the table are the redox measurements for each salt. As seen in the table, the salt batches which contain a higher level of impurities have redox potentials which are farther away from zero – and therefore are more oxidizing, as expected.

Further characterization of the FLiBe prepared from raw materials was carried out by measuring the salt's redox potential. An electrochemical probe featuring a dynamic beryllium reference electrode was used for the redox potential measurements. Five 50g batches of FLiBe were used and five redox measurements per batch were taken. A large number of total measurements were taken in order to quantify the uncertainty in the measurement process. The redox measurements from each batch along with a histogram of all runs are shown in Figure 3.9. A combination of all these measurements yields an average redox voltage of -1.706 V with a standard deviation of 6.2mV. This shows that the redox potential measurement by the dynamic reference electrode method is repeatable.

Fluoride-salt-cooled High-temperature Reactor (FHR) Annual Report: 2015
MIT, U.C. Berkeley, U. of Wisconsin and U. of New Mexico
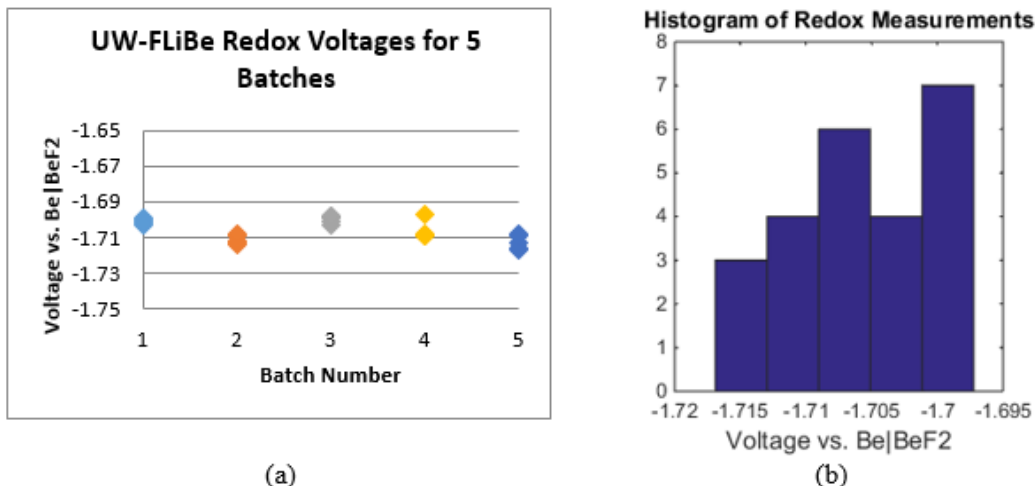For Public Distribution

Figure 3.9: (a) Redox potential measurements for five different batches of FLiBe salt prepared from raw materials (b) histogram of all measurements.

With an understanding of the redox measurement uncertainty, redox control experiments can be carried out. Both reduction and oxidation experiments have been completed in FLiBe, and measurements follow expected phenomena. To reduce the salt, several small flakes of beryllium metal were added to a frozen salt ingot in a glassy carbon crucible. The salt was then melted, and redox potential measurements were taken intermittently. As the beryllium dissolves into the melt, the redox potential is gradually reduced. Experimental results of the reduction are shown in Figure 3.10. Note here that a less negative redox voltage represents a salt that is closer to the Be|BeF$_2$ couple, and is thus more reducing.
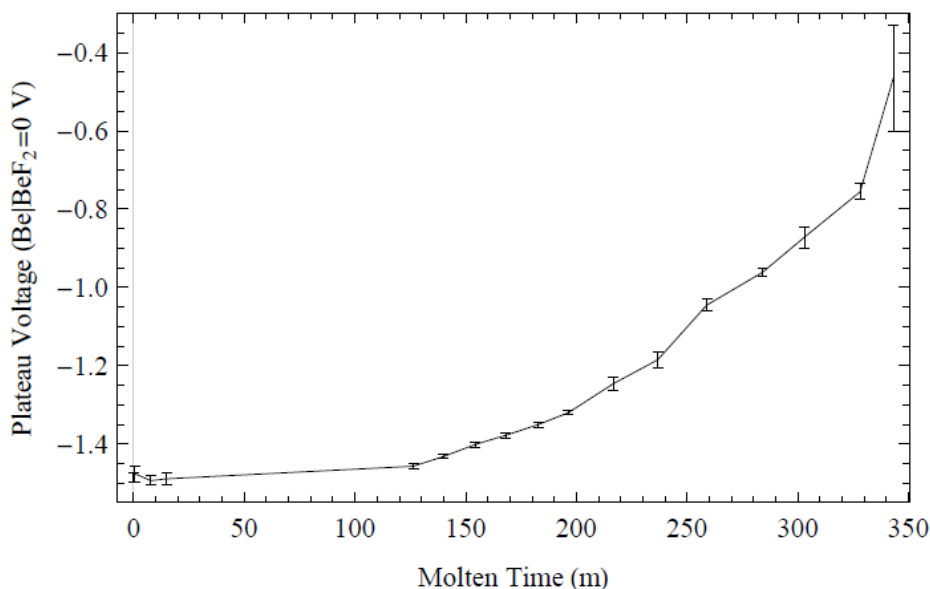
Figure 3.10: Redox voltage measurements taken as reduction from beryllium is occurring.

To investigate the robustness of this method, oxidation experiments were also carried out using purified MSRE lithium-7 enriched FLiBe salt. Nickel-fluoride was added to the salt in increasing amounts and redox potential measurements were taken after the dissolution of nickel-fluoride. The measured voltage should vary linearly with the natural log of the concentration of nickel added according to the Nernst equation. Redox measurements are plotted as a function of ppm nickel fluoride added along with a natural log fit to the data and show this linear trend. According to theory, the slope of the log fit should be

38

Fluoride-salt-cooled High-temperature Reactor (FHR) Annual Report: 2015
MIT, U.C. Berkeley, U. of Wisconsin and U. of New Mexico
For Public Distribution

RT/nF, or 0.033 V for T = 500 °C and n=2. As seen in Figure 3.11, the log fit resulted in an experimental slope of 0.036, or a percent error of 9% from the expected value.
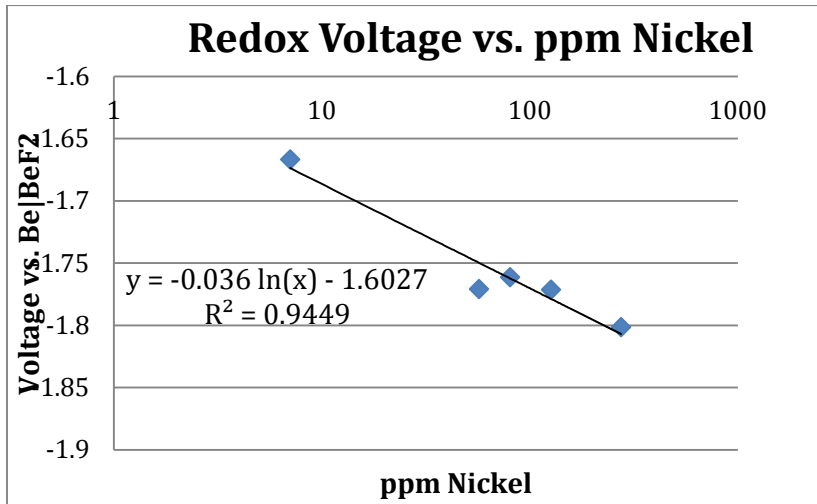

Figure 3.11: Measured redox voltages of purified MSRE salt as a function of nickel-fluoride oxidant concentration.

The design of the probe features two molybdenum electrodes, one cathode and one anode, and one glassy carbon anode. As discussed earlier, in the first phase of the measurement, a voltage is applied using the molybdenum cathode and glassy carbon anode to force the reduction of beryllium fluoride to beryllium metal, which is plated onto the molybdenum cathode. The external voltage is then cut, and the beryllium begins to dissolve back into the salt. As this happens, the beryllium recombining with fluoride ions creates a distinct reference voltage which changes over time. In the second phase, this potential is measured against a separate molybdenum anode. During this measurement, three distinct regions can be observed: a region of higher voltage during which current is applied, a "plateau" region where the distinct voltage of the salt can be deduced, and a relaxation region where beryllium begins to deplete and conditions settle back to equilibrium. The entire probe sits atop a radiant heater and is electrically insulated from heater noise via stainless steel crucible. Figure 3.12 shows a drawing of the heater and probe experimental setup.

Fluoride-salt-cooled High-temperature Reactor (FHR) Annual Report: 2015
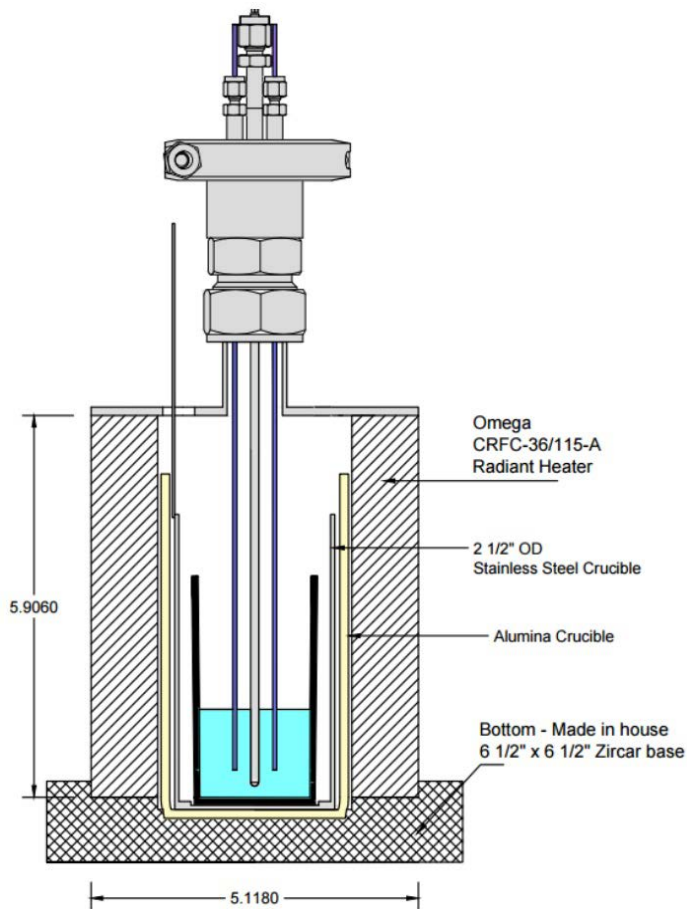MIT, U.C. Berkeley, U. of Wisconsin and U. of New Mexico
For Public Distribution

Figure 3.12: CAD drawing of electrochemical probe set atop heater with electrodes submerged in molten FLiBe. Dimensions are shown in inches.

It is important to note that surface conditions on the molybdenum electrode, in particular, have a significant effect on the redox potential measurement. When a reducing voltage is applied to the cathode, beryllium as well as less stable metal fluoride impurities are plated onto the electrode. Impurities have a much lower concentration than beryllium in typical FLiBe batches, but in repeated runs they can accumulate onto the cathode surface in significant quantities because they do not reform into fluorides as easily as the plated beryllium does. The more noble the impurity, the more likely it is to remain in its metallic state on the electrode upon reduction from its fluoride form in the salt. For example, nickel was observed on a sample of the molybdenum cathode after several redox measurements in UW raw materials FLiBe. A scanning electron microscope (SEM) picture and energy-dispersive X-ray spectroscopy (EDS) image is shown in Figure 3.13 below.

Fluoride-salt-cooled High-temperature Reactor (FHR) Annual Report: 2015
MIT, U.C. Berkeley, U. of Wisconsin and U. of New Mexico
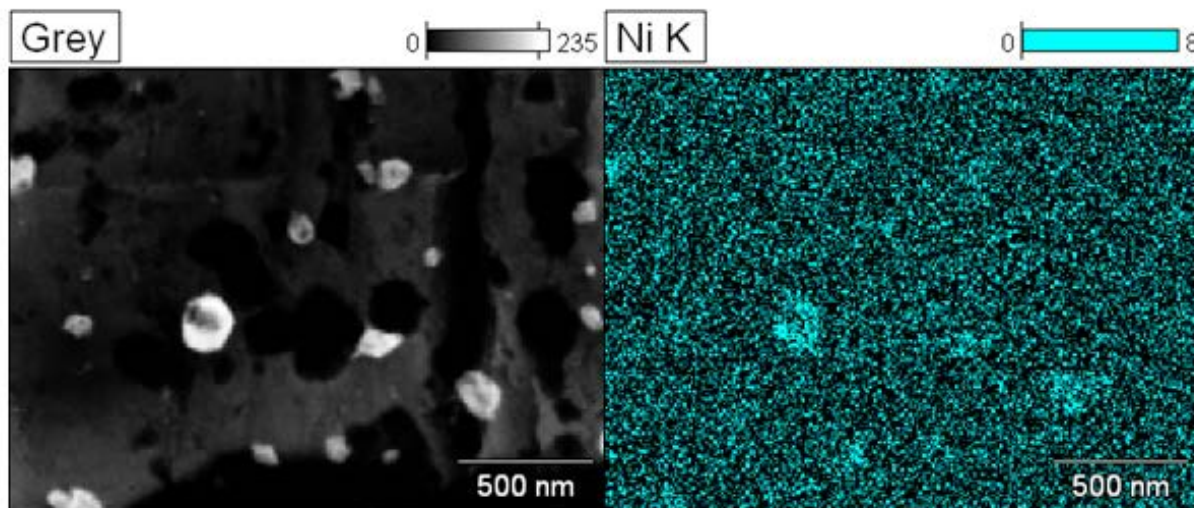For Public Distribution

Figure 3.13: SEM and EDS images of a sample molybdenum cathode after several redox potential measurements. The electrode sample was soaked in DI water for 24 hours to dissolve FLiBe frozen on the surface.

As a direct consequence of the realization that an applied potential on a noble electrode can cause impurity fluorides dissolved in FLiBe to plate out as their reduced metal counterparts, an electro-purification experiment using the same probe was tested and is discussed in the next section.

Electro-purification Experiments:

An electrochemical reduction method was tested as a replacement for reduction by beryllium metal addition as a means of salt chemical control. The probe was modified using a coiled nickel wire as the cathode instead of a straight molybdenum cathode. The Ni coil before and after plating are pictured in Figure 3.14. The Solartron 1287A potentiostat was used to provide time dependent voltages and to measure current. In this experiment, the goal was to apply a voltage to force impurities to plate out of the salt and onto a sacrificial Ni electrode for purification. During electro-purification experiments, a 2-3 V potential is held across the Ni cathode and glassy carbon anode for approximately 10 minutes. Two of the trials successfully reduced the salt by approximately 100mV, however, overall redox potential changes due to electroplating following relaxation were minimal. In the future, a nickel plate electrode geometry will be tested because of the increased surface area and improved current density distribution for even plating coverage.

Fluoride-salt-cooled High-temperature Reactor (FHR) Annual Report: 2015
MIT, U.C. Berkeley, U. of Wisconsin and U. of New Mexico
For Public Distribution

Figure 3.14: Nickel coil before (left) and after (right) electroplating. Plating results in a dark electrode surface likely from salt impurities.

The feasibility of an iridium wire as a replacement for the glassy carbon electrode will also be tested in the future. As shown in Figure 3.15, it has been observed that during electroplating, anodic reactions occurring at the glassy carbon electrode eroded the material and caused carbon to leach into the salt, turning it grey. In order to observe a more significant reduction, longer plating times would be required. Therefore, an iridium anode would improve electoplating performance by replacing this reaction with the production of pure F_2 gas, which would simply bubble out of the salt. In addition, the increased nobility of iridium could also yield more accurate redox potential results for basic measurements.

Figure 3.15: Initial MSRE FLiBe (left) and a salt ingot following an electro-purification run (right). The bottom of the ingot is facing upwards in the bottom right photo. The green tint in the initial salt is likely caused by dissolved metal fluorides. Reduction of these metals during plating also results in the dissolution of the carbon anode.

Preparation of reduced UW FLiBe consisted of 0.5mg Be metal additions to 50g batches of FLiBe. The FLiBe salts to be used in future corrosion studies will be purified in unreduced and Be-reduced states

Fluoride-salt-cooled High-temperature Reactor (FHR) Annual Report: 2015
MIT, U.C. Berkeley, U. of Wisconsin and U. of New Mexico
For Public Distribution

which constitutes a difference of 282 mV in redox potential. These salts have already been prepared and photograph of the salts is shown in Figure 3.16.
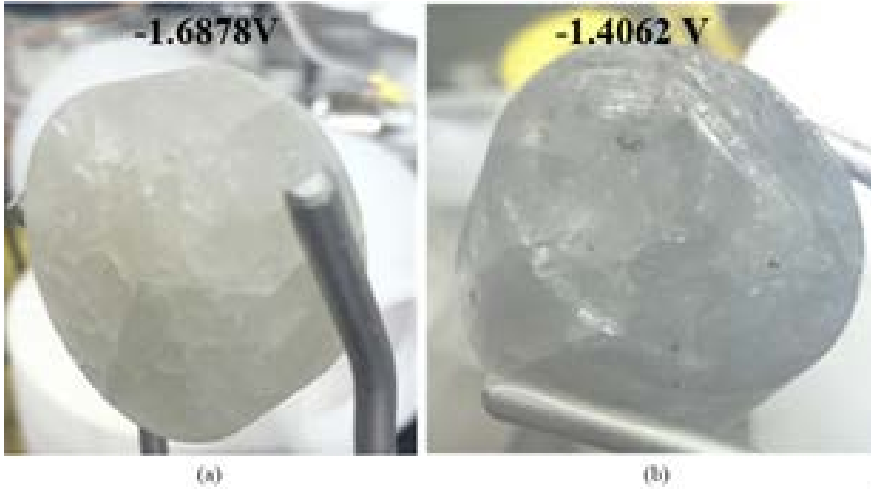

Figure 3.16: Unreduced (a) and reduced (b) variants of UW raw-materials FLiBe. Salt was reduced by adding a 0.5mg Be metal to four 50g melts and allowing to dissolve for at least 24 hrs. A total of 200g of FLiBe has been Be reduced for corrosion testing.

The results of redox potential testing of UW FLiBe before (Figure 3.17) and after (Figure 3.18) Be reduction are shown in Table 3.3.
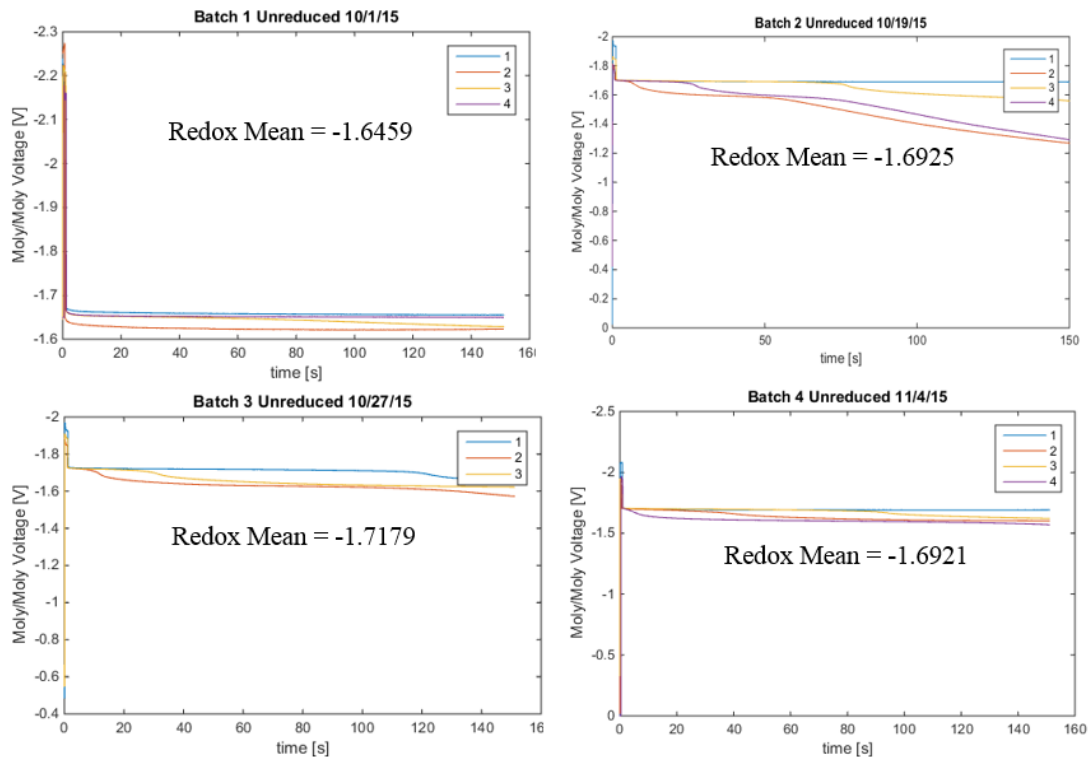
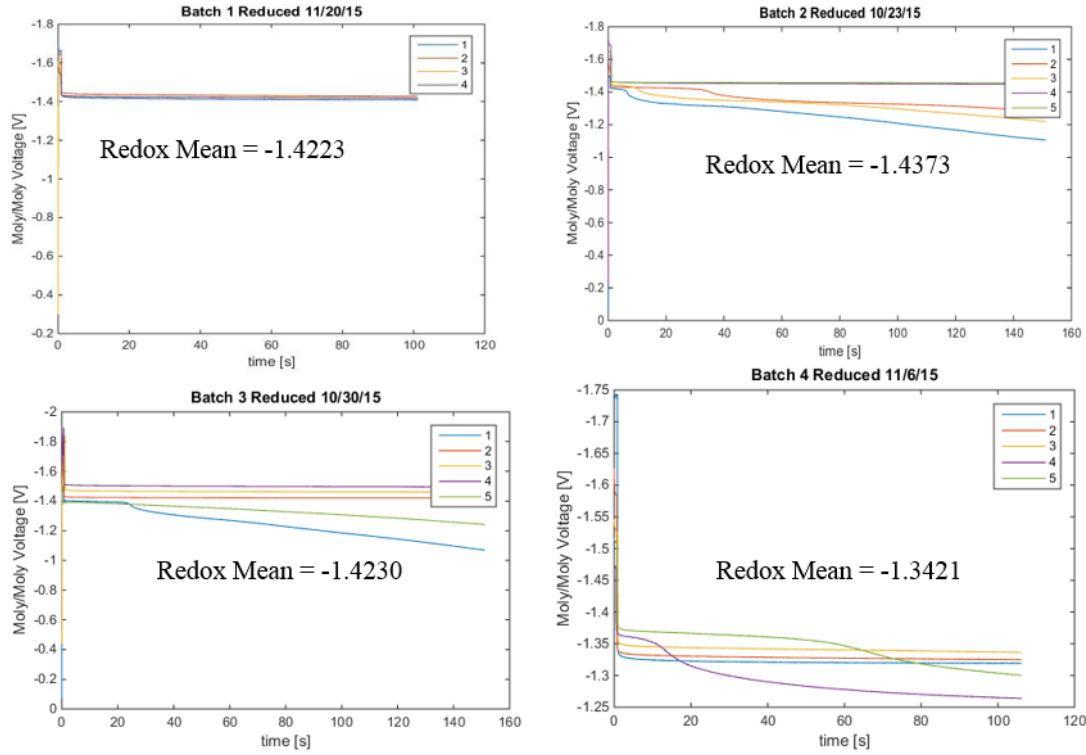Figure 3.17: Redox potential measurements of 4 batches of UW-made FLiBe prior to Be reduction.

Fluoride-salt-cooled High-temperature Reactor (FHR) Annual Report: 2015
MIT, U.C. Berkeley, U. of Wisconsin and U. of New Mexico
For Public Distribution

Figure 3.18: Redox potential measurements of 4 batches of UW-made FLiBe after to Be reduction and 24 hr dissolution at 600ºC.

Table 3.3: Redox potential results of batch-wise reduction of UW-made FLiBe. Average redox potentials shown below.

Batch Number	Batch 1			Batch 2			Batch 3			Batch 4	
	Unreduced	Reduced		Unreduced	Reduced		Unreduced	Reduced		Unreduced	Reduced
Mean Redox Potential [V]	-1.6459	-1.4223		-1.6925	-1.4373		-1.7179	-1.4230		-1.6921	-1.3421
Combined Mean Redox Potential [V]	Unreduced = -1.6871 V						Reduced = -1.4062 V				

Fluoride-salt-cooled High-temperature Reactor (FHR) Annual Report: 2015
MIT, U.C. Berkeley, U. of Wisconsin and U. of New Mexico
For Public Distribution

Oxidation of FLiBe with Impurity Fluorides:

Following the demonstration of a repeatable dynamic reference electrode method for measurement of the redox potential of FLiBe salt, the next step was to show the robustness of this method by conducting oxidation experiments. Three separate oxidation experiments were conducted at 500°C using the common corrosion impurities nickel, iron and chromium fluorides starting in a thoroughly purified FLiBe salt batch donated by MSRE. In each experiment the redox potential of four additions of a metal impurity were measured. In Figure 3.19, the voltage is observed to vary linearly with the natural log of the concentration of the metal impurity added as predicted by the Nernst equation.
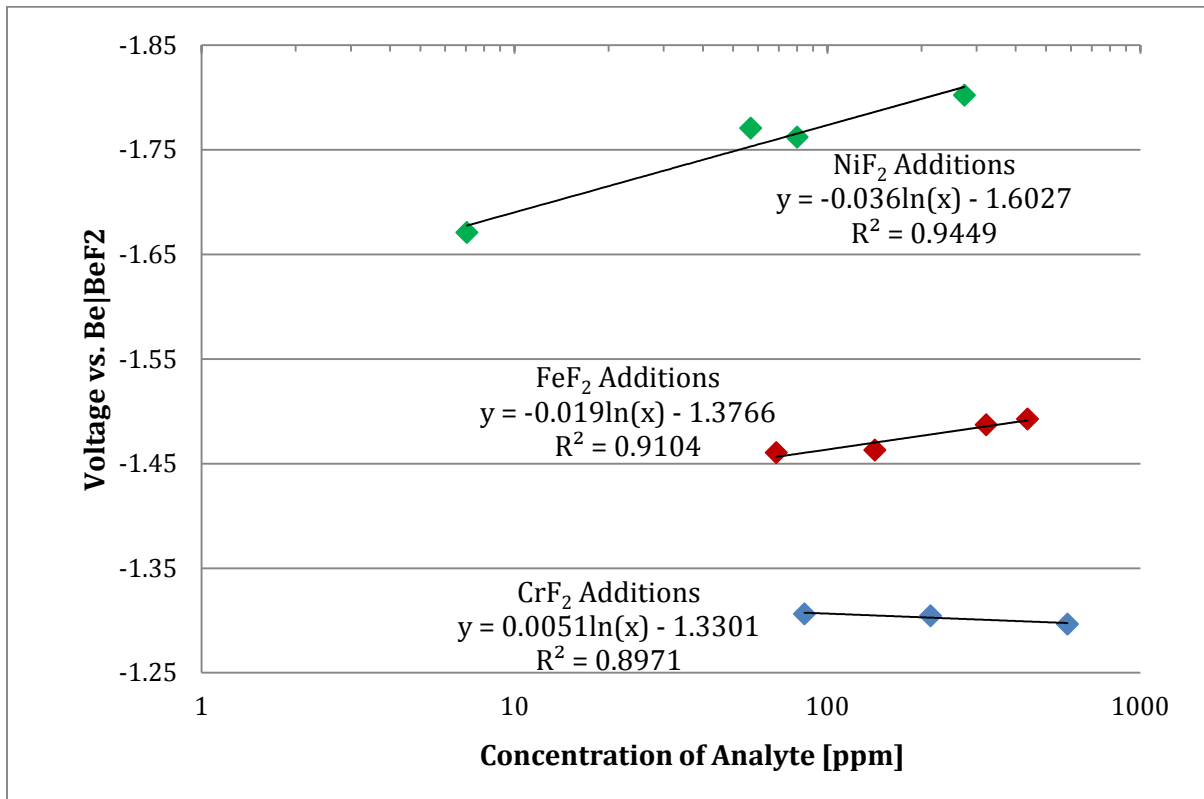

Figure 3.19: Combined results from the nickel, iron, and chromium fluoride additions to purified MSRE FLiBe.

While the data shows the expected relative relationships between the added metal fluorides, not all data conformed to the theoretical trends. As predicted, nickel fluoride caused the most significant oxidation because it is the least stable of the three metal fluorides. Iron presented a mild oxidizing behavior. While it was expected that chromium would be the most stable fluoride and have the least effect on the redox potential, chromium produced a result inconsistent with theory by reducing the salt rather than oxidizing it. Several factors contributed to the variation in the data plotted above including: varying initial salt redox potential, inconsistent beryllium dissolution, and difficulty measuring plateau signals for chromium addition. In future work, further experimentation with these three common corrosion impurities using the identical baseline salt will be conducted in order to better predict their oxidizing effects using the dynamic reference electrode method.

Fluoride-salt-cooled High-temperature Reactor (FHR) Annual Report: 2015
MIT, U.C. Berkeley, U. of Wisconsin and U. of New Mexico
For Public Distribution

Task 2.1(c) - Out-of-Reactor Materials Corrosion Testing:

Corrosion of 316 Stainless Steel and Hastelloy N:

Analysis of samples of two candidate structural materials for FHRs, namely 316 stainless steel and Hastelloy N tested up to 3000 hours and 1000 hours, respectively in [7]Li-enriched FLiBe is progressing satisfactorily. 316 stainless steel performed well in FLiBe in when tested in 316SS crucible with a predicted attack depth of 17.1 µm per year. In graphite crucibles, the corrosion was noted to be accelerated with a predicted attack depth of 316SS of 31.2 µm per year. Corrosion in both 316SS and graphite occurred by the dissolution of chromium from the stainless steel into the salt which led to the depletion of chromium predominantly along the grain boundaries the material. Carburization in the subsurface of 316 stainless steel occurred during corrosion tests in graphite crucibles. Cr_7C_3 precipitate particles were observed throughout the depth of the corrosion layer. The corrosion results showed that if the FLiBe is very pure or slightly reducing as desired, the corrosion rate of 316 stainless steel may be acceptable for building the reactor vessel and other components in FHRs.

Hastelloy N showed outstanding corrosion resistance in FLiBe when tested in a pure Ni crucible. Similar to the corrosion of 316 stainless steel in a graphite crucible, the graphite accelerates the corrosion of Hastelloy N in FLiBe and also carburization occurred in the subsurface of Hastelloy N during a 700ºC/1000 hour corrosion test. Results also indicate that while graphite accelerates the corrosion in the short-term, this may not be true over a period of years. Further study is needed on the effects of graphite on long term corrosion and service life of structural materials for FHRs.

The corrosion of structural alloys in FLibe is mainly controlled by diffusion of Cr in the grains and grain boundaries. Based on the experimental corrosion results of 316 stainless steel in 316 stainless steel crucible at 700ºC for 1000, 2000 and 3000 hours, a preliminary model was developed to predict the Cr concentration depletion after a specified exposure time in FLiBe thus predicting the corrosion attack depth after long term corrosion. As shown below, after corrosion time *t*, the Cr concentration $C(x, t)$ can be expressed as $C(x,t) = \int_0^x dC(x,t) = \int_0^x \frac{C_0}{\sqrt{\pi D t}} s e^{-\frac{u^2}{4Dt}} du = C_0 erf(\frac{x}{2\sqrt{Dt}})$ where D is the effective diffusion coefficient of Cr in 316SS and the value of D can be experimentally determined based on weight loss ($\Delta M = 2AC_0\sqrt{\frac{Dt}{\pi}}$), where A is the total surface area, C_0 is the initial Cr concentration, *t* is the corrosion test time). Figure 3.20 shows the Cr concentration profile after a specified corrosion time *t*. Since the diffusion coefficient is directly calculated from the weight changes, this model would be applicable specifically to corrosion in FLiBe. Figure 3.21 shows a comparison between the model and experimentally derived data for Cr depletion due to corrosion of 316 stainless steel and Hastelloy-N
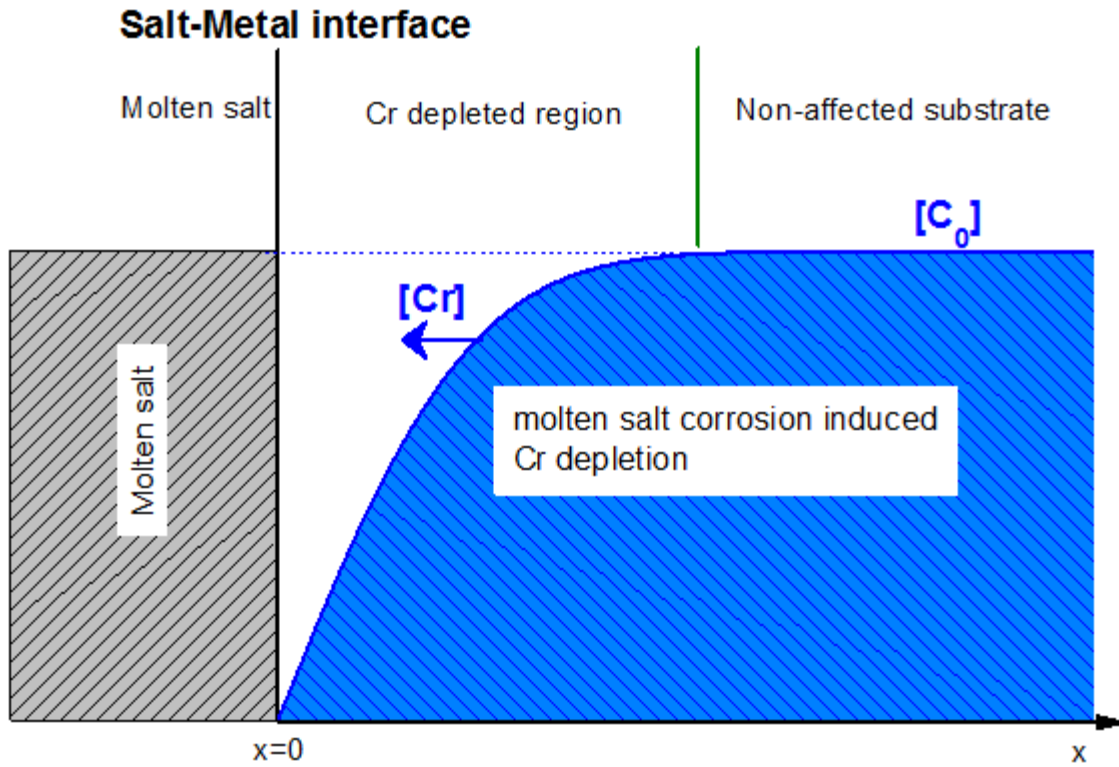
Fluoride-salt-cooled High-temperature Reactor (FHR) Annual Report: 2015
MIT, U.C. Berkeley, U. of Wisconsin and U. of New Mexico
For Public Distribution

Figure 3.20: Schematic illustration of Cr depletion model in alloy corrosion in molten fluoride salts.

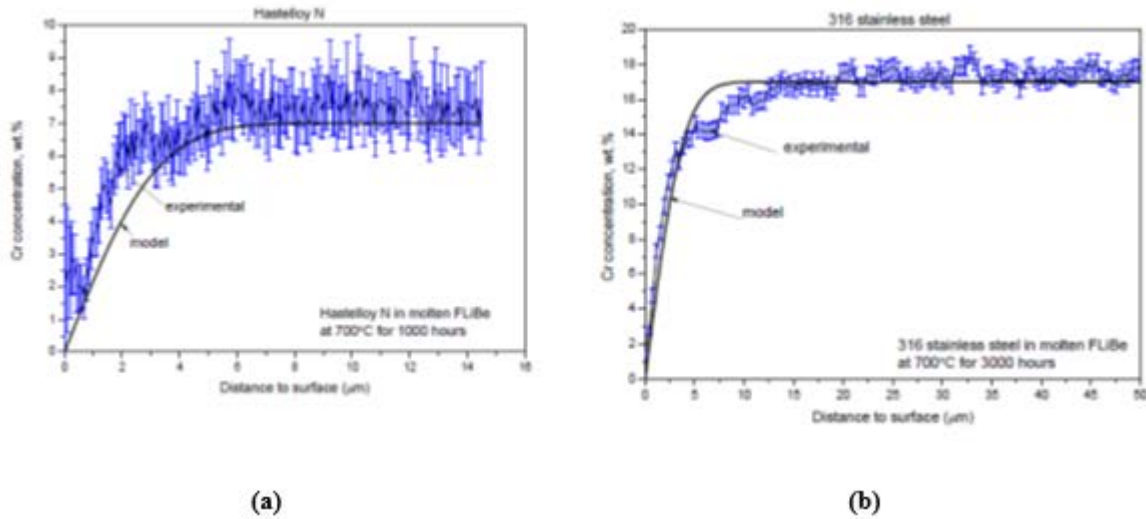(a)   (b)

Figure 3.21: Comparison of experimental data and model for Cr depletion due to corrosion in FLiBe at 700ºC after 1000 hours exposure: (a) Hastelloy N and (b) 316 stainless steel.

Corrosion of Binary Ni-Cr alloys:

In addition to the extensive studies that we have performed on FHR specific structural and fuel materials such as 316 stainless steel, Hastelloy-N, TRISO particles, and SiC-SiC composites, we have also conducted research on Ni-Cr binary alloys to gain a fundamental understanding of corrosion in

47

Fluoride-salt-cooled High-temperature Reactor (FHR) Annual Report: 2015
MIT, U.C. Berkeley, U. of Wisconsin and U. of New Mexico
For Public Distribution

molten FLiBe salt at 700ºC. Two binary alloys, Ni-5%Cr and Ni-20%Cr, were tested in FLiBe at 700ºC for up to 1000 hours. The weight loss of the two alloys after corrosion is shown in Figure 322. The weight loss results from the Cr depletion from alloys and then dissolution into molten salt in form of chromium fluoride.
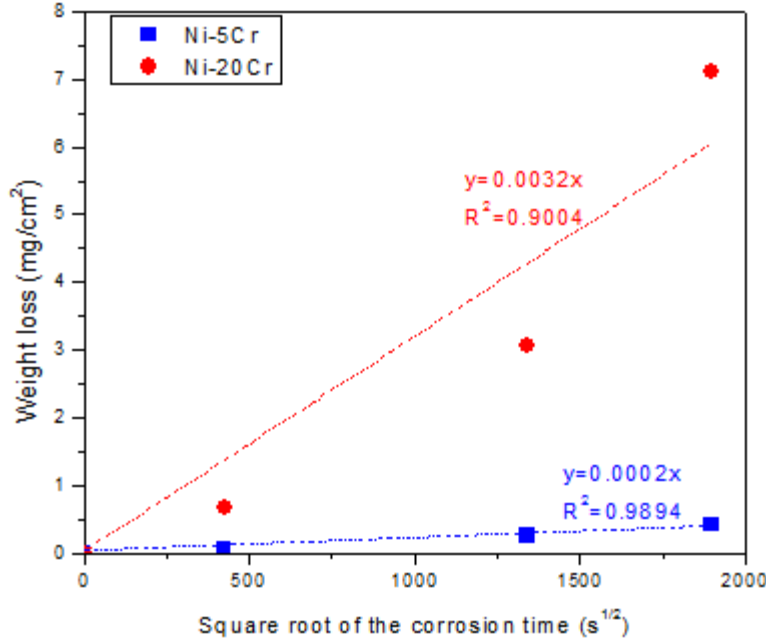

Figure 322: Weight loss as a function of square root of the corrosion time for Ni-5%Cr (blue) and Ni-20%Cr (red) alloys that were exposed to molten FLiBe at 700°C for 50, 500 and 1000 hours. Linear trend lines (dashed lines) and R-squared values are included for both alloys.

Figure 3.23 shows the surface morphology of samples tested in molten FLiBe for varying durations. The intergranular corrosion attack was observed on the surface of all samples, and the attack becomes deeper and wider with increasing of exposure time. This is indicative of preferential Cr leaching along grain boundaries in the near-surface region. From these corrosion images, it is obvious that the fraction of grain boundaries per unit area on the surface of Ni-20%Cr is larger than that on Ni-5%Cr, which also contributes to the overall Cr depletion rate. Using ImageJ, the area fraction of attacked grain boundaries is 3.85% and 28.42% for Ni-5%Cr and Ni-20%Cr, respectively after 1000 hours corrosion in molten FLiBe. In general, the density of grain boundaries is inversely proportional to grain size for polycrystalline materials. Therefore, the Ni-20%Cr with a relatively smaller grain size has higher fraction of grain boundaries per unit area.

Fluoride-salt-cooled High-temperature Reactor (FHR) Annual Report: 2015
MIT, U.C. Berkeley, U. of Wisconsin and U. of New Mexico
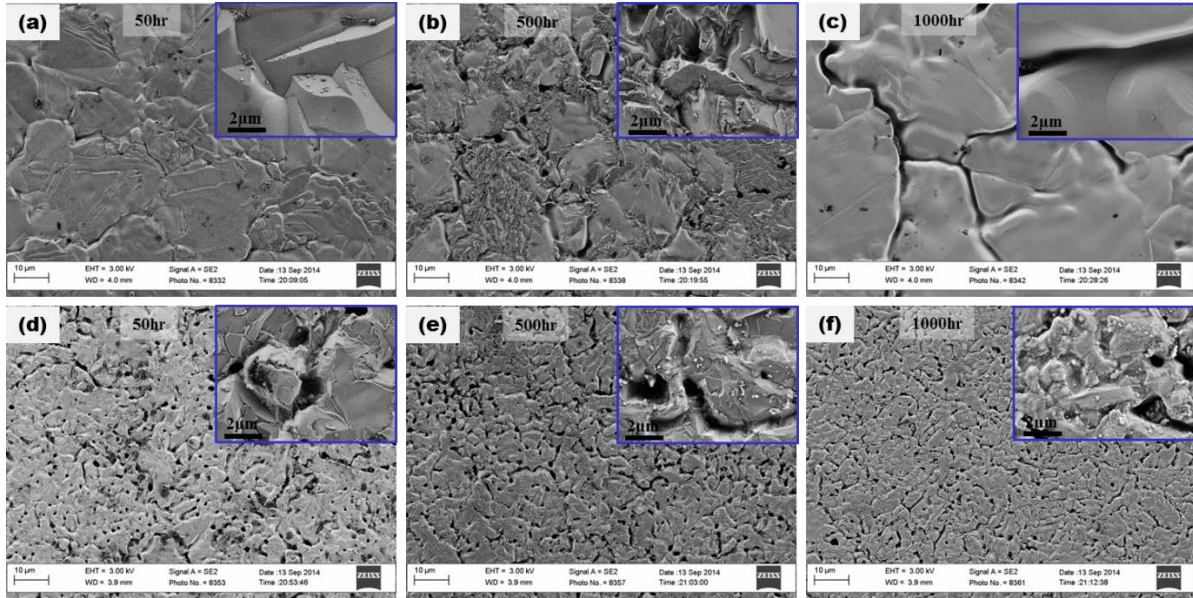For Public Distribution

Figure 3.23: Surface SEM images of (a, b, c) Ni-5%Cr and (d, e, f) Ni-20%Cr tested in molten FLiBe for 50, 500 and 1000 hours (from left to right) respectively. Inset on upper right corner shows the morphology of grain boundaries.

The cross-section of the near-surface layer of post-corrosion Ni-5%Cr and Ni-20%Cr model alloys is shown in Figure 3.24. The corrosion surface (denoted with red arrow in SEM images) was protected by a layer of electroplated Cu prior to polishing. The voids with a couple of microns in diameter randomly distribute within the near-surface layer of Ni-20%Cr alloys, but they are not observable in post-corrosion Ni-5%Cr alloy. Furthermore, the void size in Ni-20%Cr slightly increased with increasing corrosion time.
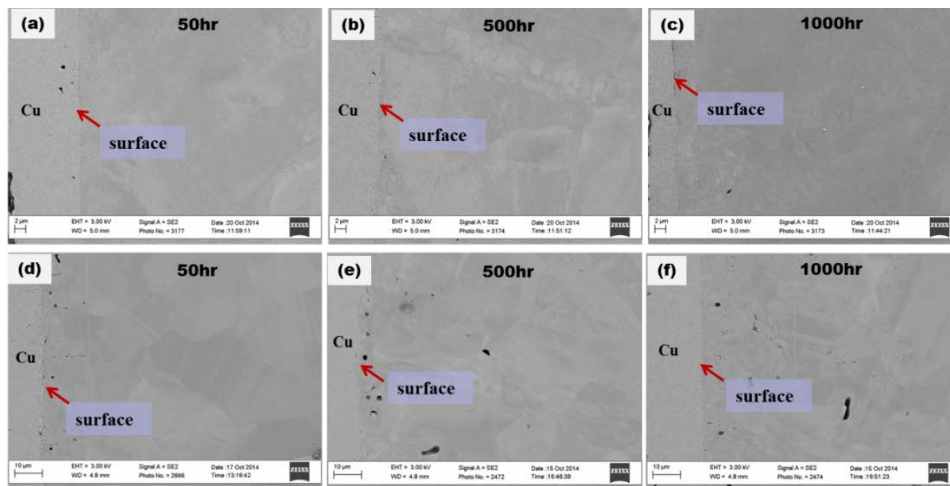

Figure 3.24: Cross-sectional SEM images of (a, b, c) Ni-5%Cr and (d, e, f) Ni-20%Cr exposed to molten FLiBe for 50, 500 and 1000 hours. A layer of Cu was electroplated on all samples surface for edge protection during polishing. Arrow denotes corrosion surface.

Figures Figure 3.25 and Figure 3.26 show the elemental distributions of main constituents Ni and Cr in the cross-section of the near-surface region in FLiBe-exposed Ni-5%Cr and Ni-20%Cr for 50, 500 and 1000 hours. The relatively low concentration of Cr was observed in the near-surface region for all corrosion samples. Unlike the corrosion surface where preferential grain boundary attack was observed, the Cr depletion is also observed in the grains. It is likely that the Cr depleted grain boundaries are too

49

Fluoride-salt-cooled High-temperature Reactor (FHR) Annual Report: 2015
MIT, U.C. Berkeley, U. of Wisconsin and U. of New Mexico
For Public Distribution

thin to be identified by EDS imaging technique. This is consistent with above cross-sectional observation. Additionally, the Cr depletion is not uniform in same depth. To evaluate corrosion attack depth, the maximum Cr depletion distance was measured and labeled in EDS Cr mappings. With the increasing of corrosion time, from 50 hours to 1000 hours, the maximum Cr depletion distance increases from 5.4μm to 21.7μm and from 18.2μm to 140.8μm for Ni-5%Cr and Ni-20%Cr respectively.
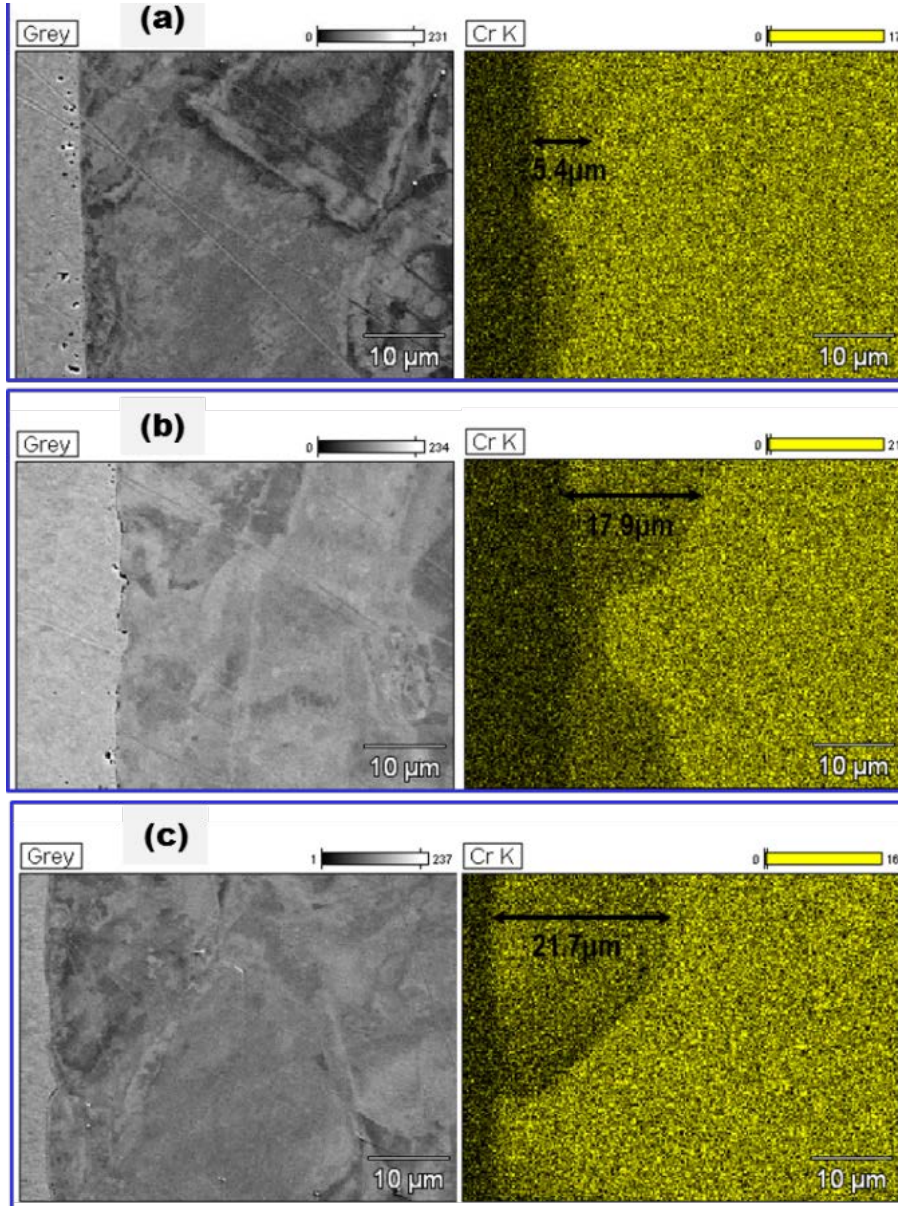

Figure 3.25: EDS mapping of Cr elemental distribution in the near surface layer of the Ni-5%Cr samples tested in molten FLiBe for (a) 50 hours, (b) 500 hours and (c) 1000 hours.

The Cr depletion in Ni-5%Cr only occurred in certain grains adjacent to the surface. Actually, only partial Cr depletion occurred within those grains. In Ni-20%Cr, the Cr depletion occurred in a wide range crossing multiple connected grains. This is because the grain size in Ni-5Cr (~100μm-200μm) is much larger than Ni-20Cr (~10μm-30μm), even larger than the maximum Cr depletion distance. The reason why Cr depletion preferentially occurred in certain grains, not in all the grains to the same depth, will be further analyzed using EBSD technique.

Fluoride-salt-cooled High-temperature Reactor (FHR) Annual Report: 2015
MIT, U.C. Berkeley, U. of Wisconsin and U. of New Mexico
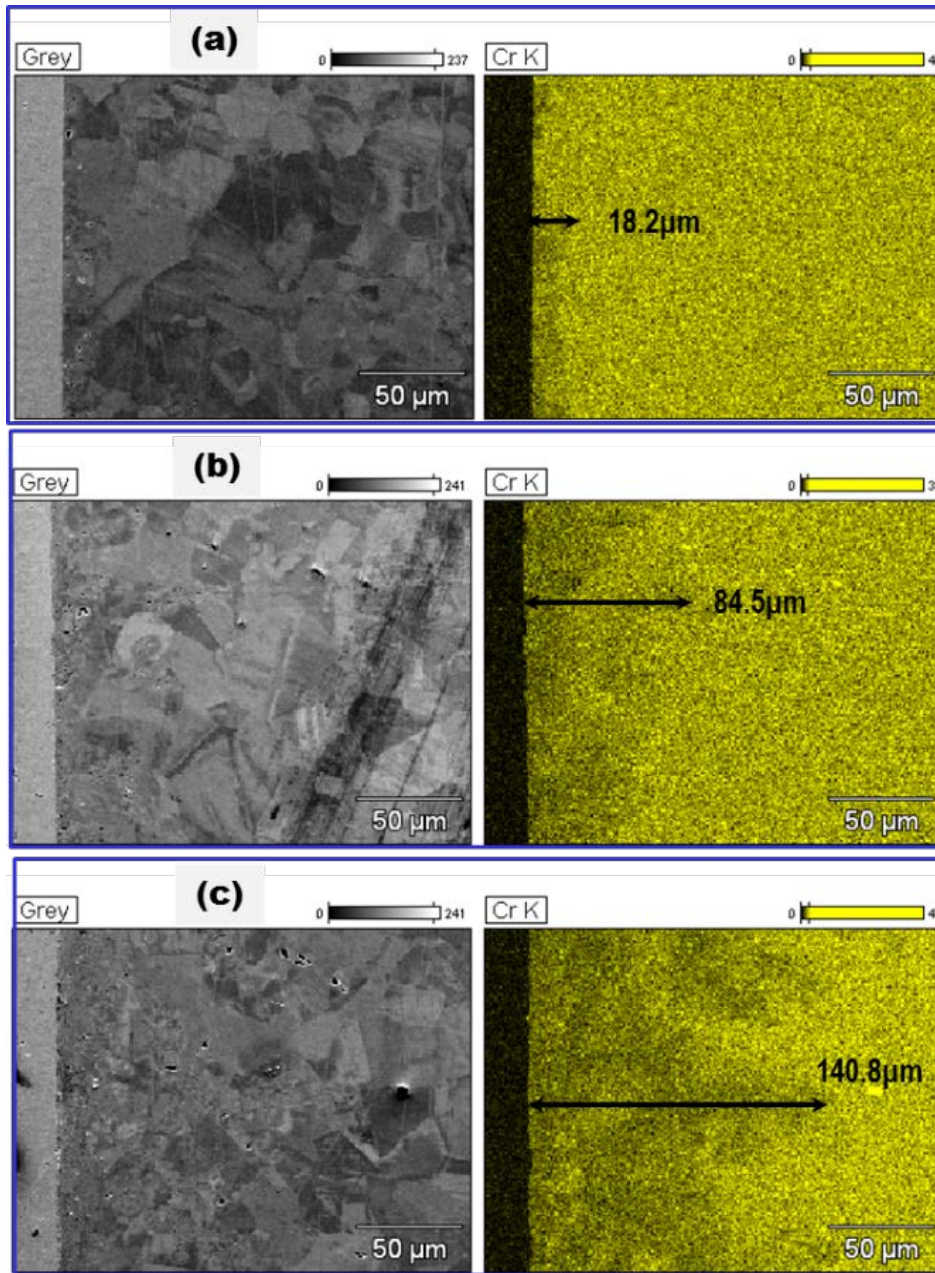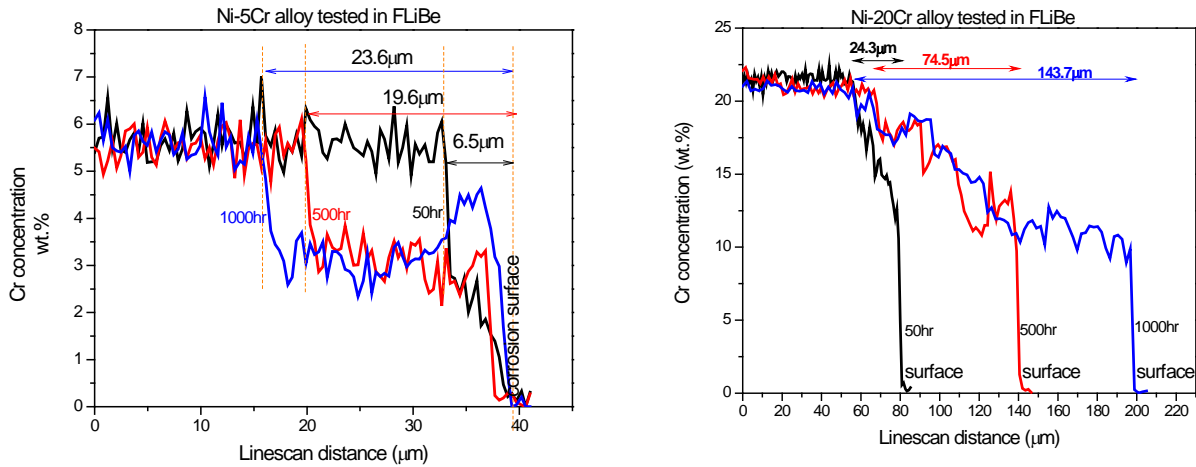For Public Distribution

Figure 3.26: EDS mapping of Cr, Ni and Cu elemental distribution in the near surface layer of the Ni-20%Cr samples tested in molten FLiBe for (a) 50 hours, (b) 500 hours and (c) 1000 hours.

Fluoride-salt-cooled High-temperature Reactor (FHR) Annual Report: 2015
MIT, U.C. Berkeley, U. of Wisconsin and U. of New Mexico
For Public Distribution

(a)   (b)

Figure 3.27: Cr concentration profiles (EDS linescan after exposure to molten FLiBe salt at 700ºC for 50, 500 and 1000 hours (a) Ni-5%Cr and (b) Ni-20%Ni.

Figure 3.27 shows quantitative results of Cr concentration profiles in post-corrosion Ni-Cr alloys based on EDS linescan. Each linescan path crosses the maximum Cr depletion region that is referred to the observation of EDS Cr mappings. The linescan direction is from the unaffected substrate to corrosion surface. From these Cr concentration profiles, the Cr depletion distance is 6.5µm, 19.6µm, and 23.6µm for Ni-5%Cr, and 24.3µm, 74.5µm, and 143.7µm for Ni-20Cr, exposed to molten FLiBe for 50 hours, 500 hours and 1000 hours respectively. From these Cr concentration profiles, it was observed that the Cr concentration drops down dramatically from the unaffected substrate (no Cr depletion) to the Cr depleted region and then maintains at about half of initial Cr concentration in Ni-5%Cr, but gradually decreases in Ni-20% Cr.

Effects of Grain boundaries on Corrosion:

Generally, less corrosion occurred in CSL Σ3 grain boundaries in Ni-Cr alloys. Similar phenomenon was observed in the corrosion of 316 stainless steel in FLiBe. Figure 3.28 shows the EBSD of 316 stainless steel tested in FLiBe at 700ºC for 1000hrs. It was found that Cr depleted along random high angel grain boundaries (15-180º, blue lines) but no Cr depleted along CSL Σ3 grain boundary. Because of substantial Cr depletion, α phase (NiFe$_x$) developed in the subsurface area, which extended to ~6µm in depth.

Fluoride-salt-cooled High-temperature Reactor (FHR) Annual Report: 2015
MIT, U.C. Berkeley, U. of Wisconsin and U. of New Mexico
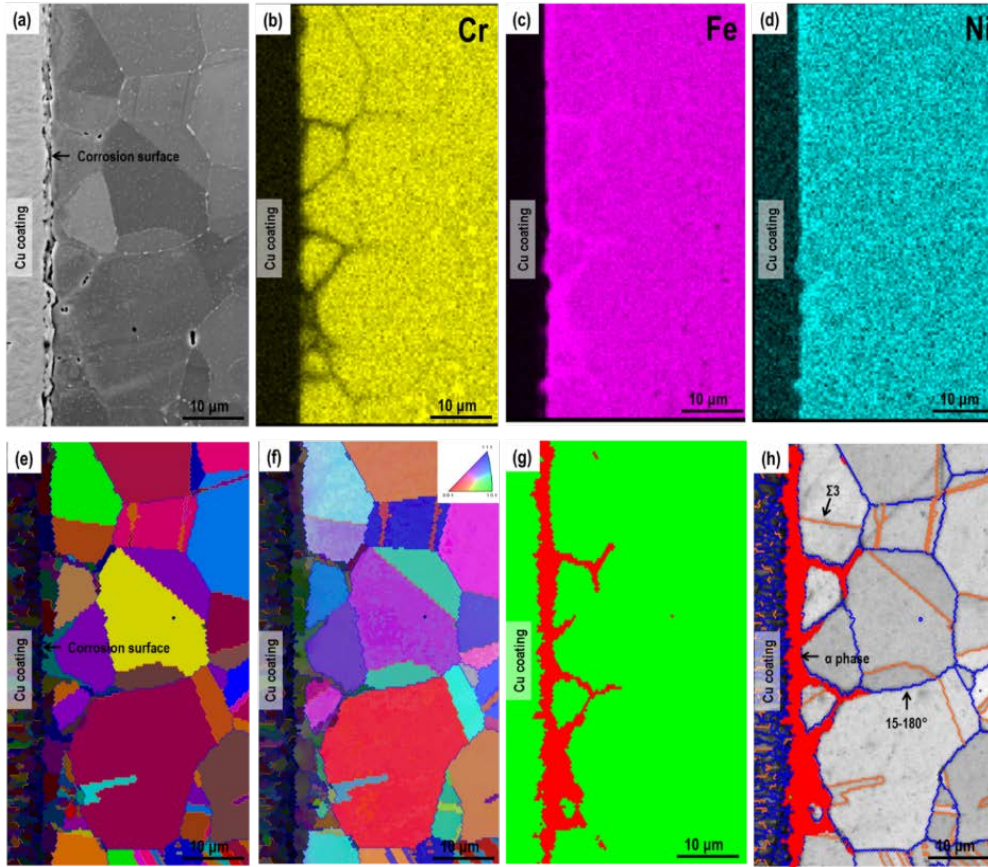For Public Distribution

Figure 3.28: EBSD of 316SS tested in FLiBe at 700°C for 1000 hours.

Proposed Future Corrosion Tests:

The currently planned static FLiBe corrosion test will focus on testing the following effects in two identical graphite crucibles:

1) Redox potential on corrosion in FLiBe

2) Presence of graphite on corrosion in FLiBe

Part of the FLiBe batch that was produced from raw materials and purified with HF/H_2 sparge will be used in one crucible of the planned corrosion test. This salt has a well-characterized redox potential of -1.706V, and will serve as the baseline salt for comparison. The other crucible (identical sample arrangement) will contain a filtered, Be-reduced FLiBe that will be reduced by adding stoichiometrically equivalent Be(s) to replace impurity fluorides estimated from NAA. The goal of the experiment is to compare corrosion behavior of new and conventional samples as a function of redox potential.

Conventional materials tested previously include 316 Stainless Steel, CVD SiC, and nuclear graphite. New materials for testing in FLiBe include a Mo-Hf-C alloy sourced from H.C. Starck, a SiC-coated SiC-SiC composite sourced from General Atomics, and a W/ZrC Cermet sourced from Georgia Tech. The new materials are listed in Table 3.4.

Fluoride-salt-cooled High-temperature Reactor (FHR) Annual Report: 2015
MIT, U.C. Berkeley, U. of Wisconsin and U. of New Mexico
For Public Distribution

Table 3.4: Potential FHR-relevant materials for next phase of static corrosion testing in FLiBe.

Material	Location	Supplier	Attractive Properties and Motivation	Compatibility with FLiBe
SiC coated SiC$_m$-SiC$_f$ Composite	Fuel cladding	General Atomics – Bob Schleicher	Improved fuel cycle and lower fuel costs for FHRs using SiC clad pellet fuel over TRISO fuel. High temperature irradiation resistance and strength.	CVD SiC shows good compatibility, but composites depend on manufacturing process.
Nuclear Graphite	Core structure	Available	High temperature stability and strength.	Chemically inert to FLiBe, but maybe issues with high Be content salt.
Mo-Hf-C alloy	Control rod	H.C. Starck – Chip Urban	High temperature stability and strength.	Unknown
ZrC/W Cermet	Valves and sensors	Georgia Tech – Ken Sandhage	Good thermal shock resistance. Easy to form into large complicated shapes.	Unknown

Characterization of the samples before and after exposure to FLiBe will include optical microscopy, SEM/EDS, surface profilometry, and XRD. All samples will be flat polished to 1200 grit using metallographic SiC polishing papers prior to all characterization and corrosion testing. Sample preparation of the above samples is being carried out at present.

Table 3.5 shows the experimental setup of the planned corrosion test and Fig. 3.29 shows the experimental design for the corrosion test.

Table 3.5: Experimental setup of next phase of static corrosion testing in FLiBe.

Crucible 1: -1.68V UW FLiBe	Crucible 2: -1.40V UW FLiBe

Hole 1: SiC materials. 2x General Atomics SiC-SiC, 1x CoorsTek bonded SiC-SiC, 1x CVD SiC for reference.

Hole 2: C materials. 1x matrix graphite sample, 1x IG-110 sample, 1x C-C composite.

Hole 3: Mo-Hf-C. 3x Mo-Hf-C alloy samples with Mo wire suspension, no liner.

Hole 4: W-Zr-C. 3x W-Zr-C Cermet samples with W wire suspension, no liner.

Hole 5: 316 SS. 3x 316 samples with SS wire suspension, no liner.

Hole 6: 316 SS. 3x 316 samples with SS wire suspension, with 316 SS liner.

*Avoid dissimilar materials in contact in FLiBe wherever possible

Fluoride-salt-cooled High-temperature Reactor (FHR) Annual Report: 2015
MIT, U.C. Berkeley, U. of Wisconsin and U. of New Mexico
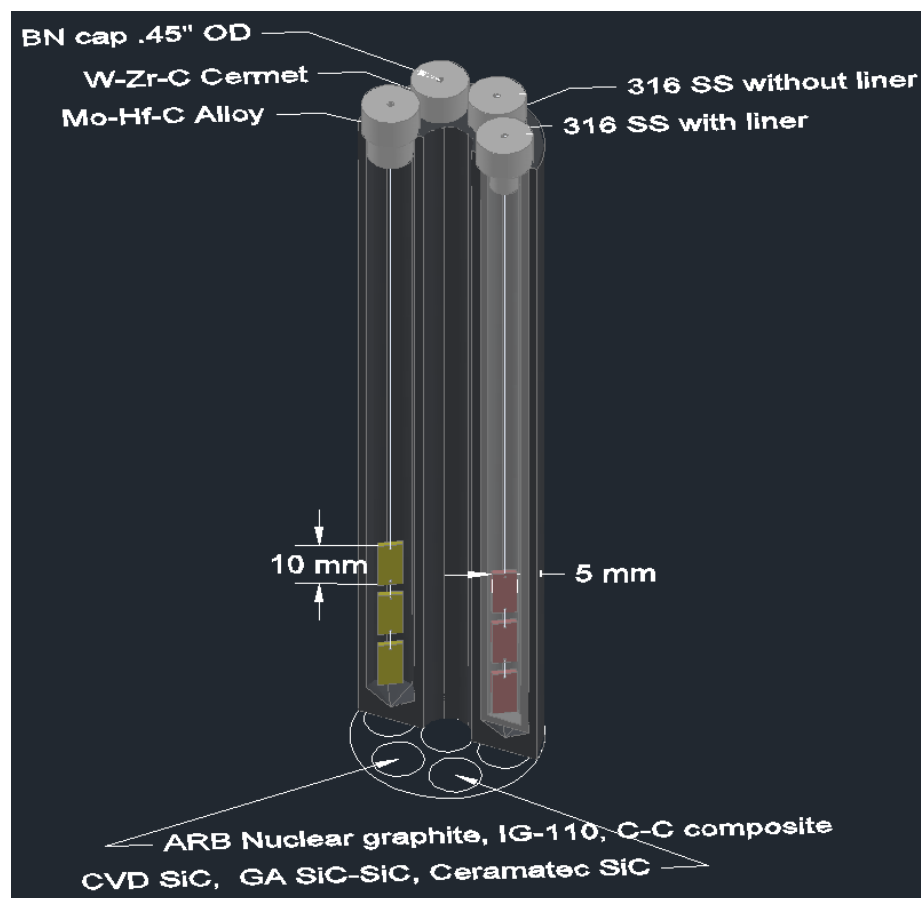For Public Distribution

Figure 3.29: CAD drawing of corrosion crucible and sample locations. Metallic samples will be suspended with wire, whereas ceramic samples will be placed in the crucible freely. A total of about 150g of FLiBe per crucible is required.

Once all samples are fully prepared, corrosion crucibles will be filled with respective salts and covered with graphite plugs. The temperature of FLiBe for the corrosion test will be 600^{0}C, with an exposure time of 1000 or 2000 hours.

Procedure for future corrosion test:

Crucible filling will be done inside of an atmosphere controlled glovebox with salt in a solid form. This will be accomplished by first carefully crushing the salt in a steel mortar and pestle to obtain a granulated consistency. Then, salt will be deposited into each .405" diameter hole with samples either hung on wires or resting in the bottom of the crucible. Once solid salt is filled to the top of each hole in the crucible, it will be moved into a heater to melt the salt. It is expected that the volume of the liquid salt will be much less than solid, so a loss of salt height is expected. In order to combat this issue, samples will be hung near the bottom of the crucible so that it is guaranteed that they will be submerged in the salt. In the case that samples are not fully submerged following the melting step, more granulated salt will be carefully added to the hot crucibles to raise the salt level. It is anticipated that this step will require dexterous handling in a glovebox.

Once the salt is filled and samples submerged to satisfaction, the heaters will be ramped up to the desired temperature of 600ºC and monitored for 1000 hours. During this time, additional samples will be

Fluoride-salt-cooled High-temperature Reactor (FHR) Annual Report: 2015
MIT, U.C. Berkeley, U. of Wisconsin and U. of New Mexico
For Public Distribution

characterized in optical microscopy as well as electron microscopy to observe the surface microstructure and topography, chemical composition, and overall appearance. In addition, all samples will be carefully weighed prior to adding to crucibles in order to monitor weight changes due to corrosion mechanisms. Additionally, surface hardness measurements will be take of all samples before and after corrosion to observe changes in mechanical properties in the structural material.

Pre-corrosion characterization of the materials in the test have begun, however multiple hurdles had to be crossed. First and foremost was the cutting of holes in composite and refractory metal samples for hanging in the crucible. Since W-Zr-C cermet samples are too hard to drill with conventional bits, EDM or diamond drill bits are required to cut holes into the samples, which caused a delay in preparation. Also, the W-Zr-C samples were found to be too porous for proper corrosion testing, so a new set of fully dense samples had to be delivered. Lastly, the Mo-Hf-C samples suffer a similar fate due to the fact that the samples contain carbides that increase the hardness substantially. These materials will need to be polished with diamond grinding pads to a 1200 grit finish to obtain a surface that is satisfactory for cross sectional analysis and accurate corrosion rate measurement.

Task 2.1 (d) - FliBe Salt Loop:

To order to advance salt studies to more realistic reactor conditions, it is important to expose the samples to corrosion within a dynamic flow system. Static corrosion testing has two severe limitations: firstly, the corrosion rate risks becoming limited by the rate of diffusion for the corrosion species through the salt, secondly, the static corrosion tests have no method of chemistry control during the test, and incorporate such a small volumes of salt that the post-test chemistry can differ markedly from the chemistry. To abate these concerns, a natural circulation flow loop is under design to expose two sets of small removable samples to a continually flowing system for extended periods of time, under carefully controlled chemical conditions. The design of the loop will allow it to test a wide variety of sample materials under a variety of flow conditions at two different temperatures, with one set of samples held in the hot leg riser and one set in the cold leg.

The current loop design, shown in Figure 3.30, is built of type 316 stainless steel tubing with an inner-diameter of 0.76 inches. The tubing forms a parallelogram shape that is approximately 1.5 meters wide and 2 meters tall, with a 6 inch NPS flow through expansion tank on the top of the riser, and a 3 inch outer-diameter expansion tank on top of the down-comer. The lower cross and riser legs are heated by 4 sets of clamshell radiant heaters, each with a 24-inch heated length, capable of a combined output of 4 kW, which should drive flow velocities up to 5 cm/s. Both of the expansion tanks provide access ports to the salt, allowing racks of samples to be inserted into the vertical hot and cold legs of the loop, as well as porviding access to the bulk salt for salt monitoring instruments. The corrosion environment will be characterized by redox, temperature, and flow velocity. The salt chemistry will be monitored using the UW redox potential probe and the salt temperature and flow velocity will be measured using surface mounted thermocouples. Flow velocity can be calculated by timing the progression of a heat pulse around the loop; since no sufficiently accurate low flow velocity instrumentation has been found that is capable of operating at high temperatures while withstanding corrosion and not contributing to a significant pressure drop.

Chemistry control in the loop will be achieved through periodic additions of beryllium to the salt, based on the readings of the UW redox potential probe. By adding beryllium, the salt chemistry will become more reducing, causing impurity fluorides to plate out of solution. Reduction of static salt normally requires filtration after beryllium addition, in order to filter out the small metal slivers that are formed by impurities. In place of a fine mesh filter, the loop design relies upon a down-comer cold trap to help capture material and allow it to settle out of solution. It is hoped that at some later time, the cold trap can be removed from the loop and the material deposition analyzed to lend insight to the internal loop corrosion. While the loop is in operation, salt analysis will have to be carried out externally, using either neutron activation analysis (NAA) or Inductively Coupled Plasma Optical Emission Spectroscopy (ICP-

Fluoride-salt-cooled High-temperature Reactor (FHR) Annual Report: 2015
MIT, U.C. Berkeley, U. of Wisconsin and U. of New Mexico
For Public Distribution

OES). Salt tests will need to be carried out on a regular basis so that impurities concentrations can be related to the measurements of the salt.
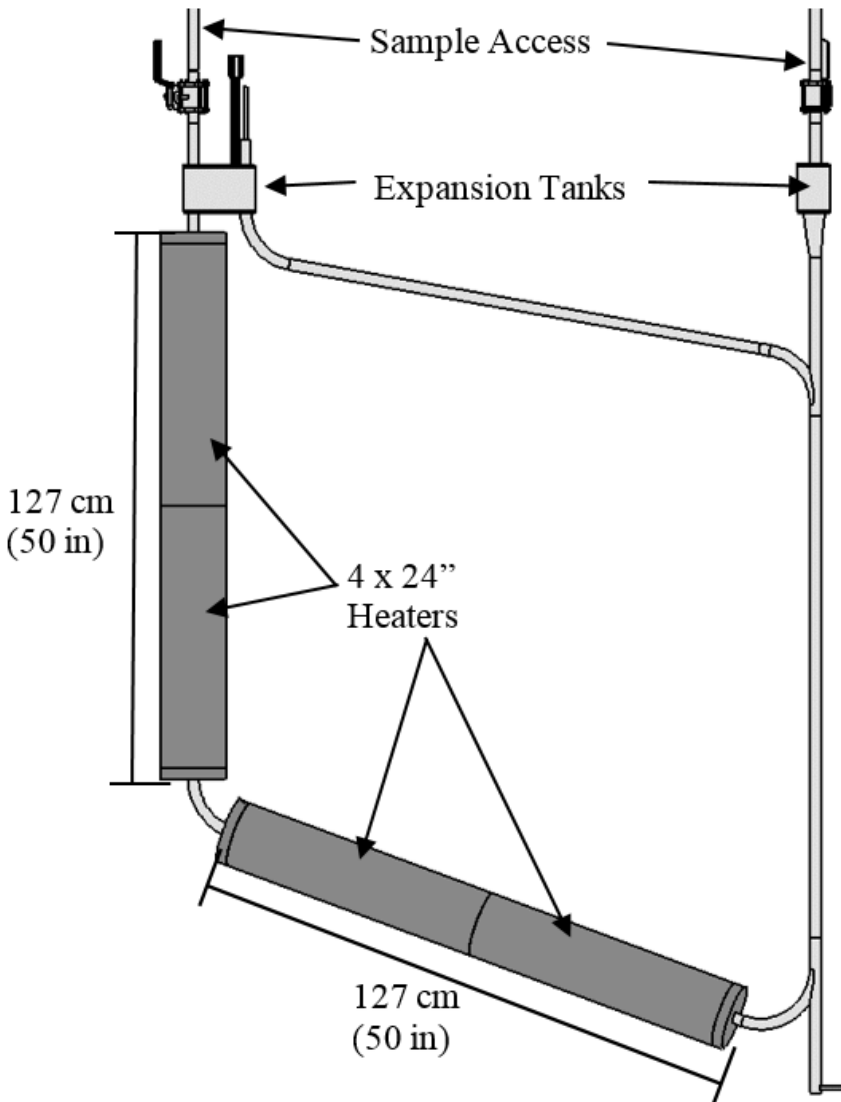

Figure 3.30: Working drawing of UW FLiBe natural circulation flow loop.

Fluoride-salt-cooled High-temperature Reactor (FHR) Annual Report: 2015
MIT, U.C. Berkeley, U. of Wisconsin and U. of New Mexico
For Public Distribution

Task 2.2(a): In-Reactor FHR Materials Corrosion Testing

Heated Irradiation Facility Design

Work continues on the design of the new irradiation capsule for tritium and activation product release measurement. An electric "cartridge" heater with a capacity of a few hundred watts is being designed for installation in the center of the sample zone, with radiation-hardened leads extending to the top of the reactor core tank. This electric heater will provide "booster" heating at low reactor power to keep the salt temperature above 300°. It is believed that this will mitigate the radiolytic production of fluorine and volatile fluoride products encountered during the FS-2 irradiation.

Task 2.2(b): Irradiated FHR Materials Post-Irradiation Examination and Flibe Salt Analysis

Preparatory Work for Analyzing In-reactor Corrosion Tested Alloys

To start analyzing the microstructure of in-reactor corrosion tested alloys, all samples have to be sectioned to small size for reducing activity during transferring, handling, and analyzing in instruments. The size of original tested samples is approximately 13mmx6mmx1mm. Although these samples have been tested in MIT nuclear research reactor in 2013, they are still too hot to transfer between laboratories. Some preparatory work has been done to section these hot materials including setting up a sectioning saw in fume hood, building a shielding space, covering plastic bag to limit contamination, and preparing lead caskets for storing and transferring samples and so on. Additionally, other precautions are required to handle these radioactive materials in laboratory. Exposure dose must be monitored online during handling. Contaminated cutting water was stored in a special container. Working area was repeatedly cleaned and wipe samples were counted to ensure no contaminant. With the support of radiation protection officers (RPO), one in-reactor corrosion tested (FS-1) Hastelloy N sample was first glued on an aluminum strip, and then cut to three parts. The center part (as shown in 3.31) is selected as a sample for microstructural analysis. This sectioned sample will be adhered on a sample holder to further cut it to three parts. Then all sectioned samples will be completely cleaned in acetone.

Figure 3.31: Photograph of in-reactor corrosion tested Hastelloy N, ~6.7mmx2mmx1mm, sectioned by using a low speed sectioning saw in MIT nuclear reactor laboratory. Sample was glued on aluminum strip for cutting.

Fluoride-salt-cooled High-temperature Reactor (FHR) Annual Report: 2015
MIT, U.C. Berkeley, U. of Wisconsin and U. of New Mexico
For Public Distribution

XRD Analysis of SiCs

To continue analyzing the structural stability of three different SiC samples in high-temperature and strong irradiation environment, the as-received, out-of-reactor (provided by UW) and in-reactor corrosion tested samples were analyzed by XRD. The microstructure of the exposure surface of each type of sample was observed under SEM prior to testing in high-temperature molten FLiBe salt. Then all samples were analyzed using XRD (Brucker D8) with exactly same parameters.

Figure 3.32 shows the microstructure of the mechanically polished surface of as-received Rohm & Haas CVD SiC. This rough surface exposed to high-temperature molten FLiBe salt during corrosion tests. It is known that this relatively rough surface has much larger surface area than mirror surface to contact/interact with liquid salt. Theoretically, CVD SiC is super stable in the high-temperature molten fluoride salt with regular redox potential. It is possible that small amount of materials lost from this rough surface due to thermal effect during corrosion which causes slight weight loss.
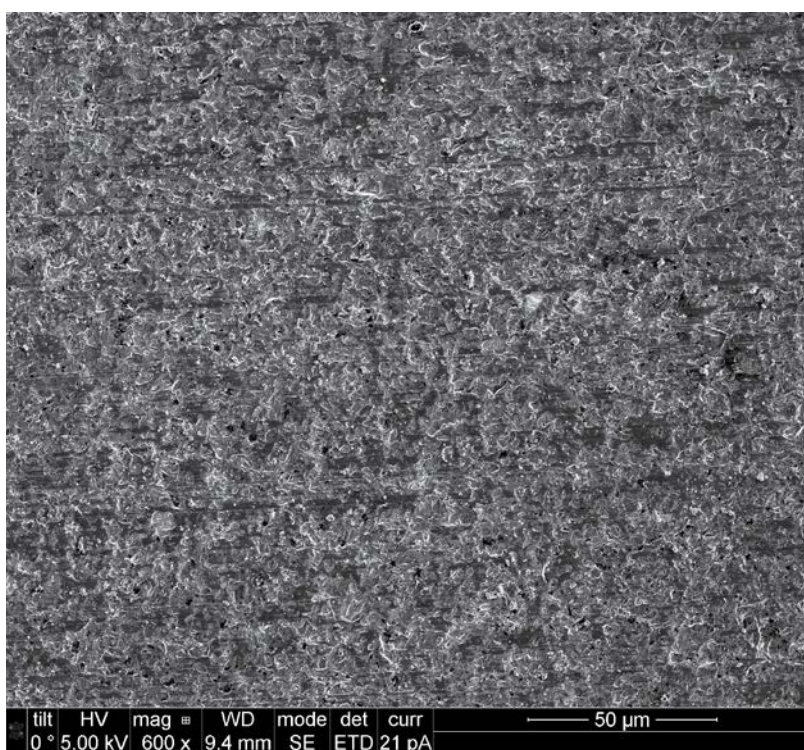

Figure 3.32: SEM image of a mechanically polished surface of as-received Rohm & Haas CVD SiC sample prior to high-temperature corrosion tests in molten FLiBe salt.

XRD patterns were collected from the mechanically polished as-received sample and exposed surface of corrosion tested samples. Figure 3.33 shows the XRD patterns pre- and post-corrosion Rohm & Haas CVD SiC samples. By comparing these three XRD patterns from 2 theta 20° to 90°, it is suggested that no change occurred for the CVD SiC samples in high-temperature molten FLiBe salt without or with neutron irradiation.
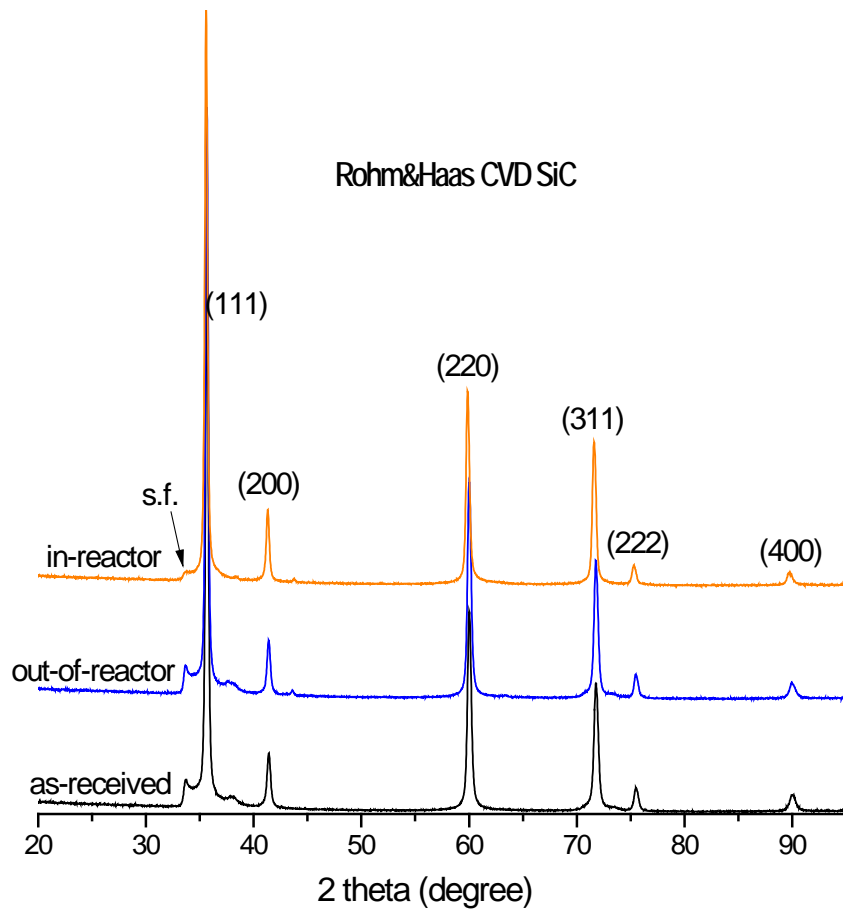
Fluoride-salt-cooled High-temperature Reactor (FHR) Annual Report: 2015
MIT, U.C. Berkeley, U. of Wisconsin and U. of New Mexico
For Public Distribution

Figure 3.33: XRD patterns of as-received, out-of-reactor and in-reactor corrosion tested Rohm & Haas CVD SiC samples. s.f. denotes stacking fault.
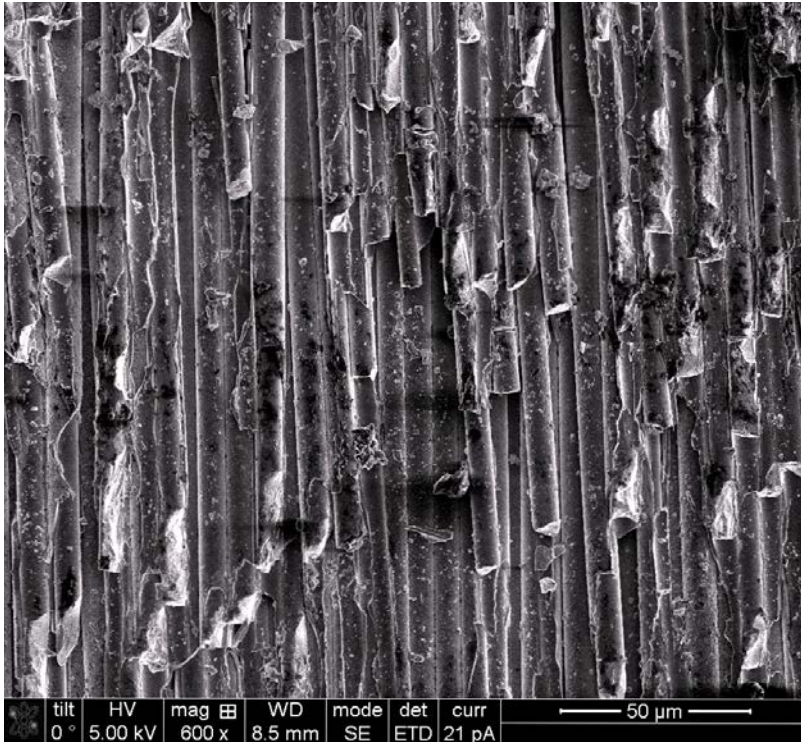
Fluoride-salt-cooled High-temperature Reactor (FHR) Annual Report: 2015
MIT, U.C. Berkeley, U. of Wisconsin and U. of New Mexico
For Public Distribution

Figure 3.34: SEM image of original surface of as-received Tyranno-SA3 CVI SiC/SiC composite sample, focusing on a bunch of SiC fibers.

Fluoride-salt-cooled High-temperature Reactor (FHR) Annual Report: 2015
MIT, U.C. Berkeley, U. of Wisconsin and U. of New Mexico
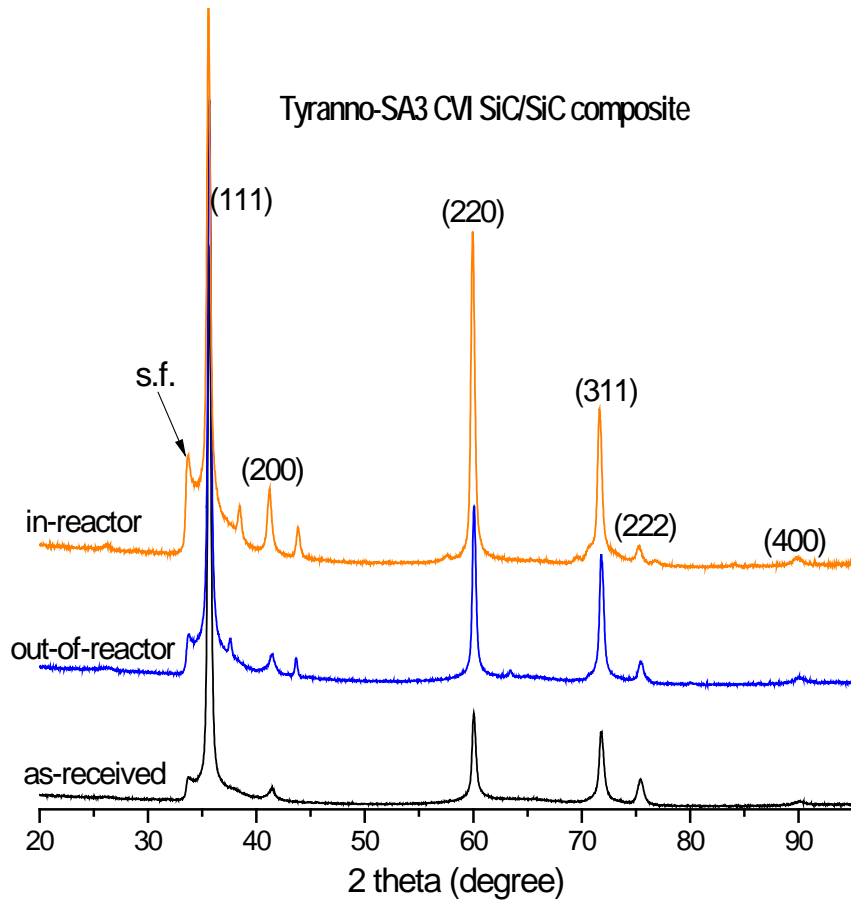For Public Distribution

Figure 3.35: XRD patterns of as-received, out-of-reactor and in-reactor corrosion tested Tyranno-SA3 CVI SiC/SiC composite samples. s.f. denotes stacking fault.

Fluoride-salt-cooled High-temperature Reactor (FHR) Annual Report: 2015
MIT, U.C. Berkeley, U. of Wisconsin and U. of New Mexico
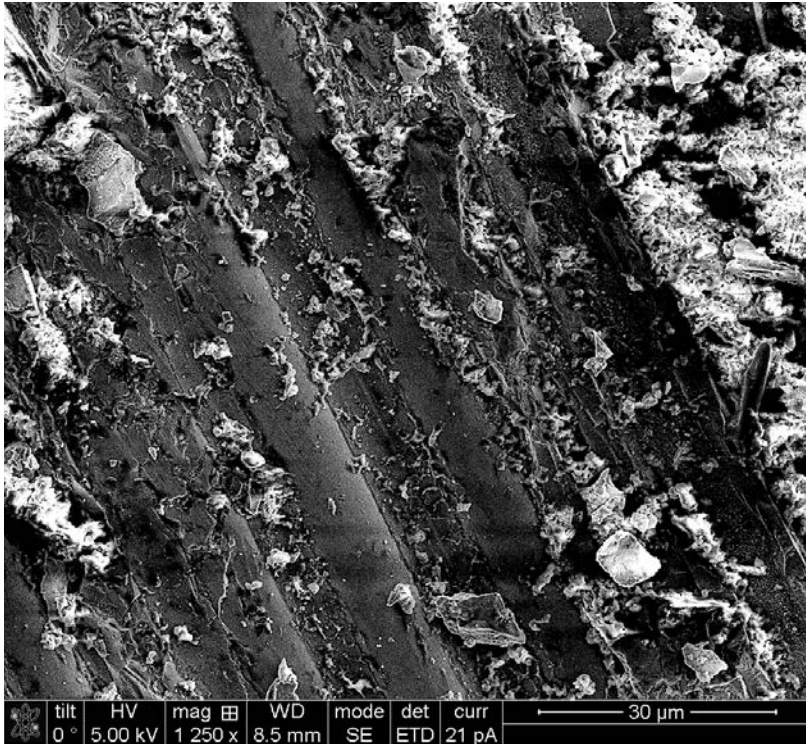For Public Distribution

Figure 3.36: SEM image of original surface of as-received Hi-Nicalon Type-S CVI SiC/SiC composite sample, focusing on an area with visible SiC fibers.

Fluoride-salt-cooled High-temperature Reactor (FHR) Annual Report: 2015
MIT, U.C. Berkeley, U. of Wisconsin and U. of New Mexico
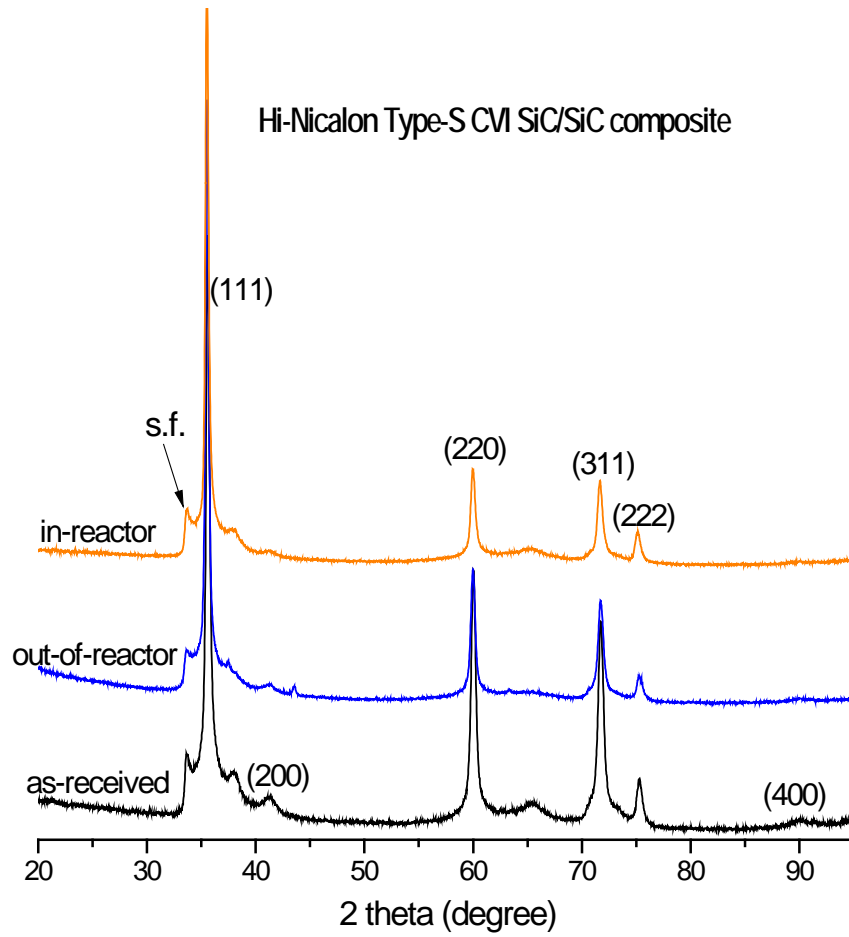For Public Distribution

Figure 3.37: XRD patterns of as-received, out-of-reactor and in-reactor corrosion tested Hi-Nicalon Type-S CVI SiC/SiC composite samples. s.f. denotes stacking fault.

.

Fluoride-salt-cooled High-temperature Reactor (FHR) Annual Report: 2015
MIT, U.C. Berkeley, U. of Wisconsin and U. of New Mexico
For Public Distribution

4   Task 3: FHR Experiments and Modeling for Thermal Hydraulics, Neutronics, and Structural Mechanics (UCB, UNM)

The objective of this task is to perform modeling and to provide experimental data for benchmarking of evaluation models for FHR safety and transient response.

Task 3.1: FHR Experiments and Modeling for Thermal Hydraulics, Neutronics, and Structural Mechanics (UCB)

This task involves developing an experimental program and modeling capability of FHR thermal hydraulics, neutronics, and structural mechanics, especially in relation to safety modeling of passive decay heat removal systems during accident scenarios. Experimental data will be used to validate models where possible, which will be part of a benchmark campaign involving all IRP members as well as outside participants. The coupling of models in thermal hydraulics, neutronics, and structural mechanics for a holistic view of FHR phenomena and response is also a goal for this task area.

Task 3.1(a): Conduct CIET test program for existing CIET configuration

CIET Test Program and Simulation Models

Parasitic heat loss evaluation

Parasitic heat loss tests have been performed on the Compact Integral Effects Test (CIET) facility. The goals are:

1. To identify major sources of heat losses between the fluid loop and ambient air, and to reduce these heat losses to a minimum by adding thermal insulation wherever needed and possible, and
2. To develop empirical correlations for overall heat transfer coefficient between the fluid loop and ambient air between pairs of temperature measurement locations.

These goals were achieved during the first quarter of 2015 by measuring fluid flow rates in each branch of the loop and fluid temperatures at many locations along the loop. Figure 4.8 shows a piping and instrumentation diagram for the loop, indicating the locations of all instrumentation.

The tests were divided in several phases:
1. Parasitic heat losses in the primary loop: fluid is flowing through the heater and CTAH branches. The DHX, bypass branches, and DRACS loop, are isolated.
2. Parasitic heat losses in the DHX branch: fluid is flowing through the heater, DHX and CTAH branches. Because of relative friction losses in the heater vs. the DHX branch, about 80% of the flow goes through the heater and gets heated up while about 20% of the flow goes through the DHX branch. The DRACS loop is isolated.
3. Parasitic heat losses in the DRACS loop: the DRACS loop is connected to the primary loop (similar configuration used for pressure drop measurements in the DRACS loop). Fluid is flowing through the heater, DHX and CTAH branches, and through the DRACS. Because of relative friction losses in the heater vs. the DHX branch and the DRACS, about 90% of the flow goes through the heater and gets heated up while about 10% of the flow goes through the DHX branch and the DRACS.
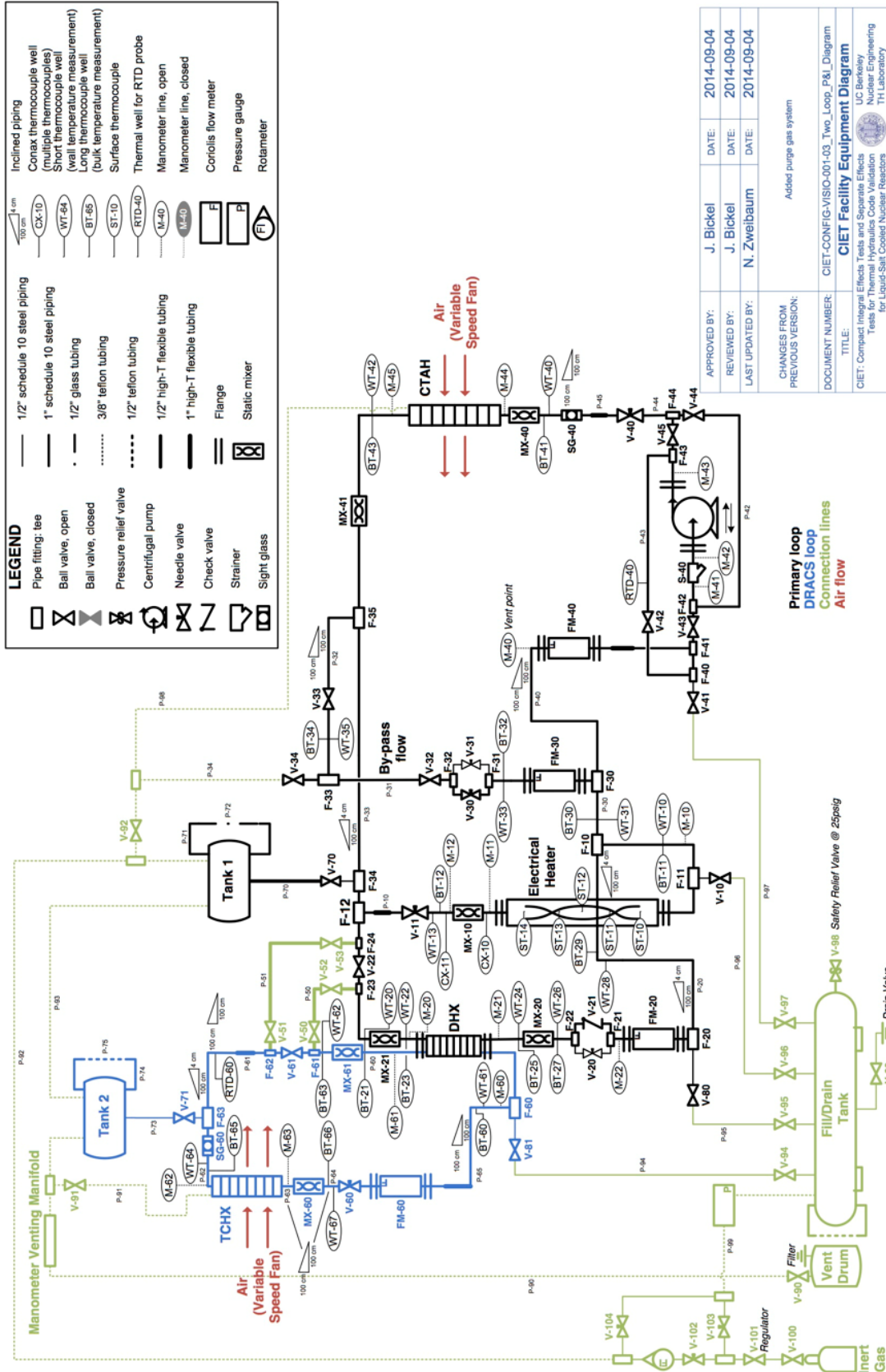
Fluoride-salt-cooled High-temperature Reactor (FHR) Annual Report: 2015
MIT, U.C. Berkeley, U. of Wisconsin and U. of New Mexico
For Public Distribution

Figure 4.8. CIET piping and instrumentation diagram.

Fluoride-salt-cooled High-temperature Reactor (FHR) Annual Report: 2015
MIT, U.C. Berkeley, U. of Wisconsin and U. of New Mexico
For Public Distribution

An infrared camera (FLIR E4) was used to measure surface temperatures along the primary loop and identify locations where major heat losses occur. As expected and measured, significant heat losses occurred at the CTAH heat exchanger (

Figure **4.9**). These do not need to be minimized since it is the role of the CTAH to extract heat from the primary loop. On these pictures, manometer and thermocouple ports also appear as significant heat loss sources. These were subsequently covered with insulation to minimize heat losses.
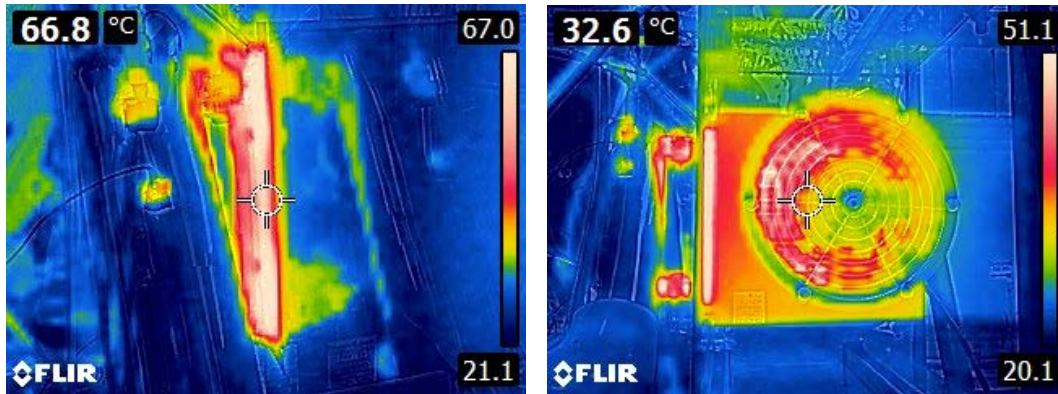

Figure 4.9. Infra-red pictures of the manifold (left) and body (right) of the CTAH fan-cooled heat exchanger.

Non-negligible heat losses occurred at other locations that can be covered with easily removable insulation, such as needle valve knobs and sight glasses (
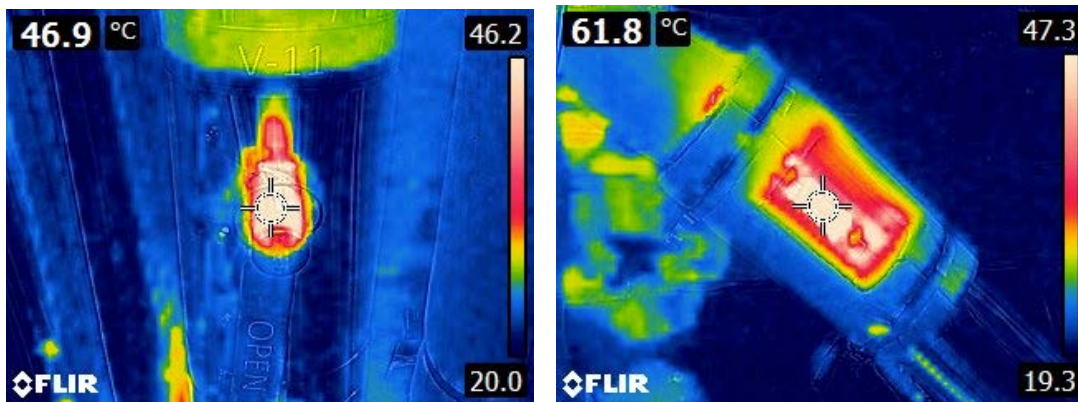
Figure **4.10**).

Figure 4.10. V-11 needle valve knob (left) and S-40 sight glass (right).

Finally, significant heat losses occurred at locations that could be better insulated with permanent insulation, particularly flanges for connections of the pump and electrical heater (

Figure **4.11**).

Fluoride-salt-cooled High-temperature Reactor (FHR) Annual Report: 2015
MIT, U.C. Berkeley, U. of Wisconsin and U. of New Mexico
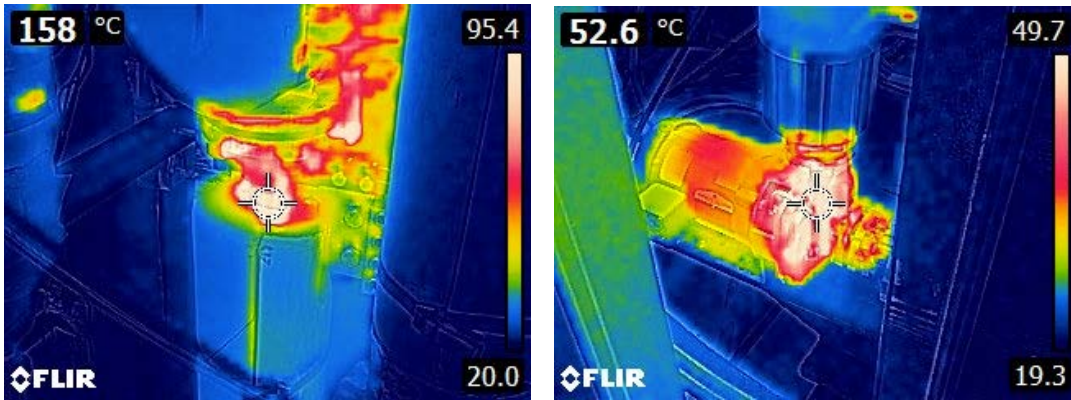For Public Distribution

Figure 4.11. Electrical heater top flange (left) and primary pump (right).

All identified parasitic heat losses will be reduced by:
1. Installing additional thermal insulation wherever possible (now complete), and
2. Implementing guard heating in the enclosure of the CIET facility, to raise the ambient temperature to the average temperature of the fluid in the loop (modification underway).

At locations where only thin, removable insulating pads had been installed have been complemented with flexible fiberglass insulation, as shown in
Figure **4.12**.

Figure 4.12. Installation of flexible fiberglass insulation underneath thin, removable insulating pads.

CIET Experimental Program Audit

Fluoride-salt-cooled High-temperature Reactor (FHR) Annual Report: 2015
MIT, U.C. Berkeley, U. of Wisconsin and U. of New Mexico
For Public Distribution

During the months of May and June, the CIET experimental program's quality assurance program was audited. The conclusion from the audit was very positive:

"The CIET program has taken considerable actions to address the findings and corrective actions from the previous year's audit results. The corrective actions to address the findings were mainly addressed with only a few portions of a couple requirements remaining to be addressed. These few portions are represented by the 3 findings. This demonstrates a significant improvement over previous year's results."

This is a strong reflection of the CIET Test Program's commitment to quality assurance in its research efforts, and the three issues in need of address are currently being addressed. The CIET Program Quality Assurance Program is currently in compliance with NQA-1-2008 with 2009 Addenda Requirements following this year's audit's completion.

Beginning of NE-KAMS and CIET Integration

Oak Ridge National Laboratory's Nuclear Energy – Knowledge Base for Advanced Modeling and Simulation (NE-KAMS) has been selected as the data repository and method for interacting with and sharing all FHR IRP data. This was one of several outcomes from the previous FHR IRP Workshop in March held at UC Berkeley. Currently, several CIET test results and supporting documentation have been uploaded to NE-KAMS in order to understand and implement the tools for sharing this data. This work is also being supported by similar activities from the University of New Mexico.

This work will continue, and as NE-KAMS increases its functionality and data management abilities, more data from UC Berkeley and the other FHR IRP universities will be added. This will allow for the sharing and understanding of experimental research across the FHR IRP universities and will be vital during the benchmark campaign over the course of the coming two years. NE-KAMS will also allow for streamlined data sharing to and from partner organizations, particularly internationally.

CIET Mass Flow Meter Replacement

A minor but important maintenance activity was carried out for the CIET facility during the second quarter of this year: three out of four mass flow meters, which had been identified to erroneously "drift" and give poor quality data, have been replaced and fully calibrated for use in the CIET facility. Previous data may be subject to poor mass flow measurement, but fortunately this malfunction was identified early on and steps were taken to limit the effects of this problem, such as moving the correctly functioning flow meter to a more important position in the flow loop, and limiting the amount of heat used in the system which was identified to be a cause of mass flow drift during experimentation.

Loss of Forced Circulation (LOFC) Transient Testing

Loss of forced circulation (LOFC) transient testing has begun using the CIET facility. LOFC transient tests are being performed to understand the performance capabilities of the DRACS system to remove decay heat in CIET, and subsequently in FHRs. Experimental data from these tests will be subsequently used in FHR TH models to optimize the DRACS design.

Further understanding of the LabVIEW control system is also planned under LOFC testing. Currently, control trials for the control of the fan-cooled oil-to-air heat exchanger, representing the coiled tube air heat exchanger (CTAH), have been performed. The initial control algorithm was developed to vary fan speed to control the average fluid outlet temperatures of the TCHX and CTAH heat exchangers.

Fluoride-salt-cooled High-temperature Reactor (FHR) Annual Report: 2015
MIT, U.C. Berkeley, U. of Wisconsin and U. of New Mexico
For Public Distribution

An additional benefit from the development of this feedback control system involves the opportunity to collect extensive heat transfer data for these heat exchangers. This data can be used to improve models to better characterize heat rejection from the CIET 1.0 fan-cooled heat exchangers at various fan speeds, and oil and air temperatures. Throughout these tests, the heater power input was manually varied, and the CTAH feedback control system was used to control the CTAH steady-state outlet temperature. Several options were examined for feedback control of the CTAH, including proportional, proportional-integral and proportional-integral-derivative controllers.

Figure 4.13 shows results obtained using a simple proportional controller to vary CTAH fan speed based on CTAH outlet temperature set-points, with a fixed heat input of 1.06 kW through the resistive heater. The proportional controller, activated 4000 seconds into the test, was successful in reaching steady CTAH outlet temperatures of 40°C (step up), 38°C (step down) and 41.5°C (step up), successively.

Further transient testing is also planned, especially to develop the capability to integrate simple neutronics models into the control and response of the power input into the CIET facility. These efforts will be the first steps in transitioning the control of the CIET facility to a system that behaves similarly to a nuclear powered system, specifically an FHR.
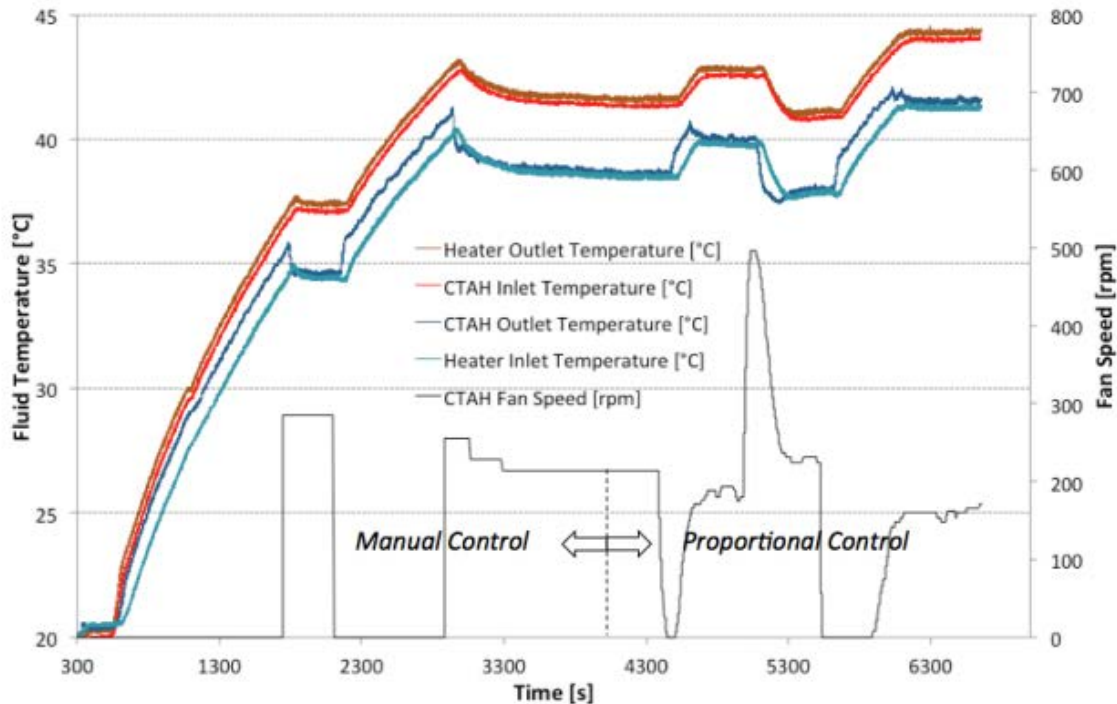

Figure 4.13. CTAH proportional feedback control test.

Dynamic Input Capabilities

Looking forward to more complicated transient scenarios and the integration of reactor feedback responses, dynamic input capabilities have been tested using the current control scheme for the CIET facility. The power supplied by the heating element was input as a sine function with varying frequency and amplitude to test the capabilities of the LabVIEW control system as well as the data acquisition resolution. The control and data acquisition abilities of the current system are adequate but will necessitate upgrading in the near-term future. However, these oscillations have provided very interesting data that may lead to insights into how the thermal inertia of structural components are coupled to the

70

Fluoride-salt-cooled High-temperature Reactor (FHR) Annual Report: 2015
MIT, U.C. Berkeley, U. of Wisconsin and U. of New Mexico
For Public Distribution

fluid temperature and core power conditions. Figure 4.14 shows part of the experimental run where the heater power was varied sinusoidally with an increase in amplitude at 2100 seconds and an increase in frequency at 2410 seconds.
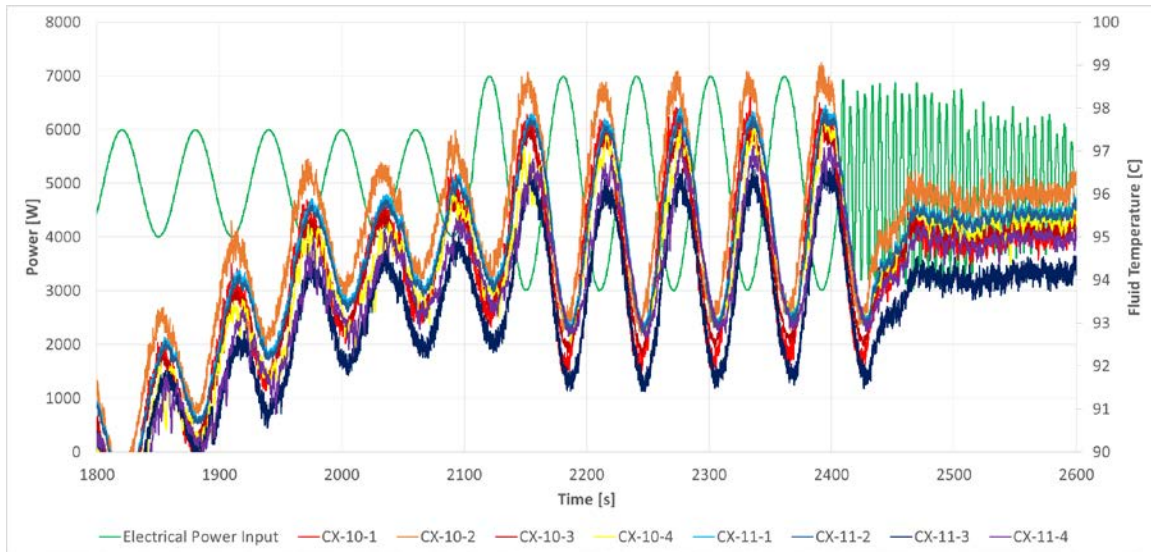

Figure 4.14. CIET input power oscillations experiment.

Figure 4.15 provides a close-up of a 4 kW amplitude (maximum heater power of 7 kW, minimum heater power of 3 kW), 60-second period region; the figure colors are adjusted such that it is easier to tell the difference between the four Conax thermocouples at the heater outlet before the mixing element (CX-10) and the four Conax thermocouples at the heater outlet after the mixing element (CX-11).
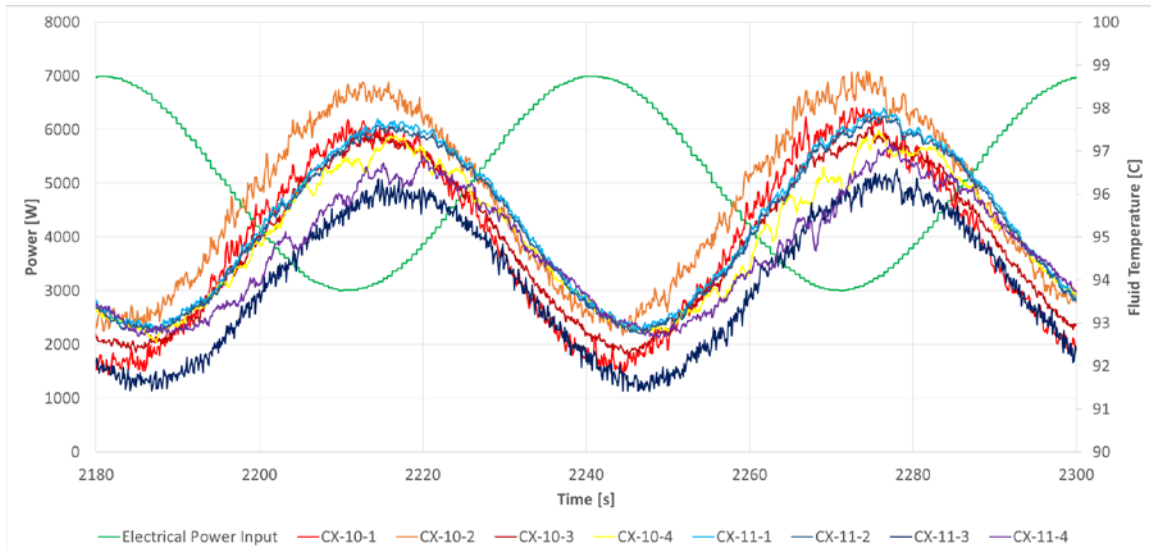

Figure 4.15. CIET input power oscillations experiment close-up; 4 kW amplitude, 0.017 Hz frequency.

There is approximately a 35 second phase delay between the heater power and the CX-10 thermocouples' response. Estimating, the CX-11 thermocouples have about a 3 second delay from the

Fluoride-salt-cooled High-temperature Reactor (FHR) Annual Report: 2015
MIT, U.C. Berkeley, U. of Wisconsin and U. of New Mexico
For Public Distribution

CX-10 thermocouples, which is commensurate with oil residence time in the annular heating element of 3.5 seconds.

This data is encouraging for understanding the conjugate heat transfer between fluoride salts and structural components such as graphite and steel piping. Testing the system's conjugate heat transfer by oscillating power input and monitoring system temperatures to understand system thermal inertias may be able to provide thermal hydraulic and structural element validation data for prototypical FHR systems, which would be an extremely valuable tool and merits further study. This effort will also be explored further in UC Berkeley's SET Program.

Evaluation of Dynamical System Scaling (DSS) methodology applied to CIET

The DSS approach is recommended for application to tightly-coupled systems with many independent parameters for which spatial and temporal decoupling is difficult, and especially for systems with important time-dependent phenomena. Work this year at UC Berkeley reveals the added complexity associated with application of the DSS approach in the development of governing balance equations, the careful consideration of viable assumptions needed to reduce the scaling search space, and the creation of a solution algorithm that updates guesses for loss coefficients in order to yield steady initial system states that correspond to the permutation selections of the scaling design. The lowest transient-integrated distortion obtained by the DSS method was directly compared to the distortion estimates of the CIET facility to relate the eventual DSS scaling selection to the actual H2TS scaling design of CIET. For each dimensionless Pi term associated with the H2TS scaling, there is one distortion estimate, and reconciling these independent distortions into a single value proves difficult and to the discretion of the experimenter. The strong advantage of providing a time-dependent distortion motivates the use of the DSS method in future scaled IETs for salt systems that are tightly coupled due to the single-phase nature of the coolants. While the DSS approach does involve more upfront effort that other scaling methods, the reduction in distortion may be substantial enough to justify its use. The value of the DSS method over other methods will of course depend on the specific experimental system, and for salt IETs, the DSS method has been shown to be a valuable new tool for viewing a new dimension of the scaling. Further examination of the applicability of this scaling methodology to scaled experiments for molten salt thermal hydraulics is underway, and a more thorough discussion will be produced during the next year.

Observations and investigations of flow instability in the CIET heating element

During the initial heated testing of CIET, including steady-state and transient operation, oscillations in coolant temperature were observed at the heating element outlet, as shown in
Figure **4.16**. The fluctuating fluid temperature at the CIET heating element outlet was not expected, but provided insights on the dynamic response of the CIET loop and its heat structures. As Figure 4.3 shows, a clear phase lag exists between oscillations at the heating element outlet, and oscillations at the inlet to the coiled tube air heater (CTAH), simulated by an oil-to-air cooler with a variable speed fan, immediately downstream. The phase lag and amplitude reduction occurs due to a combination of the advection time for the coolant from the heating element outlet to the CTAH inlet (8.5 seconds for 0.18 kg/s mass flow), and heat transfer to and from solid heat structures between the heating element and CTAH.

Fluoride-salt-cooled High-temperature Reactor (FHR) Annual Report: 2015
MIT, U.C. Berkeley, U. of Wisconsin and U. of New Mexico
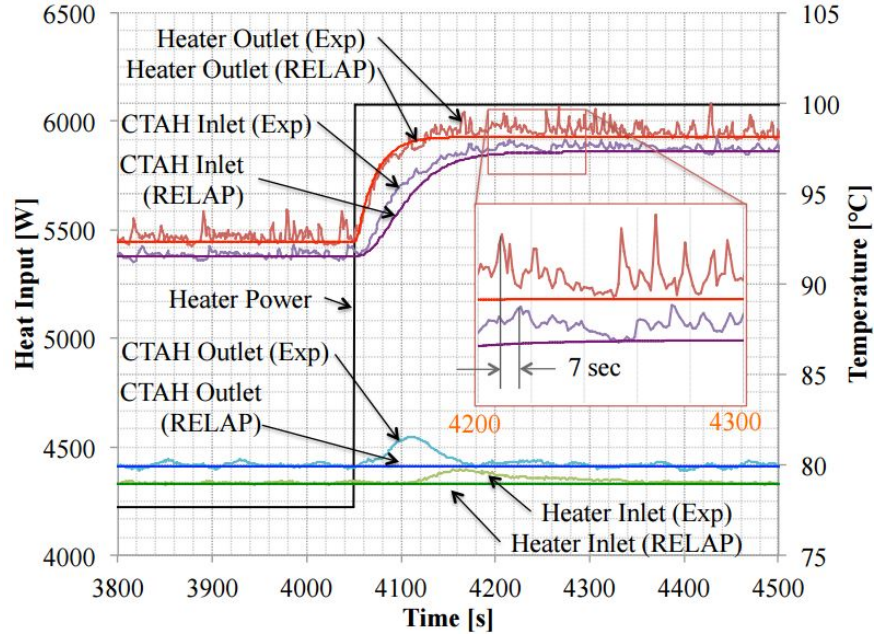For Public Distribution

Figure 4.16. Oscillating coolant temperatures observed during CIET forced-circulation test 2015-04-28_Power_Step_Change_Transient_Test, involving a step change in heating element power from 4220 W to 6070 W at 4050 seconds.

By the time the fluid exits the CTAH the fluctuations damp greatly. However, it can be seen that the proportional–integral–derivative control of the CTAH fan speed is imperfect in maintaining a constant CTAH outlet temperature immediately after the power step change, resulting in a temperature anomaly at the outlet. The time delay and amplitude reduction for this temperature anomaly to arrive back at the heating element inlet is also readily apparent, and agrees closely to the predicted delay due to the 28.8 second fluid transit time from the CTAH outlet to the heating element inlet. CIET 1.0 was modeled in RELAP5-3D (Version 4.0.3ie) providing excellent prediction for the time averaged fluid temperatures, but this model was not capable of simulating the high-frequency fluid temperature oscillations.

Figure **4.16** depicts power step changes under forced cooling operation with a fixed mass flow rate that were performed primarily for validating the RELAP5-3D model for thermal inertia of the system's solid structures and fluid inventory, which affects its response time to such transients. In particular, because the thermal capacity of the solid structures in the loop is of the same order of magnitude as the thermal capacity of the oil (approximately 50 kJ/K and 20 kJ/K, respectively), it is important to account for the fact that some heat structures are more tightly coupled to the system's fluid inventory to accurately predict the system's transient behavior. During model optimization, closer agreement between code results and experimental data is obtained by separating the weakly coupled thermal masses (e.g. flanges, valves) and the strongly coupled thermal masses (e.g. pipe walls) into separate heat structures in the RELAP5-3D model, based upon measured values for weights of individual components and the fact that weakly coupled thermal masses account for roughly 20% of the total weight of the system's solid structures.

While the unexpected oscillations of the heating element outlet temperature led to a number of insights about the dynamic behavior of the CIET experiment, these oscillations are undesirable because they degrade the quality of the transient data collected in CIET for use in code validation. Likewise, such

73

Fluoride-salt-cooled High-temperature Reactor (FHR) Annual Report: 2015
MIT, U.C. Berkeley, U. of Wisconsin and U. of New Mexico
For Public Distribution

instabilities would be undesirable in an actual FHR, because they have the potential to drive heated surfaces to excessively high local temperatures and to generate fluctuating thermal stresses that could lead to high-cycle fatigue and failure of structures. For this reason, additional experiments were performed to identify the cause of the instabilities in the annular heating element.

In the heated experiments, the flow rate of the coolant in the loop was measured with a Siemens SITRANS FC430 Coriolis mass flow meter. No fluctuation of the mass flow rate was observed, indicating that the instability occurs with a constant average mass flow rate. This observation implicated local buoyancy and/or viscosity induced flow instabilities as the likely cause of the temperature oscillations as temperature is observed to fluctuate independent of the bulk mass flow rate. Temperature oscillations were measured by two thermocouples in-line with the fluid at the exit of the heating element after a flow mixer. One thermocouple is close to the wall of the pipe and the other is closer to the center of the pipe. The average temperature measurement difference between these thermocouples during the most recent test (2015-10-22_Power_Step_Change_Transient_Test) was 0.63°C with a standard deviation of 0.13°C, indicating good agreement within the expected combined uncertainty of both thermocouples of +/- 1.0°C. Therefore the temperature measurement of the fluid at the heating element outlet correctly reflects the fluid's bulk temperature.

To identify the cause of the temperature oscillations, the outside surface of the heating element was instrumented with multiple thermocouples at elevations of 0.75 m (ST-12) and 1.52 m (ST-14) above the bottom of the 1.62 m long heated section.

These experiments showed that the CIET heating element has substantial azimuthal temperature non-uniformity around its circumference caused by flow instability. Figure 4.17 shows azimuthal temperatures at the vertical center (ST-12) and vertical top (ST-14) of the heating element during a low power step change test with power changing from 1500 W to 5000 W in 500 W steps; azimuthal positions are labeled based on their cardinal direction on the outer tube surface. Temperature distributions in the azimuthal direction at varying vertical locations are the most convincing evidence that flow instability does occur within the heating element. Figure 4.17 not only shows distinct azimuthal temperature distributions at the vertical center and vertical top of the heating element, but shows that the relative positions of the hottest and coldest azimuthal temperatures change throughout the test, a clear indication of flow instability within the annular heating element.

Fluoride-salt-cooled High-temperature Reactor (FHR) Annual Report: 2015
MIT, U.C. Berkeley, U. of Wisconsin and U. of New Mexico
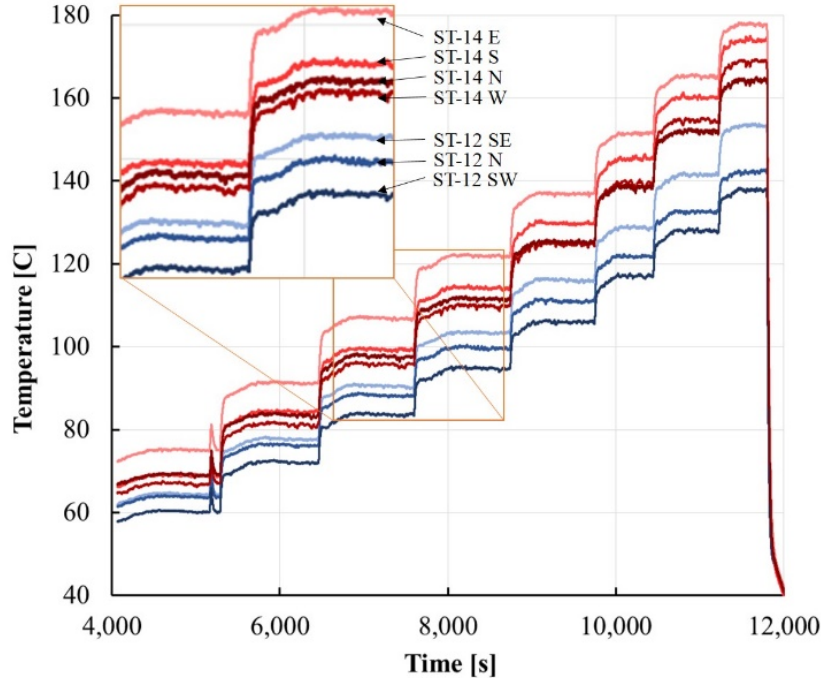For Public Distribution

Figure 4.17. Azimuthal temperature distribution at the vertical center (ST-12, 3 blue lines) and vertical top (ST-14, 4 red lines) of the annular heating element during a low power step change test 2015-10-22_Power_Step_Change_Transient_Test.

This low power step change test also disproves an initial hypothesis explaining the flow instability within the heating element: buckling of the outer tube due to thermal stress at high power levels. Buckling of a beam requires a minimum amount of stress and therefore is a threshold effect. The CIET annular heating element experiences flow instability even at low power levels, well below the temperatures required to initiate any potential buckling of the outer tube due to thermal stress in the tube.

Separate Effects Test (SET) Program

Two main separate effects tests are currently underway:

1.   Pebble-Bed Heat Transfer Experiment (PBHTX)
2.   Cartridge Heater Experiment (CHEX)

   1. PBHTX

The Pebble-Bed Heat Transfer Experiment (PBHTX) is a scaled facility designed to measure heat transfer coefficients within a pebble-bed test section for the conditions applicable to the Pebble-Bed Fluoride-Salt-Cooled High Temperature Reactor (PB-FHR). A simulant oil called Dowtherm A is used as the heat transfer fluid, which matches the Prandtl number of flibe at temperatures lower than the PB-FHR conditions. A dimpled test section 0.0889m long is filled with randomly packed 0.00635m diameter copper pebbles, some of which are instrumented with thermocouples to measure temperature. The inlet and outlet fluid temperatures are also recorded. A Coriolis flowmeter is used to measure the mass flow rate of the oil within the loop. A power supply is used to vary the heater power sinusoidally, and in this way the frequency response of the test section can be measured to a high accuracy. The facility is designed so that the range of Reynolds and Prandtl numbers are matched with the prototypical conditions. The loop has been built using flexible stainless steel piping and tri-clamp fittings. It is built in a modular

Fluoride-salt-cooled High-temperature Reactor (FHR) Annual Report: 2015
MIT, U.C. Berkeley, U. of Wisconsin and U. of New Mexico
For Public Distribution

fashion, implying that the pebble-bed test section could be replaced for future tests. Preliminary data is in the process of being collected, and heat transfer data will be collected in early 2016.

The pebble-bed core can be regarded as a porous medium and thus porous media governing equations can be used to develop models for the PB-FHR core. The interfacial heat transfer coefficient is a parameter that is determined either from predictive correlations or from experimental data.

The Pebble-Bed Heat Transfer Experiment (PBHTX) is a new experimental facility at the University of California, Berkeley (UCB) in which frequency response techniques will be used to determine heat transfer coefficients in a representative pebble-bed test section. Previously at UCB, step change response tests were carried out.

The primary objective of PBHTX is:

- To measure the interfacial heat transfer coefficient in a pebble bed geometry for a range of Reynolds and Prandtl number that encompass the PB-FHR operating conditions, and compare to correlations in the literature, especially Wakao's correlation. This will be done for two heat transfer fluids: Drakesol 260AT and Dowtherm A.

The secondary objectives are:

- To measure the friction head loss in the test section geometry
- To measure permeability of the test section and compare to the analytical Carman-Kozeny relationship
- To gain experience designing and developing modular scaled Dowtherm A loops that allow for flexibility in testing
- To use sinusoidal oscillations in order to extract thermal inertia information from the collected data

There are several advantages to using sinusoidal oscillations to measure heat transfer coefficients as opposed to step change responses.

- Accurate measurements of thermal inertia of the test section can be made with frequency response data.
- In the data reduction procedure, the interfacial heat transfer coefficient is a function of the derivative of the pebble temperature Ts. With a sinusoidal temperature variation in the pebble temperatures, the derivative can be easily obtained to a higher accuracy than could be done for the step change responses.
- More data can be collected over a longer interval of time when periodic steady state conditions are achieved. This would help reduce any potential distortions due to transient effects.

With PBHTX we can exercise more control over the minimum and maximum temperatures of the fluid. This is because a larger power to the heater can be achieved. A larger temperature difference between the pebbles and oil can be obtained than was possible during the step change response tests. In this way data can be collected for a larger variety of non-dimensional numbers.

The PBHTX facility was fully constructed on October 31st. Preliminary testing of key components has been completed to check that they function as intended. This was done for the heater, heat exchanger, power supply and instrumentation. Currently, head loss data is being collected in the test section and the heat exchanger.

Fluoride-salt-cooled High-temperature Reactor (FHR) Annual Report: 2015
MIT, U.C. Berkeley, U. of Wisconsin and U. of New Mexico
For Public Distribution

Figure **4.18** shows two pictures of the facility from different directions with callouts indicating major components.
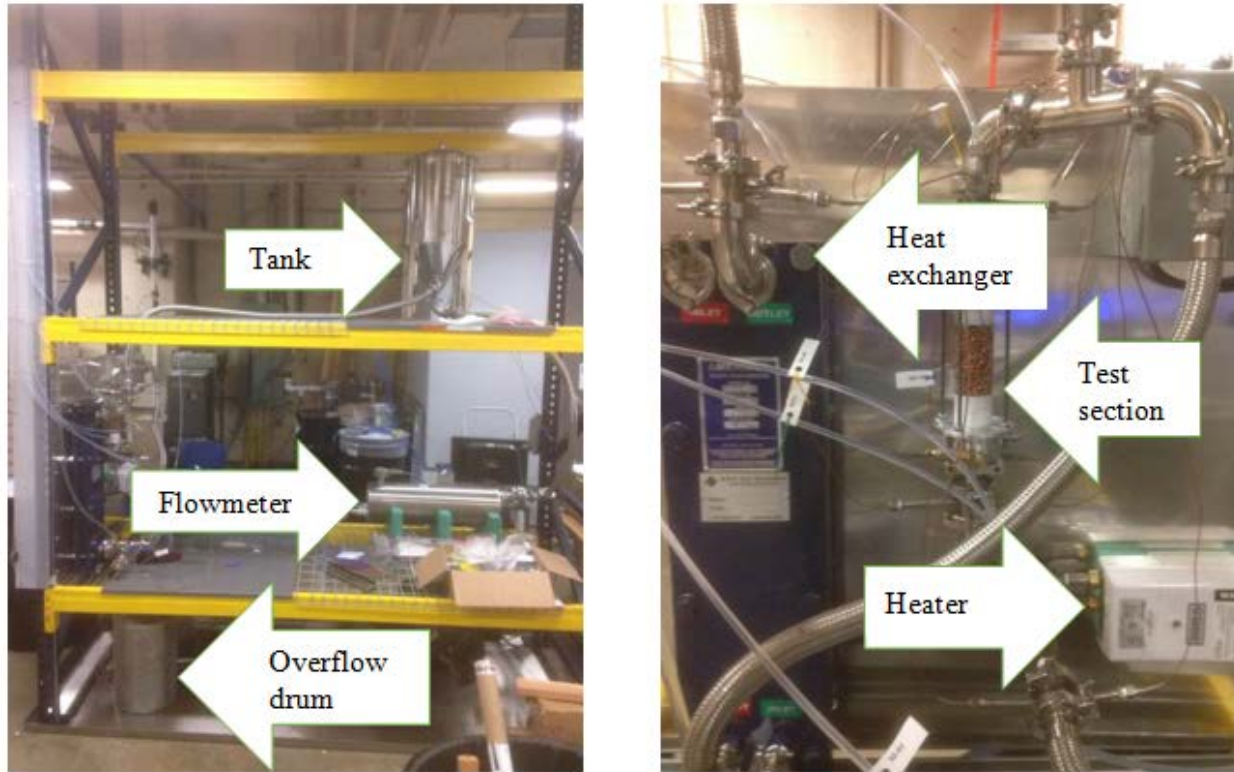

Figure 4.18. PBHTX view from the North showing the tank, flowmeter and overflow drum (left) and View from the West showing the heater, test section and heat exchanger (right)

2. CHEX

The Cartridge Heater Experiment (CHEX) was designed to test similitude between Dowtherm A and fluoride salt for natural convection heat transfer from a vertical cylinder. Experiments were conducted in Dowtherm A and were compared to results from Oak Ridge National Laboratory (ORNL) using flinak. Both laminar, transition and turbulent conditions were investigated. Data collection and data processing is complete, and simulation work is underway to complement the experimental results. Figure 4.19 shows the CHEX experimental setup and Figure 4.20 shows experimental results demonstrating Dowtherm A and flinak similitude.

Currently, COMSOL models of CHEX are being refined in order to make comparisons between the experimental data and CFD solutions. This will allow us to pinpoint sources of distortions, which is critical in assessing the capability of Dowtherm A as a simulant fluid for flibe.
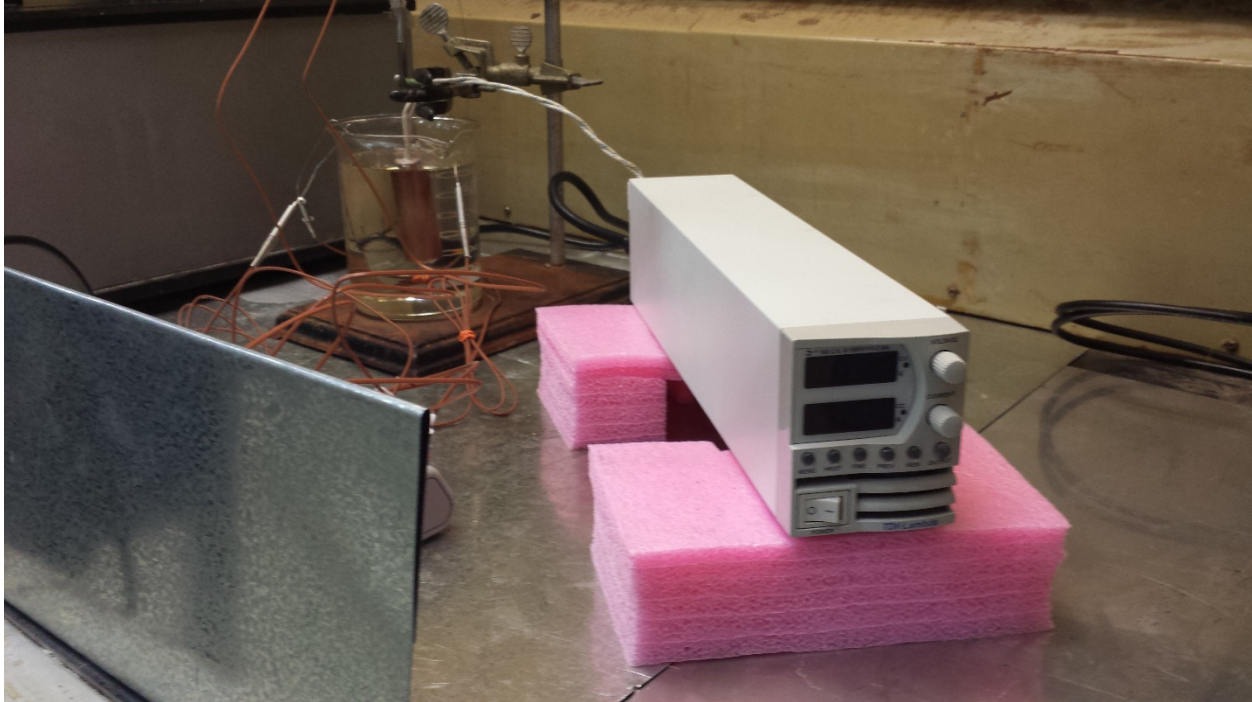
Fluoride-salt-cooled High-temperature Reactor (FHR) Annual Report: 2015
MIT, U.C. Berkeley, U. of Wisconsin and U. of New Mexico
For Public Distribution

Figure 4.19. CHEX experimental setup with a DC power supply to control the power to the cartridge heater located within a copper sleeve.
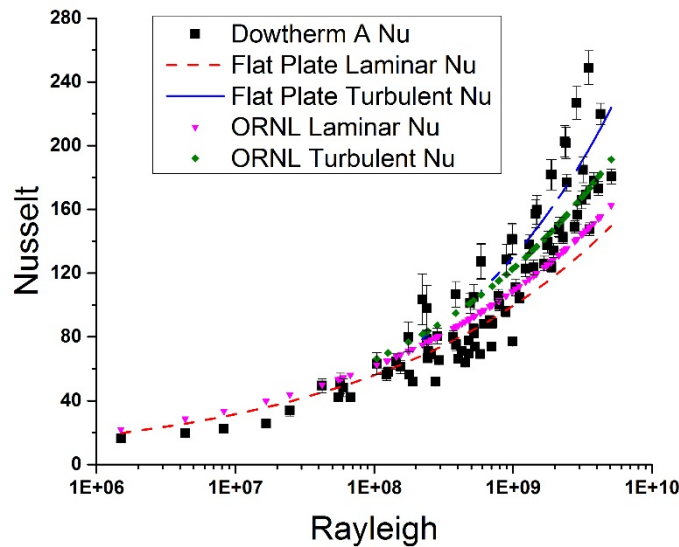
Figure 4.20. Experimental results showing comparisons between Dowtherm A and ORNL flinak data.

Task 3.1(b): Develop TH simulation models and assess CIET/prototype system similitude

Beginning of verification and validation efforts for the CIET 1.0 facility

A second major activity regarding CIET this year has been the verification and validation of RELAP5-3D and FANCY models of coupled natural circulation. The RELAP5 and FANCY models of

Fluoride-salt-cooled High-temperature Reactor (FHR) Annual Report: 2015
MIT, U.C. Berkeley, U. of Wisconsin and U. of New Mexico
For Public Distribution

CIET 1.0 reproduce its geometry (i.e. components lengths, elevations, hydraulic diameters and flow areas), pressure and temperature boundary conditions, and working fluid thermophysical properties. Material properties for the stainless steel and copper tubing, as well as the fiberglass insulation, are manually implemented in the models. In particular, thermal mass of the system will have an impact on future transient modeling and validation. Therefore, masses of individual components were measured and recorded throughout the assembly process of CIET 1.0, and these individual masses can be added to heat structures in the RELAP5 and FANCY models when transient model validation is performed. Figure 4.21 shows a labeled 3-dimensional model of CIET 1.0 and the corresponding nodalization diagram for the RELAP5 and FANCY models. On the diagram, the primary loop and the DRACS loop are highlighted in green.
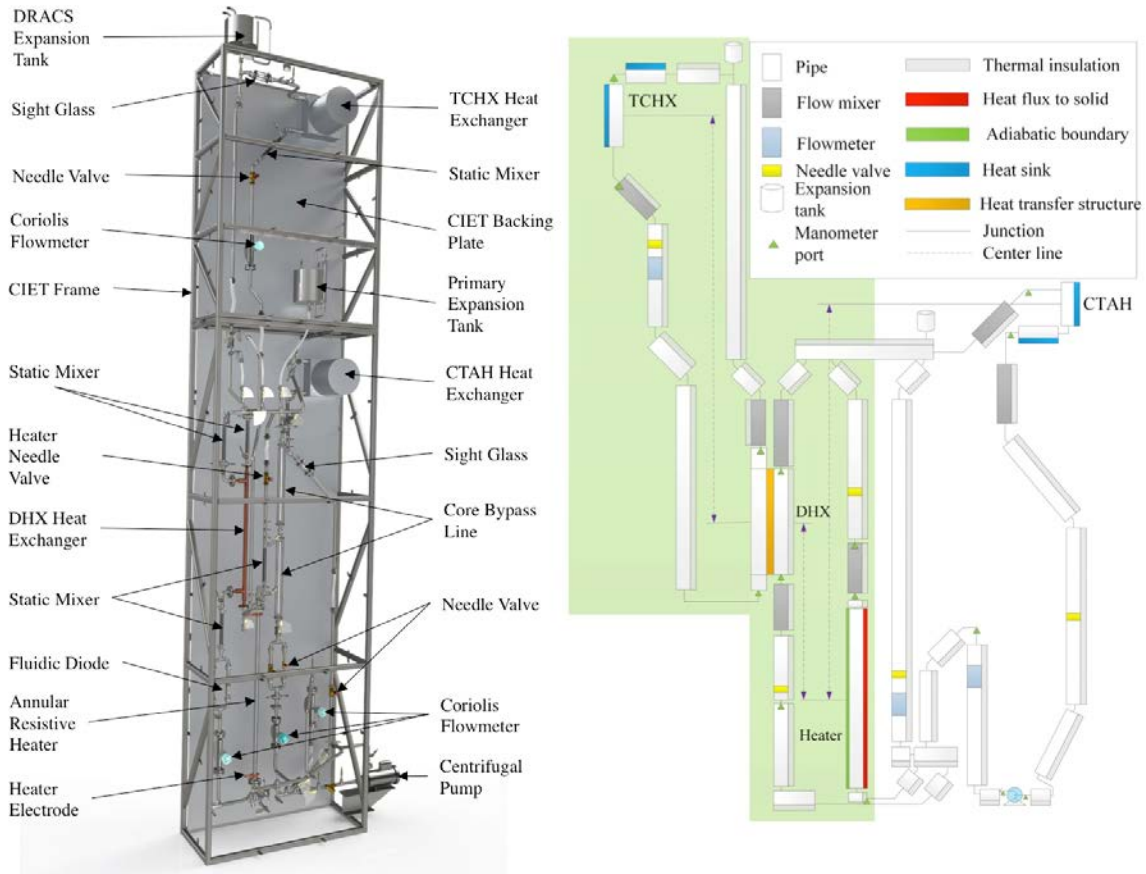

Figure 4.21: CIET 1.0 3-dimensional model, not showing insulation (left) and corresponding nodalization diagram for the RELAP5 and FANCY models (right).

Prior to the V&V effort, pressure drops were measured at various flow rates in each branch of the CIET 1.0 loop at room temperature during the previous quarter. The flow rate ranges selected for this series of tests covered Reynolds numbers (Re) up to 1,600 in each branch, corresponding to expected regimes during forced and natural circulation operation of CIET 1.0. The goal of these tests was to generate CIET-specific component-scale friction number correlations in the following non-dimensional form, which were subsequently implemented in RELAP5 and FANCY:

$$K + f\frac{L}{D} = A + B\,\mathrm{Re}^{-C}$$

Fluoride-salt-cooled High-temperature Reactor (FHR) Annual Report: 2015
MIT, U.C. Berkeley, U. of Wisconsin and U. of New Mexico
For Public Distribution

where K is the sum of form losses, f the friction factor, L the component length, D the component hydraulic diameter, and A, B and C empirically-derived coefficients. This series of tests validated the analytical correlation for laminar flow friction factor in straight, cylindrical pipes ($f = 64/\mathrm{Re}$) and its applicability to the CIET 1.0 annular heater, with an agreement within 10% between experimental data and the analytical correlation. Moreover, CIET-specific correlations were derived for static mixers, Coriolis flowmeters and fan-cooled heat exchangers, as listed in Table 4.1. These correlations yield higher friction numbers than vendor-provided charts over the range of Re of interest, therefore confirming the value of performing such tests prior to any V&V effort.

Table 4.1: CIET-specific friction number correlations for static mixers, Coriolis flowmeters and fan-cooled heat exchangers.

Component	Friction Number Correlation
Static Mixer	$K + f\dfrac{L}{D} = 21 + \dfrac{4{,}000}{\mathrm{Re}}$
Coriolis Flowmeter	$K + f\dfrac{L}{D} = 18 + \dfrac{93{,}000}{\mathrm{Re}^{1.35}}$
Fan-Cooled Heat Exchanger	$K + f\dfrac{L}{D} = 400 + \dfrac{52{,}000}{\mathrm{Re}}$

For this study, all calculations were run with RELAP5-3D/Ver. 4.0.3 and FANCY/Ver. 2.0 in transient mode until steady-state conditions are reached for fluid temperatures and mass flow rates in each loop.

For code verification, the following tests are performed at steady-state:
- Is the heat input to the fluid equal to the sum of the heat removed through the TCHX and parasitic heat losses along the loop?
- Is the mass flow rate uniform in each loop?
- Is energy and mass conservation verified in each loop?

The code results have passed these tests, hence partly verifying proper solving of the fundamental conservation equations.

For single natural circulation loops, at all power input levels and TCHX outlet temperatures tested at this point in time, the agreement between RELAP5 and experimental data for the loop mass flow is within 1% and the agreement between FANCY and experimental data is within 3%. For coupled natural circulation between the primary loop and the DRACS loop, the agreement between RELAP5 and experimental data remains within 8% and the agreement between FANCY and experimental data remains within 13% in both loops. The comparison between best estimate code solutions and experimental data in the non-dimensional space shows an excellent agreement between both code calculations and experimental data in the coupled loops, where flow is in the fully laminar regime. The results also show remarkable agreement with the correlation proposed by Vijayan for steady flow in a fully laminar natural circulation loop, which is the case here. These conclusions are supported by Figure **4.22**. For further information on model V&V for CIET performed at UCB a more detailed discussion of model V&V for CIET performed at UCB is included in a paper available in the NURETH-16 proceedings.

Fluoride-salt-cooled High-temperature Reactor (FHR) Annual Report: 2015
MIT, U.C. Berkeley, U. of Wisconsin and U. of New Mexico
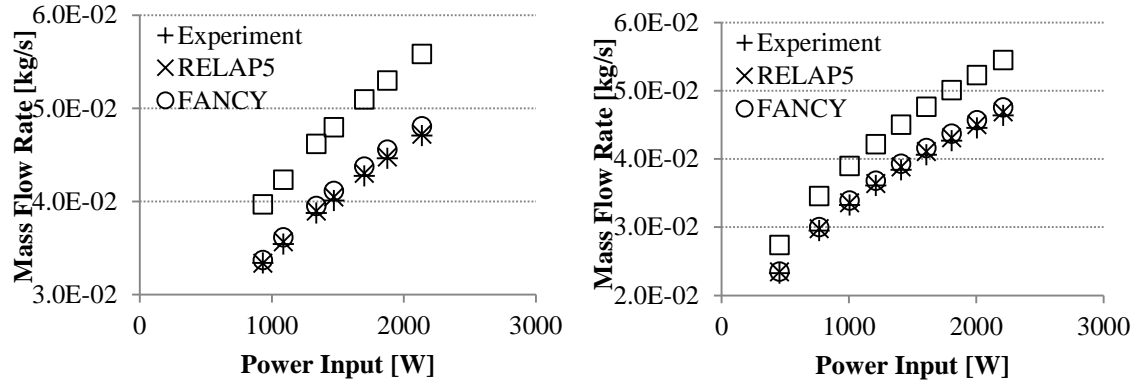For Public Distribution

Figure 4.22: Comparison of experimental, RELAP5, FANCY, and analytical natural circulation mass flow rates for various heat inputs and TCHX outlet temperatures of 46ºC (left) and 35ºC (right).

Forced Cooling, Power Step Change Model Validation

Experimental data has been collected for transient, forced cooling model validation using heat input step changes, a fixed coolant mass flow rate of 0.18 kg/s in the CTAH loop and a controlled CTAH outlet temperature of 80°C. Corresponding boundary conditions have been reproduced in RELAP5-3D. The only discrepancy between the model and the experiment is that RELAP5-3D uses a fixed CTAH outlet temperature boundary condition of 80°C instead of the more complex real evolution resulting from the CTAH controller on CIET, because of the lack of a detailed model for the CTAH at the time of this study. Power step changes under forced cooling operation with a fixed mass flow rate are aimed at validating the model for thermal inertia of the system's solid structures and fluid, which affects its response time to such transients.

Thermal capacities for each heat structure are documented in the RELAP5-3D input deck provided in Nicolas Zweibaum's PhD dissertation (see, "Published papers, reports, and theses,"). In particular, because the thermal capacity of the solid structures in the loop – ~50 kJ/K – is of the same order of magnitude as the thermal capacity of the oil – ~20 kJ/K –, it is important to account for both types of heat structures to accurately predict the system's transient behavior.

Figure 4.23 shows a comparison of RELAP5-3D results and experimental data for an entire test, and Figure 4.24 shows details of this comparison for a selection of power step changes up and down. Throughout the test, the agreement between RELAP5-3D results and experimental data is within 2°C. More specifically, the agreement is within instrumentation accuracy (±0.5°C) for the heater outlet temperature and there is a delay of ~100 s in the response of the CTAH inlet temperature to power step changes compared to experimental data. The agreement between code results and experimental data for the CTAH outlet and heater inlet temperatures is within instrumentation accuracy, except for the short periods during which the code uses an idealized CTAH outlet temperature boundary condition of 80°C instead of the more complex controller implemented on CIET 1.0.

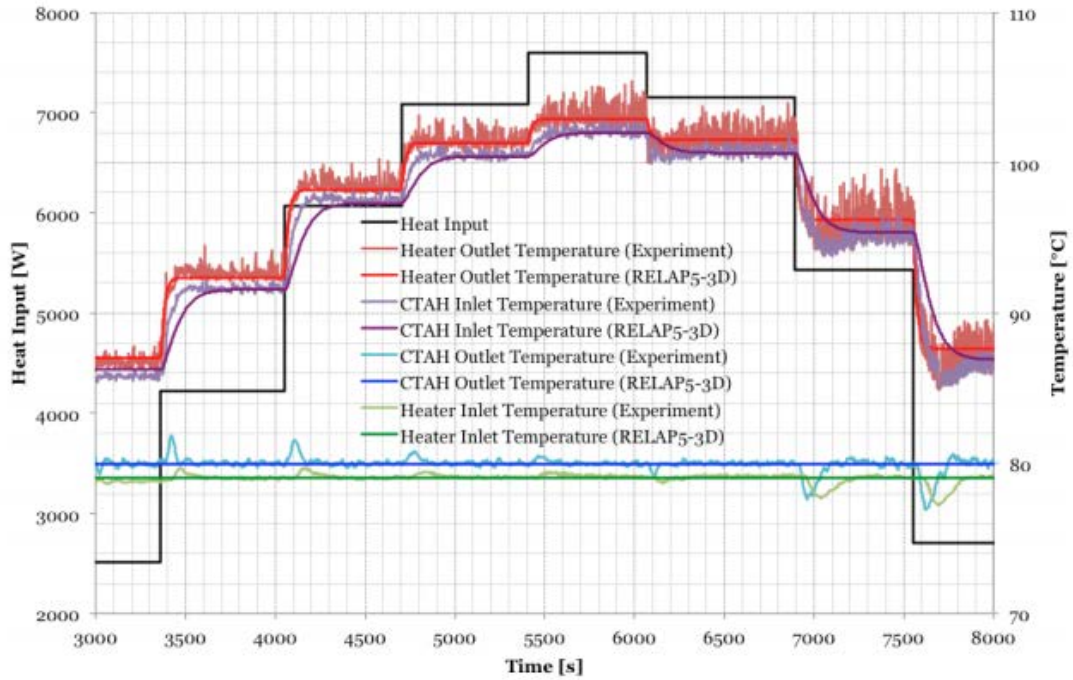Fluoride-salt-cooled High-temperature Reactor (FHR) Annual Report: 2015
MIT, U.C. Berkeley, U. of Wisconsin and U. of New Mexico
For Public Distribution

Figure 4.23. Experimental data and RELAP5-3D results for transient forced cooling in the CTAH loop.

Fluoride-salt-cooled High-temperature Reactor (FHR) Annual Report: 2015
MIT, U.C. Berkeley, U. of Wisconsin and U. of New Mexico
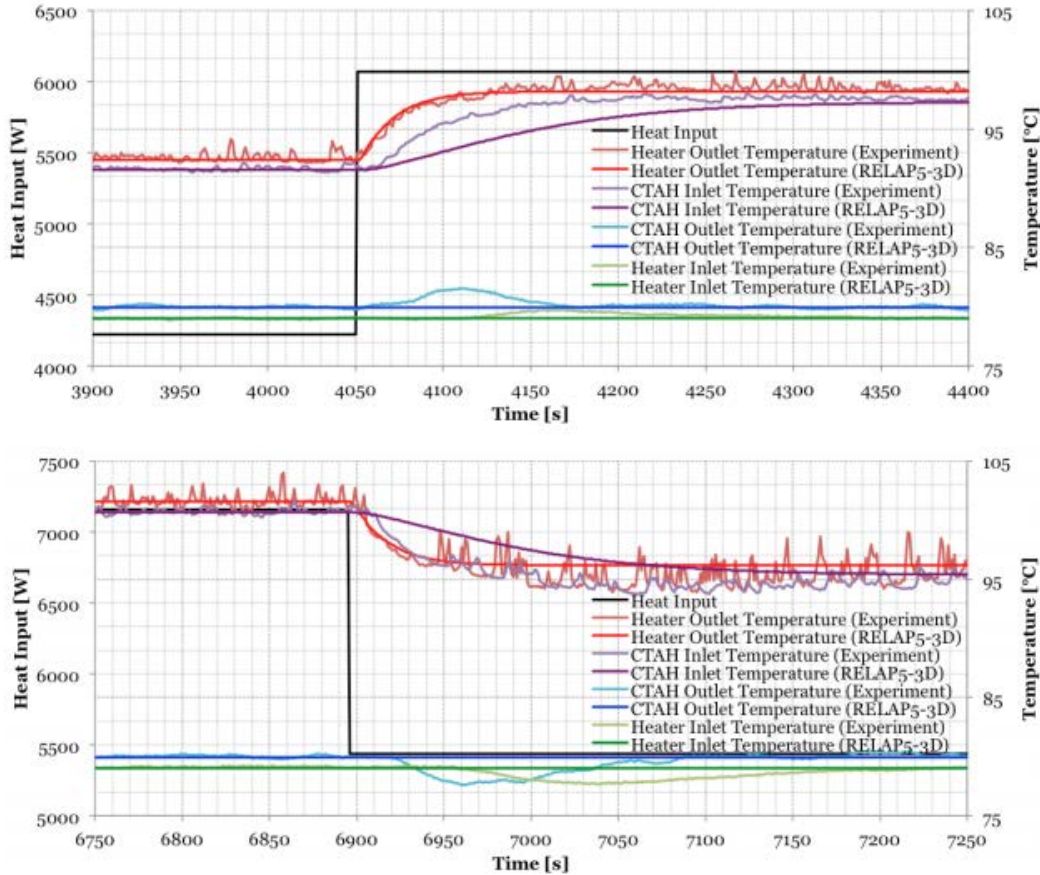For Public Distribution

Figure 4.24. Experimental data and RELAP5-3D results for transient forced cooling in the CTAH loop (details).

The fact that RELAP5-3D accurately predicts the transient increase of the heater outlet temperature indicates that the model has the correct thermal capacity for the heater element. Conversely, the thermal capacity between the heater outlet and the CTAH inlet does not appear to be modeled perfectly, since RELAP5-3D predicts a slower response of the CTAH inlet temperature than CIET produces. Because accurate data for the masses of the CIET thermal structures, and therefore for their thermal capacities, was measured during fabrication of the CIET 1.0 facility and implemented in the code, this disagreement may be due to the approach to modeling these structures, and the fact that some of the thermal structures (e.g. pipe walls), which have a large surface area compared to their thermal inertia, are more tightly coupled to the fluid than components with small surface areas compared to their thermal inertia (e.g. flanges, valves). As shown in Figure 4.25, closer agreement between code results and experimental data is indeed obtained by separating the weakly and the strongly coupled thermal masses into separate heat structures in the RELAP5-3D model, based upon measured values for weights of individual components and the fact that weakly coupled thermal masses account for ~20% of the total weight of the system's solid structures.
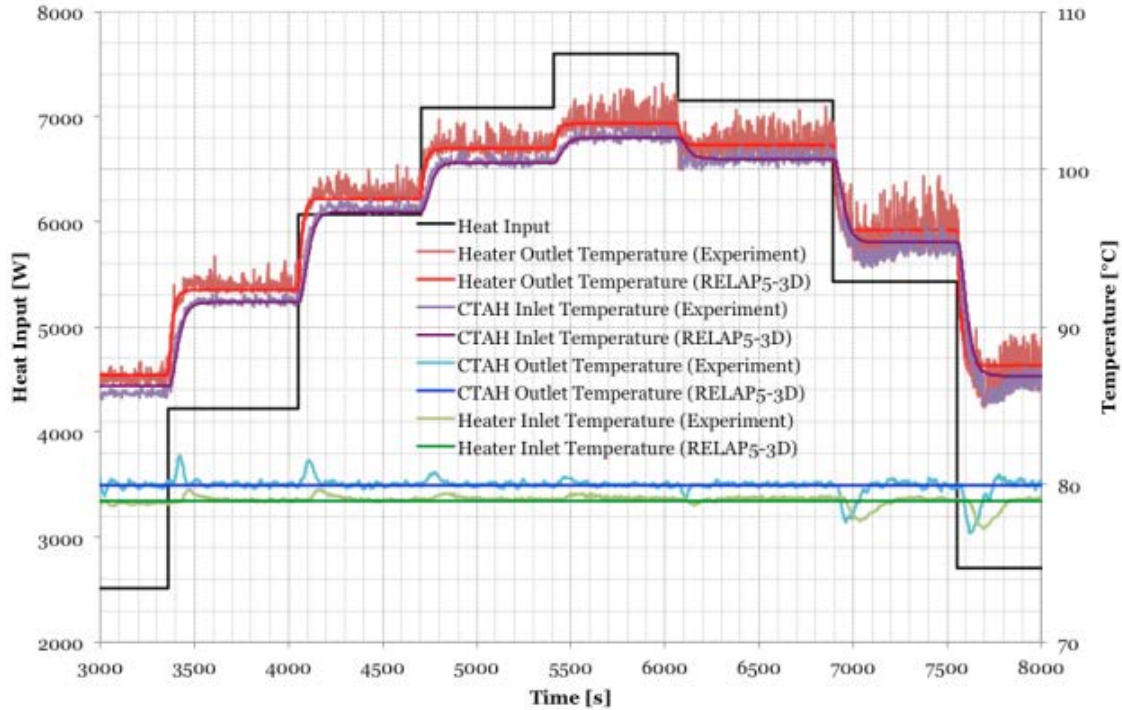
83

Fluoride-salt-cooled High-temperature Reactor (FHR) Annual Report: 2015
MIT, U.C. Berkeley, U. of Wisconsin and U. of New Mexico
For Public Distribution

Figure 4.25. Experimental data and RELAP5-3D results for transient forced cooling in the CTAH loop using decoupled heat structures.

More information can be found in Nicolas Zweibaum's PhD dissertation, (see, "Published papers, reports, and theses,").

COMSOL Mk1 PB-FHR Core Model

In the Mark I design, about 30% of the coolant flow is injected from the downcomer at the bottom of the core while the rest of the flow is injected radially from the center reflector channels. This cross flow design aims to reduce the pressure drop across the core and therefore reduce the total salt inventory and reduce the flow resistance under natural-circulation heat removal.

A hydrodynamics study has been conducted on coolant flow across the reactor core. Results of pressure loss under different inlet/outlet widths show that the pressure loss in the core can be reduced significantly by opening flow channels in the reflectors for radial injection and suction of the coolant, as shown in Figure 4.26.
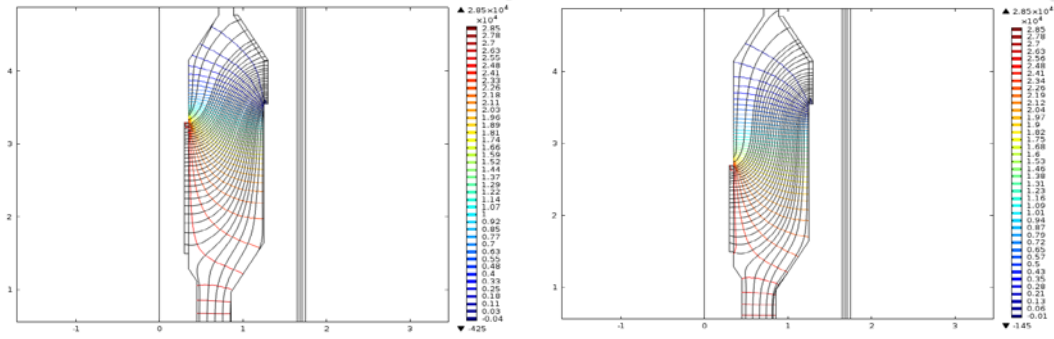
Fluoride-salt-cooled High-temperature Reactor (FHR) Annual Report: 2015
MIT, U.C. Berkeley, U. of Wisconsin and U. of New Mexico
For Public Distribution

**Figure 4.26. Streamlines (grey) and isobars (with color map) in the core
Left: H_inlet = 1.2m, H_outlet = 0.6m; Right: H_inlet = 1.8m, H_outlet = 0.6m.**

The next step consists of investigating the effects of changing the geometry on the heat transfer efficiency, and then an optimal design that results in a small pressure loss and a high equivalent heat transfer coefficient will be selected.

Preliminary model validation of transient behavior using LOFC testing

The next step in transient model V&V is validation of the RELAP5-3D model's ability to predict system behavior in the case of design basis accidents. The first experiment designed and conducted for this purpose using CIET 1.0 is the LOFC. The LOFC event is performed experimentally using CIET 1.0 by following the modified LOFC experimental procedure document (CIET-TEST-PLAN-012M-00_LOFCM_Test_Procedure) updated on 7/24/2015. This is a later iteration of the experimental procedure which includes improved clarity in its description of steps. There are two aspects to implementing the LOFC in the RELAP model. The first is the inclusion of appropriate steady-state conditions prior to the LOFC event and the second is the implementation of the specific procedures needed to reproduce the LOFC event. The steady-state conditions defined by the experimental procedure are listed below:

- CTAH Outlet Temp: 80°C
- TCHX Outlet Temp: 46°C
- DHX flowrate: 0.018 kg/s
- CTAH flowrate: 0.18 kg/s

The temperature and flow initial conditions are implemented by setting hydrodynamic component, junction, and branch initial conditions. Additionally, the flowrate in the CTAH is enforced by setting the time-dependent junction which represents the pump to supply a flowrate of 0.18 kg/s. An additional initial condition that was determined from CIET 1.0 steady-state experimental data is the definition of the temperature in the hot leg (where the CTAH outlet is the temperature in the cold leg) of the primary loop. This is estimated from the experimental results as 95°C. The RELAP simulation then finds its own steady-state condition but this process is expedited by using a reasonable value for the first guess.

After steady-state conditions are reached in the CIET facility, the LOFC transient steps can be performed. The experimental procedure for the LOFC transient is listed here:

1. Turn the pump feedback off.
2. Set the pump frequency to 0.
3. Set the "Desired Power" to 2kW.
4. Turn the CTAH fan feedback off.

85

Fluoride-salt-cooled High-temperature Reactor (FHR) Annual Report: 2015
MIT, U.C. Berkeley, U. of Wisconsin and U. of New Mexico
For Public Distribution

5. Set the CTAH fan frequency to 0.
6. Close valve V-40 to eliminate flow through the CTAH branch, representing an insurmountable pressure head through the CTAH branch during natural circulation decay heat removal in the primary loop. Because this valve does not have a counterpart in a prototypical system, the experimental procedure may need to be updated in future experiments.

Because CIET 1.0 is configured with automated controls which can respond to system conditions in order to try to maintain target values, feedback controls need to be shut off in the simulation of equipment failure. The question of how to implement these procedures in RELAP has been explored in our preliminary study and the individual events are listed here:

- The pump is set to a frequency of 0 by setting the time-dependent junction that acts as a pump to coast down to a flowrate of 0.
- The insurmountable pressure head through the CTAH branch during natural circulation operation is simulated by using a trip valve which closes at a specific time step.
- The heater power is changed from 6 kW to 2 kW using a heater power table which consists of time values and corresponding heater values.
- The CTAH unit in CIET 1.0 is a fan but is represented in the RELAP model as a heat structure that removes heat. The CTAH fan frequency is set to 0 by changing its heat transfer coefficient to 0 at the desired time.

In order to assess the capability of these events implemented in the RELAP model as accurate predictors of CIET 1.0 behavior, we have conducted a preliminary simulation of the LOFC event using the RELAP model. The data from this study is presented along with experimental data for the LOFC experiment in CIET 1.0 in Figure 4.27 and Figure 4.28. The time period in focus for the transient is the 100-second interval which begins at steady-state, experiences flow reversal as the trips occur, and ends as the DRACS loop begins to remove decay heat. For this preliminary study, we compare two sets of data: temperatures and flowrate across components. The temperatures we examine are the inlet and outlet for both the heater and the DHX which are shown in Figure 4.27. We also examine the flowrate across the heater, the CTAH, and the DHX in Figure 4.28.

We will first compare the temperature results from the RELAP LOFC simulation with the experimental results from the CIET 1.0 facility. Each component temperature in focus is color-coded with dashed lines representing RELAP simulation results and solid lines representing experimental results. It is first important to note that the temperatures initially increase and decrease in accordance with response to the LOFC event, which supports the RELAP model's capability of producing physically consistent behavior. However, it is clear that the RELAP simulation does not predict the CIET 1.0's temperature change to the accuracy desired. More specifically, the concavity of the RELAP-predicted temperature curves do not match the more sudden changes exhibited in the physical system. The RELAP results show a heater outlet temperature that continues to increase while the CIET 1.0 data shows a peak. In all temperature profiles, the RELAP results do not capture the response of the system to the loss of heat transfer to the CTAH and increased heat transfer to the DHX. This may indicate that these preliminary results do not accurately replicate the performance of the DRACS loop in removing increased amounts of heat. This is supported by the convergence of the DHX inlet and outlet temperatures in the RELAP results, representing minimal heat removal, while the DHX inlet and outlet temperatures diverge in the experimental results. Another apparent source of inconsistency is the difference in the steady-state conditions reached by the RELAP model versus CIET 1.0, which may have a significant impact on simulated response. These inconsistencies, however, will be further explored and understood in future work with a focus on better modeling the heat transfer to the DRACS loop.
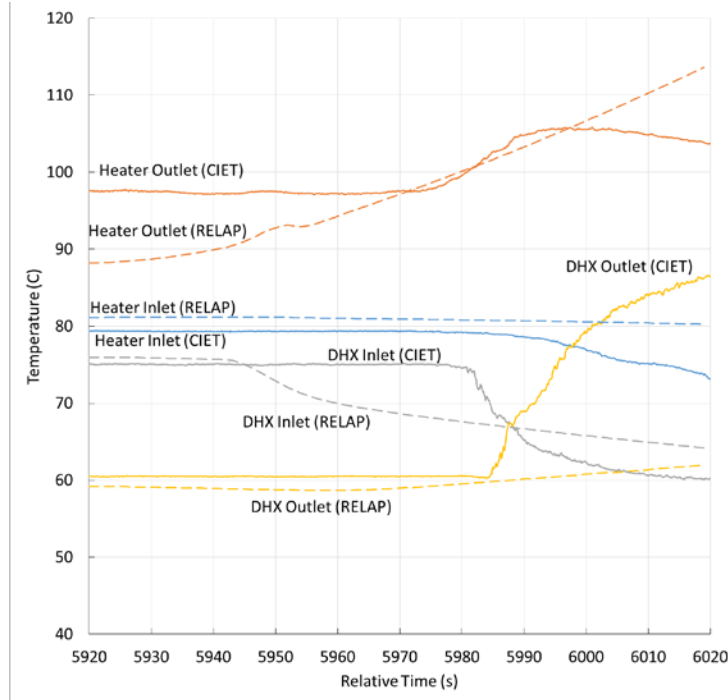
Fluoride-salt-cooled High-temperature Reactor (FHR) Annual Report: 2015
MIT, U.C. Berkeley, U. of Wisconsin and U. of New Mexico
For Public Distribution

Figure 4.27. Temperature comparison of heater and DHX inlet and outlet for CIET 1.0 experimental results and RELAP simulation results

We will next compare the flowrate results from the RELAP simulation with the experimental results from the CIET 1.0 facility. Like the temperature data, the flowrate data is color-coded and differentiated by line type. The flowrate results from RELAP seem to trend alongside the experimental results. The flowrate in the RELAP simulation across the heater and the DHX after the initial component trips, however, has a much lower magnitude than the flowrate in the experimental results. The RELAP simulation also seems to predict a much more stable response from the system while there is some fluctuation immediately following the LOFC event in CIET 1.0 which may be attributable to the time delay between experimental procedures. One possible reason for the difference in magnitude may be the improperly modeled flow losses during the LOFC event or missing information in the inertia of the DRACS loop. Discovering the source of this flowrate inconsistency will be a primary goal in the further development of the LOFC model.
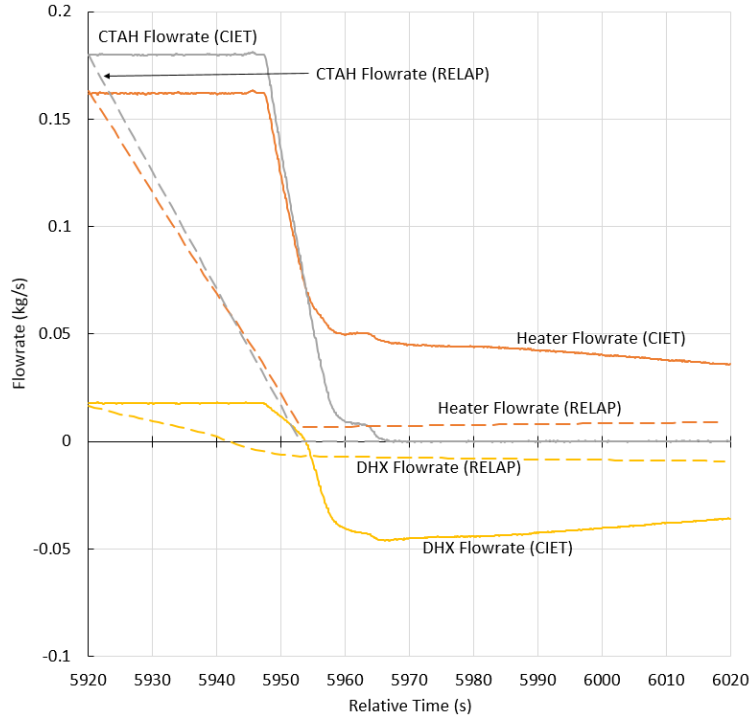
Fluoride-salt-cooled High-temperature Reactor (FHR) Annual Report: 2015
MIT, U.C. Berkeley, U. of Wisconsin and U. of New Mexico
For Public Distribution

Figure 4.28. Flowrate comparison of heater, DHX, and CTAH for CIET 1.0 experimental results and RELAP simulation results.

However, it is promising to see that each of the flowrate trends studied does follow the same trend as in the experimental system. Most importantly, flow reversal is demonstrated in the DHX, flow stoppage is demonstrated in the CTAH, and flow reduction is demonstrated in the heater as the pump shuts off and forced circulation is lost in the CTAH branch of the primary loop. One possible influential factor on the discrepancy in the magnitude of flowrate predictions in the RELAP simulation is that flowrate changes, as shown in Figure 5, are much more gradual than in the experimental configuration of the LOFC event. This may be due to some lack of fidelity in modeling the pump coast down and heater power drop and will be a first step in improving the model.

For transient, forced cooling in the CTAH loop using step changes to heater power input, agreement between RELAP results and experimental data is within 1°C for a fixed coolant mass flow rate and controlled CTAH outlet temperature. This agreement was also accomplished by decoupling heat structures with small surface areas compared to their thermal inertia. This study both validated the use of RELAP models to predict system behavior in the case of power step changes under forced circulation, and provided insight into the modeling of heat structures using RELAP.

Our preliminary study of the LOFC transient event modeled in RELAP has yielded useful results in the improvement of models for prediction of the CIET 1.0 facility's response in design basis scenarios. It demonstrates prediction of initial trends in temperature changes as well as flow reversal and flow distribution in the reactor loops. Transition of flow from the CTAH branch of the primary loop to the DHX branch is also demonstrated. Because there are significant inconsistencies between the RELAP results and the experimental results for the flowrate across facility components in particular, there is study needed before further conclusions can be drawn in the validation effort.

Task 3.1(c): Neutronic Simulation Models with Capability to Couple to Thermal Hydraulics Models

Coupled Kinetics and Thermal Hydraulics Model for FHR Transient Analysis

Fluoride-salt-cooled High-temperature Reactor (FHR) Annual Report: 2015
MIT, U.C. Berkeley, U. of Wisconsin and U. of New Mexico
For Public Distribution

Multi-point Kinetic Equations

The (standard) point kinetics equations can compute the time dependent reactor power $P(t)$ and the delayed neutron precursors $C_i(t)$ concentration:

$$\frac{dP(t)}{dt} = \frac{(\rho(t)-\beta)}{\Lambda} P(t) + \sum_{i=1}^{6} \lambda_i C_i(t) \qquad (0.6)$$

$$\frac{dC_i(t)}{dt} = \frac{\beta_i}{\Lambda} P(t) - \lambda_i C_i(t), \, i = 1...6 \qquad (0.7)$$

where ρ is reactivity, and β is the effective delayed neutron fraction, which is the sum of all β_i, the effective delayed neutron precursor yield of group i. Λ is the prompt neutron generation time, and λ_i is the decay constant for the i-th delayed neutron precursor group. However, the one-point kinetics model does not take into account changes in flux shape during a transient. For reactivity insertion transients driven by removal of one or more control rods, the flux shape changes appreciably during the transient. For the PB-FHR of particular importance are the neutrons from the reactor fuel region which are transported to the reflectors (where the control rods are located), scatter within the reflectors for some time, and come back to the fuel region to initiate a fission reaction. In the Mk1 PB-FHR, the inner reflector and the outer reflector (including graphite pebbles) provide both moderation and reflection. As shown in Table 4.2, k_{eff} and prompt neutron lifetime changes dramatically with different control rod configurations; therefore, the effects of inner and outer reflector neutron moderation must be considered.

Table 4.2: Effect of reflectors on k_{eff} and prompt neutron lifetime.

Configuration	k_{eff}	Effective prompt neutron lifetime (s)
Fuel and both reflectors	1.03	0.000459
Fuel and outer reflector	0.95	0.000384
Fuel and inner reflector	0.88	0.000399
Fuel only	0.73	0.000227

The reflector-induced effects can be characterized by the reactivity gain due to the reflector ρ_R and the sum of neutron lifetime in the fuel region and in the reflector Λ_R. The slow neutrons coming back from the reflectors into the fuel region in each configuration can be modeled as additional delayed neutron groups from fictitious neutron emitters. In this sense, a change in configuration of the control rods alters the dynamics of the chain reaction and can be modeled by adding a group of delayed neutrons.

The multipoint kinetics model is formulated for FHR cores with additional fictitious delayed neutron groups as follows:

Fluoride-salt-cooled High-temperature Reactor (FHR) Annual Report: 2015
MIT, U.C. Berkeley, U. of Wisconsin and U. of New Mexico
For Public Distribution

$$\frac{dP(t)}{dt} = \frac{(\rho_{ext}(t) - \beta - \rho_{Ri} - \rho_{Ro})}{\Lambda_c} P(t)$$
$$+ \sum_{i=1}^{nd} \lambda i \, C i \,(t) + \lambda_R C_R(t) \qquad (0.8)$$

$$\frac{dCi(t)}{dt} = \frac{\beta i}{\Lambda_c} P(t) - \lambda i \, Ci \,(t), \; i = 1...nd \qquad (0.9)$$

$$\frac{dC_{Ri}(t)}{dt} = \frac{\rho_{Ri}}{\Lambda_c} P(t) - \lambda_{Ri} C_{Ri}(t) \qquad (0.10)$$

$$\frac{dC_{Ro}(t)}{dt} = \frac{\rho_{Ro}}{\Lambda_c} P(t) - \lambda_{Ro} C_{Ro}(t) \qquad (0.11)$$

where Λ_c is the prompt neutron generation time in the core, without any reflectors. $\lambda_{Ri} = 1/\Lambda_{Ri}$, where Λ_{Ri} is the sum of neutron lifetime in the inner reflector and neutron lifetime in the core after coming back from the reflector(s). This value can be calculated from Λ_{prt}, the mean prompt neutron lifetime in the reactor including inner and outer reflectors, and Λ_{ci}, the prompt neutron generation time in the core with only outer reflector, by the following relation:

$$\Lambda_{prt} = (1 - \rho_{Ri})\Lambda_{ci} + \rho_{Ri}\Lambda_{Ri} \qquad (0.12)$$

where ρ_{Ri} is the reactivity gain by the inner reflector(k_{eff}^{io}) comparing to the core with only the outer reflector(k_{eff}^{o})

$$\rho_{Ri} = \frac{k_{eff}^{io} - k_{eff}^{o}}{k_{eff}^{o}} \qquad (0.13)$$

Similarly for the outer reflector, $\lambda_{Ro} = 1/\Lambda_{Ro}$, where Λ_{Ro} can be calculated from Λ_{co} and ρ_{Ro} by the following relationship:

$$\Lambda_{prt} = (1 - \rho_{Ro})\Lambda_{co} + \rho_{Ro}\Lambda_{Ro} \qquad (0.14)$$

$$\rho_{Ro} = \frac{k_{eff}^{io} - k_{eff}^{i}}{k_{eff}^{i}} \qquad (0.15)$$

The reactivity is calculated as the sum of external reactivity insertion and temperature reactivity feedback.

In the current model, the reactivity feedback coefficients, α, are assumed not to vary with time or temperature and the reactivity can be computed as:

$$\rho(t) = \rho_{ext}(t) + \alpha_F (T_F(t) - T_{F,0}) +$$
$$\alpha_M (T_M(t) - T_{M,0}) + \alpha_C (T_C(t) - T_{C,0}) \qquad (0.16)$$

Fluoride-salt-cooled High-temperature Reactor (FHR) Annual Report: 2015
MIT, U.C. Berkeley, U. of Wisconsin and U. of New Mexico
For Public Distribution

The multi-point model parameters (Table 4.3) and the moderator, fuel and coolant temperature reactivity coefficients (Table 4.4), as well as the kinetic parameters (Table 4.5) are computed from a full core model using the Monte Carlo code, Serpent. To calculate the temperature reactivity coefficient, the temperature of the component is varied by 100 K in the range between 800 K and 1200 K by changing the material temperature and density in the Serpent input file. The coolant temperature reactivity coefficient includes the effect of temperature on cross sections and the effect of density change due to temperature.

Table 4.3: Parameters used in the multi-point model for Mk1 PB-FHR core.

Property	Value
λ_{Ri} [1/s]	786
λ_{Ro} [1/s]	1209
ρ_{Ri}	0.084
ρ_{Ro}	0.169
Λ_c [s]	0.000227

Table 4.4: Temperature reactivity coefficient of the layers in the Mk1 fuel pebble and the coolant.

Component	Feedback [pcm/k]
Moderator	-0.70
Fuel	-3.19
Shell	-0.70
Coolant	+0.23

Table 4.5: Kinetic parameters in Mk1 PB-FHR core.

Group	β_i	λ_i [1/s]
1	2.05E-04	1.25E-02
2	1.16E-03	3.17E-02
3	1.05E-03	1.09E-01
4	2.77E-03	3.17E-01
5	8.40E-04	1.35E+00
6	3.02E-04	8.68E+00

Heat diffusion equations

The Biot number of the fuel pebble is approximately 94, using the nominal pebble bed heat transfer coefficient is approximately 4700 W/m^{2}K and a nominal equivalent thermal conductivity estimation of the HTGR fuel pebble.

$$Bi = \frac{hD}{k} \qquad (0.17)$$

Therefore the radial variation of temperature in the pebble is not negligible compared to that in the coolant. Heat diffusion equations are used to compute the temperature profile inside the fuel pebble as a

Fluoride-salt-cooled High-temperature Reactor (FHR) Annual Report: 2015
MIT, U.C. Berkeley, U. of Wisconsin and U. of New Mexico
For Public Distribution

function of time. Assuming all the nuclear heat is deposited in the fuel and transferred to moderator kernel and graphite shell via conduction, a 1-D heat diffusion equation in spherical coordinates is:

$$\rho c_p \frac{\partial T}{\partial t} = \frac{1}{r^2} \frac{\partial}{\partial r} \left(kr^2 \frac{\partial T}{\partial r} \right) + g \qquad (0.18)$$

where r is the radial location of the point and g is the heat generation density.

A Dirichlet boundary condition at r=0 and a mixed boundary condition at r=R are imposed.

$$\frac{\partial T}{\partial r}\Big|_{r=0} = 0$$

$$\frac{\partial T}{\partial r}\Big|_{r=R} = \frac{h}{k}(T - T_\infty) \qquad (0.19)$$

This equation can be written in a simpler form by introducing a new variable $U(r,t) = rT(r,t)$ as:

$$\frac{\partial U}{\partial t} = \alpha \frac{\partial^2 U}{\partial r^2} + r \frac{g}{\rho Cp} \qquad (0.20)$$

And the boundary conditions become

$$U_0 = 0 \qquad\qquad (0.21)$$

$$\frac{\partial U}{\partial r}\Big|_{r=R} = \left(\frac{1}{R} - \frac{h}{k} \right) U + \frac{R}{k} hT_\infty \qquad (0.22)$$

This new equation system is solved numerically under finite volume discretization.

Convective heat transfer at fuel pebble surface

In this work, a single-phase convective heat transfer model is applied to the coolant as flibe remains in liquid phase between 458°C and 1400°C.

$$\frac{dT_c}{dt} = \frac{1}{\left(\rho c_p V \right)_S} * \left[-\dot{m} c_p \left(T_{out} - T_{in} \right) + hA \left(T_s - T_C \right) \right] \quad (0.23)$$

T_{out} and T_{in} are outlet and inlet coolant temperatures. The bulk coolant temperature is calculated as

$$T_C = \frac{T_{in} + T_{out}}{2} \qquad (0.24)$$

Using the Wakao correlation for the pebble bed heat transfer coefficient, the fluid-to-pebble Nusselt number is:

$$Nu = 2 + 1.1 Pr^{1/3} Re^{0.6} \qquad (0.25)$$

Fluoride-salt-cooled High-temperature Reactor (FHR) Annual Report: 2015
MIT, U.C. Berkeley, U. of Wisconsin and U. of New Mexico
For Public Distribution

The Reynolds number *Re* and the Prandtl number *Pr* are determined as follows,

$$Re = \frac{\rho d_p u}{\mu}$$

(0.26)

where *u* is the superficial velocity $u = \frac{\dot{m}}{A\rho}$, $\dot{m}$ is the mass flow rate, ρ is the density and A is the cross section surface area.

$$Pr = \frac{c_p \mu}{k}$$

(0.27)

The heat transfer coefficient h can then be calculated from

$$h = \frac{Nu.k}{d_p}$$

(0.28)

Implementation in Python

This work relied on and extended the Python for Reactor Kinetics (PyRK, pyrk.github.io) package. This package provides a modular simulation environment for coupled point-reactor kinetics and thermal hydraulics. This open source Python package provides a modular and generic material definition framework, a coupled lumped parameter thermal hydraulics model with zero-dimensional neutron kinetics, and an application program interface (API) for freely distributed ANSI standard precursor data. Its object-oriented modeling paradigm and generic structure provided an extensible, design-agnostic toolkit for this accident analysis.

Reactivity Insertion Transient Analysis for FHRs

A reactivity insertion occurs for example when a reactor control element is partially or fully removed from the core. In this paper, reactivity insertions of 1$, 1.5$, and 2$ in a 10s ramp are investigated. These events are unlikely because the maximum reactivity worth of an entire single control rod is conventionally limited to be less than 1$ in reactor design.

The fuel and coolant temperature during reactivity insertions is plotted in Figure 4.29 and Figure 4.30. The nuclear power transient is plotted in Figure 4.31.
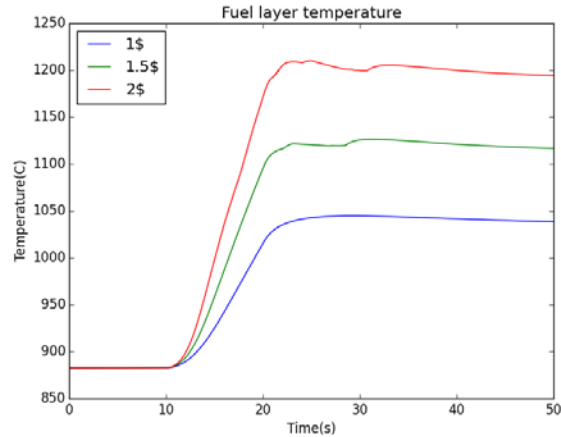
Fluoride-salt-cooled High-temperature Reactor (FHR) Annual Report: 2015
MIT, U.C. Berkeley, U. of Wisconsin and U. of New Mexico
For Public Distribution

Various temperature feedback mechanisms will stabilize the reactor at a higher equilibrium temperature. The temperature rise is proportional to the inserted reactivity. The final temperature following a 2$ reactivity insertion is 1220ºC in the fuel and 946ºC in the coolant.

Uncertainty and Sensitivity Study

Some input parameters for the model are measured with uncertainties since they vary during the reactor lifetime. This uncertainty and sensitivity study investigates the range of selected output parameters during 1$ reactivity insertion transient and their sensitivities with respect to the uncertainties in the selected input parameters. The effect of uncertainties of the following input parameters is studied:

- effective conductivity of the three layers in the fuel pebble: k_m, k_f, and k_s [W/m.K]
- specific heat capacity of the three layer in the fuel pebble and of the coolant: cp_m, cp_f, cp_s and cp_c [J/kg.K]
- pebble bed convective heat transfer coefficient: h [W/m^2.K]
- temperature reactivity feedback coefficient of the coolant: α_c [pcm/K]
- temperature reactivity feedback coefficient of the fuel: α_d [pcm/K]

Material properties are measured with uncertainties because they vary with radiation damage. The fuel element conductivity is distributed uniformly between 15 W/m.K and 19 W/m.K. Other material property uncertainties are assumed as a 5% interval around their nominal values in this study. More detailed knowledge about their uncertainties will be included in a future study. Some input parameters are calculated from correlations or other computer models with uncertainties. The pebble bed heat transfer coefficient is sampled in 30% error interval centered at the nominal value. Uncertainties in temperature reactivity coefficients are estimated using Serpent[4].

The code is run with 1500 sets of input parameters that are generated by Monte Carlo sampling in their uncertainty space (shown in Table 4.6). The range of steady state temperature and maximum fuel temperature during the transient is discussed in the following sections.

Uncertainty Range of Output Parameters

The empirical probability distribution of the peak fuel temperature and temperature rise during the transient is plotted in histograms shown in Figure 4.32 and Figure 4.33. The 95% confidence interval for the maximum temperature during the transient is [862ºC, 917ºC]. The average temperature rise in fuel pebbles during a 1$ reactivity insertion transient is about 167K ± 24K. The maximum coolant temperature ranges from 745ºC to 786ºC with 95% confidence.

Table 4.6: Probability distribution for Input parameters used in the uncertainty study.

	Input parameters	M	σ	distribution
Neutronics	α_c [pcm/K]	0.23	0.11	Gaussian
	α_d [pcm/K]	-3.19	0.1595	Gaussian
Heat transfer	k_m [W/m/K]	17	1.15	uniform
	k_l [W/m/K]	15	1.15	uniform
	k_s [W/m/K]	17	1.15	uniform
	cp_m [J/kg/K]	1818	90.9	Gaussian
	cp_f [J/kg/K]	1818	90.9	Gaussian
	cp_s [J/kg/K]	1818	90.9	Gaussian
	cp_c [J/kg.K]	2415.78	120.789	Gaussian
	h [W/m^2.K]	4700	940	Gaussian

Fluoride-salt-cooled High-temperature Reactor (FHR) Annual Report: 2015
MIT, U.C. Berkeley, U. of Wisconsin and U. of New Mexico
For Public Distribution
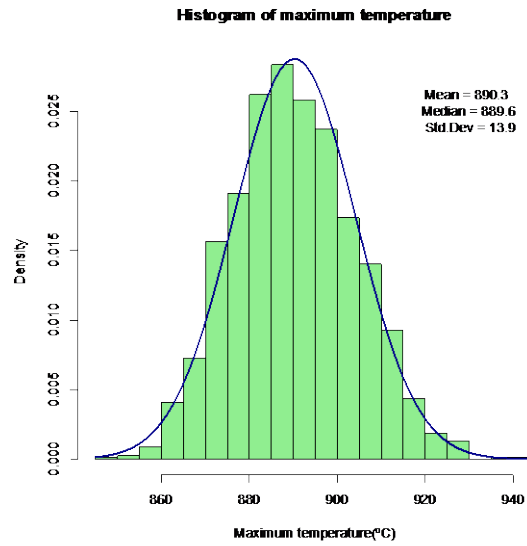
Figure 4.32: Histogram of maximum fuel temperature.
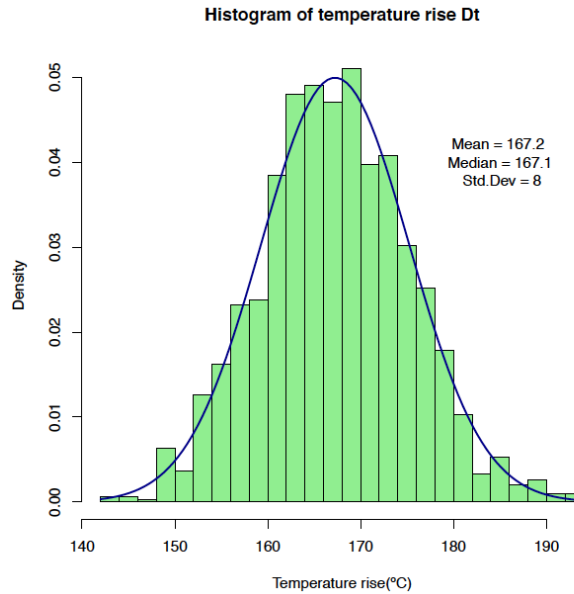
Figure 4.33: Histogram of temperature rise in fuel layer of the pebble.

Multi-Group Neutron Diffusion Model

The multi-group neutron diffusion equation is used to determine the neutron distribution in a reactor core. In eigenvalue mode, the effective multiplication factor k_{eff} is inserted to the neutron balance equation to represent the variation of neutron population from one generation to another.

$$-\nabla D_g \nabla \Phi_g + \Sigma_{Rg} \Phi_g = \sum_{g'=1}^{g-1} \Sigma_{sg'g} \, \Phi_{g'} + \frac{1}{k_{eff}} \chi_g \sum_{g'=1}^{G} \nu_{g'} \Sigma_{fg'} \, \Phi_{g'}$$

96

Fluoride-salt-cooled High-temperature Reactor (FHR) Annual Report: 2015
MIT, U.C. Berkeley, U. of Wisconsin and U. of New Mexico
For Public Distribution

D_g is the diffusion coefficient of group g, Σ_{Rg} is the removal cross section in group g, $\Sigma_{sg'g}$ is the scattering cross section from group g to g', $\nu_{g'}\Sigma_{fg'}$ is the average number of neutrons emitted per fission times the fission cross section, χ_g is the fraction of neutrons born in group g.

The energy spectrum is divided using an eight-energy group structure in Table 4.7. Two energy groups are added on the six-group structure to capture the cross section change Pu and isotopes in the flibe salt.

Temperature (density) dependent scattering and removal cross sections data are calculated as log-linear function of the fuel temperature and as linear function of the flibe density. Fission cross sections in the fuel region are also modeled as a log-linear function of the fuel temperature.

$$\Sigma(T_{fuel}) = c0 + c1 * \log(T_{fuel})$$
$$\Sigma(\rho_{flibe}) = c0 + c1 * \rho_{flibe}$$

Table 4.7: Energy group structure adopted in the multi-group diffusion model

Gr	upper bound [MeV]	lower bound [MeV]
1	1.00E+37	1.40E+00
2	1.40E+00	2.50E-02
3	2.50E-02	4.80E-05
4	4.80E-05	4.00E-06
5	4.00E-06	5.00E-07
6	5.00E-07	1.90E-07
7	1.90E-07	5.80E-08
8	5.80E-08	0.00E+00

Fluoride-salt-cooled High-temperature Reactor (FHR) Annual Report: 2015
MIT, U.C. Berkeley, U. of Wisconsin and U. of New Mexico
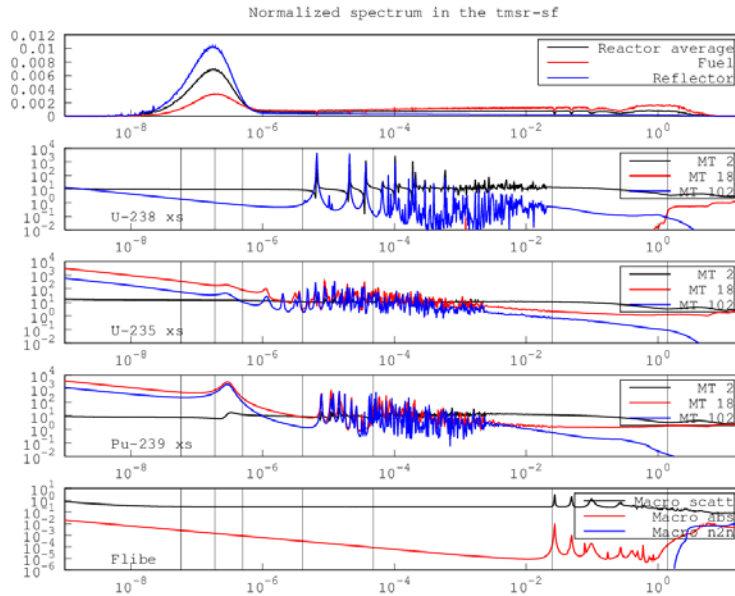For Public Distribution

Figure 4.34: Energy group structure and important isotope cross sections

Heat Transfer Model

Nuclear power is generated inside the fuel pebbles and transferred in the coolant through heat convection. Heat transfer between fuel pebble and coolant is computed:

$$Q''' = -h\frac{A}{v}(Ts - Tf)$$

where h is the convective heat transfer coefficient, computed using the Wakao correlation n. Ts is the solid temperature and Tf is the fluid temperature.

Spatial temperature distribution in the homogenized coolant/pebble material is computed with equivalent thermal properties. An equivalent composite material is defined as 40% of fuel pebbles and 60% of flibe salt. Properties such as conductivity, heat capacity is defined as a volume weighted sum of two material properties.

Implementation in COMSOL

A two-dimensional neutron diffusion model is developed for the TMSR core using the finite element software COMSOL Multiphysics. Once verified, the methodology can be applied to Mk1 PB-FHR core because of their similarities in design. The COMSOL Multiphysics is a software package that uses the finite element method for spatial discretization to solve systems of PDEs or ODEs. User can either use pre-defined multiphysics modules or specify a system of user-defined PDEs. The LiveLink™ for MATLAB® module in COMSOL allows user to define the COMSOL model parameters through a MATLAB interface, which further extends its versatility.

The group constants used in the diffusion equation are generated with the three-dimensional continuous energy Monte Carlo neutron transport code Serpent. The data are calculated at five different

Fluoride-salt-cooled High-temperature Reactor (FHR) Annual Report: 2015
MIT, U.C. Berkeley, U. of Wisconsin and U. of New Mexico
For Public Distribution

fuel temperatures(300K, 600K, 900K, 1200K, 1500K) and five different flibe densities(17 kg/m^3, 18 kg/m^3, 19 kg/m^3, 20 kg/m^3, 21 kg/m^3). In this project, a MATLAB package is developed for automatically reading data from Serpent output files and producing temperature/density dependent group constant for as many neutron energy groups as deemed necessary.

The neutron diffusion model is based on the COMSOL built-in 'PDE interfaces' in the following form:
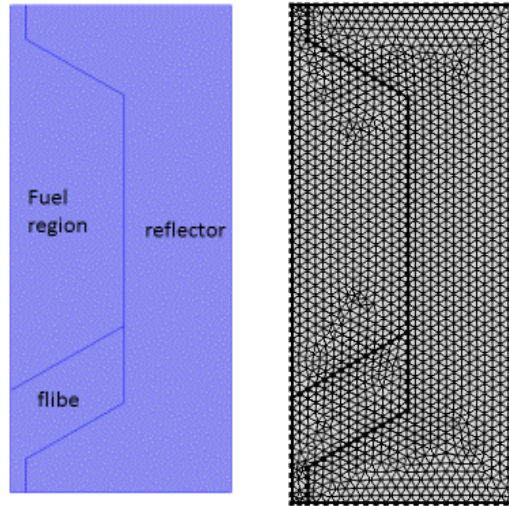

Figure 4.35: Schematic representation of the COMSOL model and the mesh (49232 degree of freedom)

$$\begin{bmatrix} -\nabla D_1 \nabla & \cdots & 0 \\ \vdots & \ddots & \vdots \\ 0 & \cdots & -\nabla D_G \nabla \end{bmatrix} \begin{bmatrix} \phi_1 \\ \vdots \\ \phi_G \end{bmatrix}$$
$$+ \begin{bmatrix} \Sigma_{R1} - \dfrac{1}{k} v_1 \chi_1 \Sigma_{f1} & -\Sigma_{s21} - \dfrac{1}{k} v_2 \chi_1 \Sigma_{f2} \cdots & -\Sigma_{sG1} - \dfrac{1}{k} v_G \chi_1 \Sigma_{fG} \\ -\Sigma_{s12} - \dfrac{1}{k} v_1 \chi_2 \Sigma_{f1} & \ddots & \vdots \\ \vdots & \cdots & \Sigma_{RG} - \dfrac{1}{k} v_G \chi_G \Sigma_{fG} \end{bmatrix} \begin{bmatrix} \phi_1 \\ \vdots \\ \phi_G \end{bmatrix} = 0$$

A symmetry boundary condition (BC) is used at the core centerline(r=0) and vacuum BC is used at the outer reflector surfaces.

In the TMSR core, coolant enters at the bottom inlet and flows upward at an average velocity of 0.18m/s. Uniform and fixed axial coolant velocity is assumed in the current model. Conservative adiabatic boundary condition is applied beyond the reflector.

At the nominal fuel temperature (900K) and the nominal flibe density (1900 kg/m3), the neutron flux of different energy groups are shown in

Figure **4.36**.
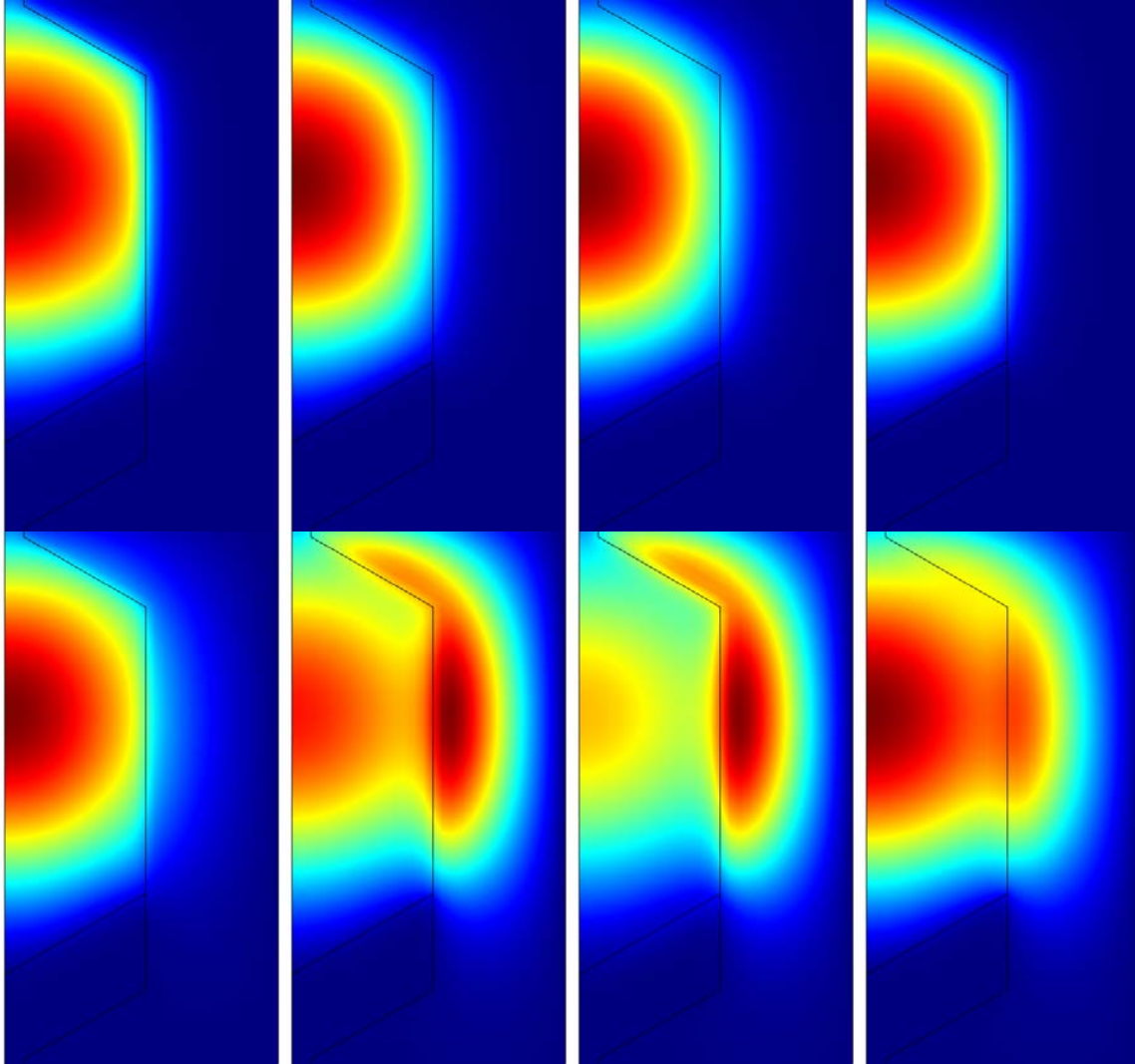
Fluoride-salt-cooled High-temperature Reactor (FHR) Annual Report: 2015
MIT, U.C. Berkeley, U. of Wisconsin and U. of New Mexico
For Public Distribution

Figure 4.36: flux of neutrons in eight energy groups, from high energy to low energy

Fluoride-salt-cooled High-temperature Reactor (FHR) Annual Report: 2015
MIT, U.C. Berkeley, U. of Wisconsin and U. of New Mexico
For Public Distribution

Model Validation

In order to validate the COMSOL model, results of the multiplication factor k_{eff} is compared to the Serpent full core model. Serpent solve the neutron transport equation in integral form using continuous energy nuclear data with virtually no approximation; therefore it produces valuable reference results for such validation process when experimental data are not available. The reactivity is calculated from k_{eff} as

$$\rho = \frac{k_{eff} - 1}{k_{eff}}$$

In
Figure **4.37**, the difference between the reactivity at various fuel temperatures and the reference reactivity at 900K is plotted. The result from the COMSOL model matches with that from the Serpent model. The diffusion model captures the neutron balance at a similar accuracy as the Serpent model.
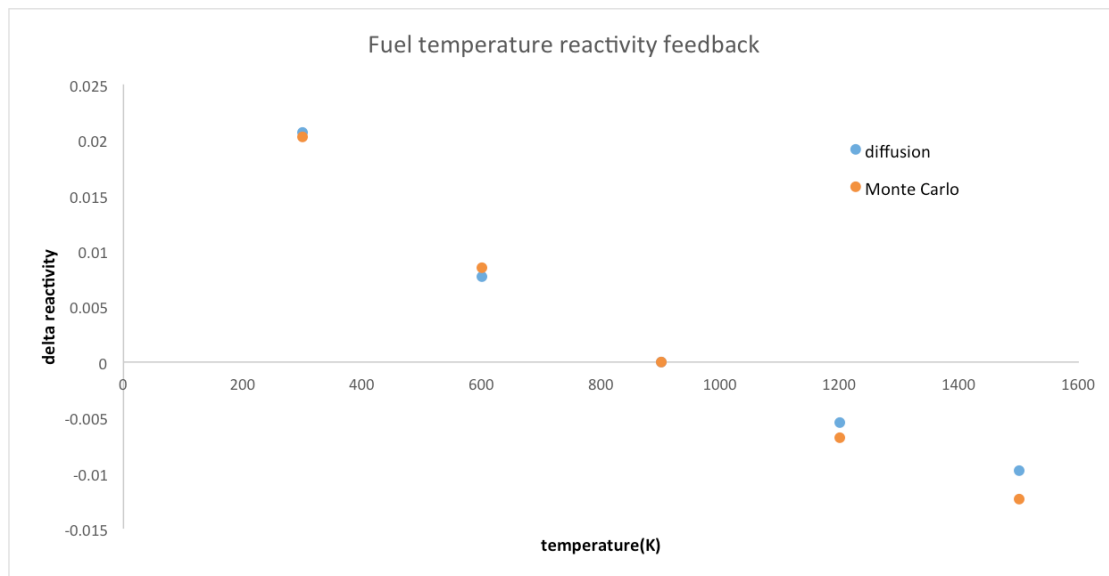

Figure 4.37: reactivity as a function of temperature

Monte Carlo – CFD Coupling for PB-FHRs: Application to the TMSR-SF Model

An advanced multi-physics modeling tools for coupled neutron kinetics and thermal-hydraulics analysis of PB-FHRs is under development. The new multi-physics tool is based on coupling the Monte Carlo code Serpent-2 for neutron transport and the CFD code OpenFOAM for thermal-hydraulics.

In the developed coupling scheme, at each collision during neutron transport, an implicit estimate of the local fission energy deposition is computed via standard Monte Carlo collisional estimator and scored in the Finite-Volume cell containing the collision point. On the other hand, the OpenFOAM mesh and field information are passed to the Monte Carlo neutron tracking routines, in order to update the material, temperature and density at collision points.

The pre-existing flexible Serpent–OpenFOAM coupling capabilities for steady-state and transient reactor analysis via both external- and internal-coupling mode are being adapted to PB-FHRs. Moreover

Fluoride-salt-cooled High-temperature Reactor (FHR) Annual Report: 2015
MIT, U.C. Berkeley, U. of Wisconsin and U. of New Mexico
For Public Distribution

extensions to these capabilities were developed to allow the exchange of information involving pebbles position, power distributions, and temperature profiles. In addition, the discrete element method (DEM) capabilities of the multi-physics toolkit OpenFOAM were integrated in the coupling scheme. DEM is a numerical simulation technique that allows modeling of assemblies of spheres via the explicit solution of the equation of motion for each element. The DEM capabilities have been adopted to study the TMSR-SF initial loading, with accurate prediction of the pebble bed random configuration.

In

Figure 4.38 and

Figure 4.39, tables with the main parameters adopted in the TMSR-SF neutronics and DEM modeling are presented.

Table I. Main parameters applied in the Serpent model of the TMSR-SF.

Parameter	Value
TRISO particles packing factor, %	7
Dispersion of TRISO particles inside pebbles	explicit random distribution
Number of fuel pebbles in the core	$\sim 11 \times 10^3$
Distribution of fuel pebbles in the core	OpenFOAM DEM model
Uranium enrichment, %	17
Uranium loading, g/pebble	~ 7
^{7}Li enrichment in flibe coolant, at.%	99.99
Coolant mass flow rate, kg s^{-1}	150
Reactor thermal power, MW	10

Figure 4.38. Table of the main parameters applied in the Serpent model of the TMSR-SF.

Table II. Parameters applied in the 3D DEM model of the pebble bed.

Parameter	Value
Diameter, cm	6
Density, g cm^{-3}	1.81
Young's modulus, Pa	1×10^{10}
Poisson's ratio	0.12
Pebble-pebble friction coefficient	0.25
Pebble-reflector friction coefficient	0.25

Figure 4.39. Table of the parameters applied in the 3D DEM model of the pebble bed.

Figure 4.40 shows vertical cross sections of the fuel elements distribution in the TMSR-SF core at different phases of the initial fuel loading (the reflector is not shown for clarity). The pebbles are injected from the central part of the bottom cone and accumulates in the top due to both the buoyancy effects and the drag forces. The 3D OpenFOAM DEM simulations in the considered conditions predict that the bed forms a cone-shaped bottom.
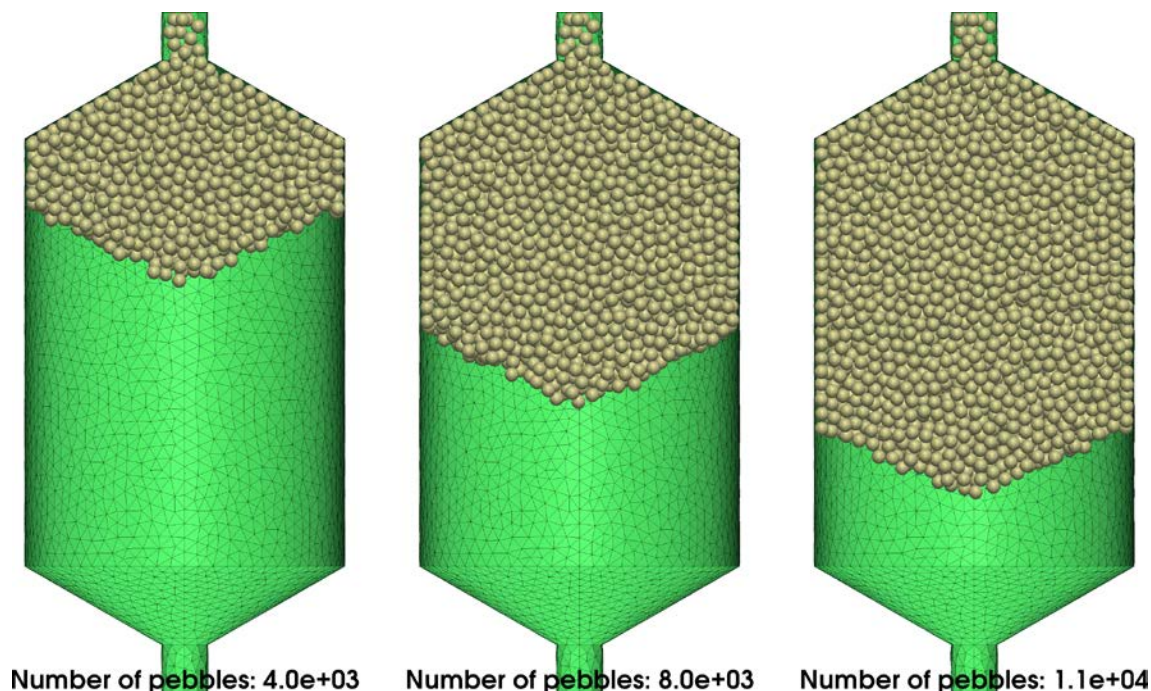
Fluoride-salt-cooled High-temperature Reactor (FHR) Annual Report: 2015
MIT, U.C. Berkeley, U. of Wisconsin and U. of New Mexico
For Public Distribution

Number of pebbles: 4.0e+03   Number of pebbles: 8.0e+03   Number of pebbles: 1.1e+04

Figure 4.40. Pebble loading in the TMSR-SF; DEM modelling.

The explicit DEM modeling allows to take into account the space-dependent packing fraction and assembly shape of the pebble bed resulting from the random sphere settling in the considered conditions. The ordered packing close to the radial reflector can be appreciated in

Figure 4.40. Figure 4.41 shows Serpent–OpenFOAM coupling results for the effective multiplication factor during reactor loading.
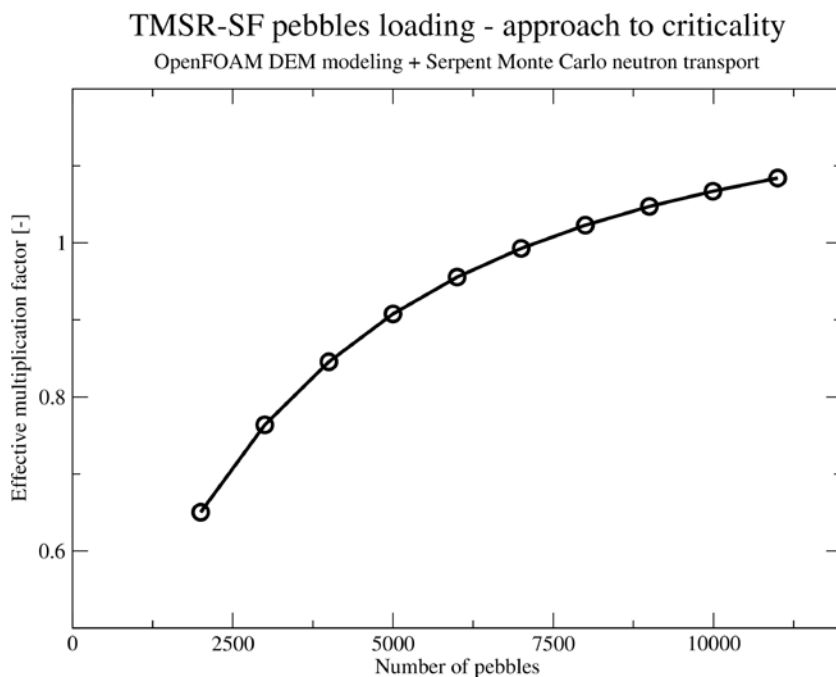

Figure 4.41. Serpent-OpenFOAM coupling results for the TMSR-SF loading.

103

Fluoride-salt-cooled High-temperature Reactor (FHR) Annual Report: 2015
MIT, U.C. Berkeley, U. of Wisconsin and U. of New Mexico
For Public Distribution

The thermal-hydraulics model selected for the present multi-physics tool makes use of the porous-media approach with incompressible flow formulation. This approach solves for homogenized values of material temperatures over the finite-volume cells, which might contain several pebbles. This approximation allows for a computationally efficient solution of the coupled problem, while maintaining the exact geometrical treatment in the Monte Carlo neutron transport. On the other hand, the power distribution is made available as both homogenized and pebble-resolved values.
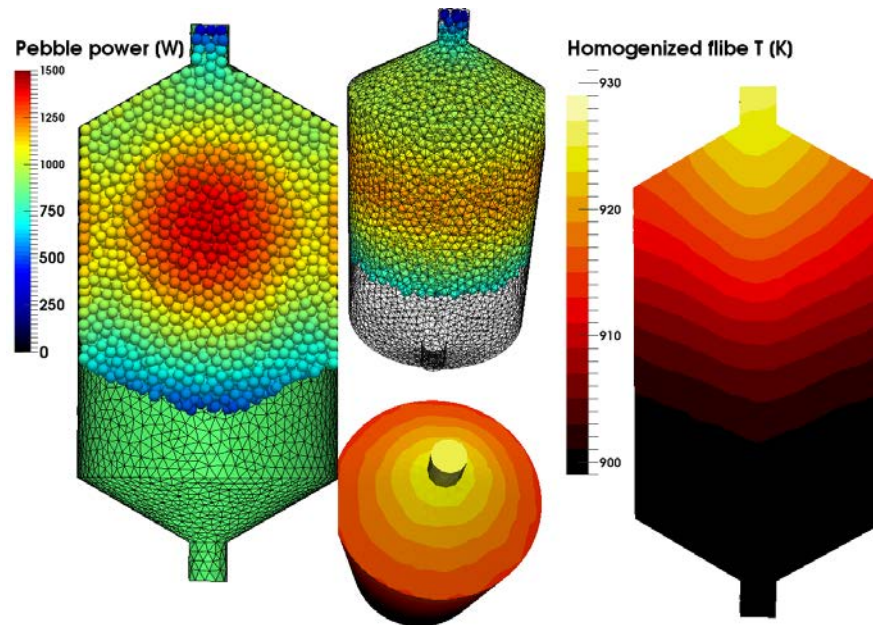
Figure 4.42. Power distribution and homogenized coolant temperature in the TMSR-SF.

In Figure 4.42, Serpent-OpenFOAM results show the pebble power distribution (left and top) and the homogenized flibe temperature (right and bottom). In

Figure *4.43*, the effect of the insertion of two control rods (not depicted) is presented. Dark blue represents pebbles with low power. In red, pebble with relative high power density are shown (up to 1.5 kW per pebble). Despite the small size of the reactor, a significant distortion of the power and temperature distributions are introduced by the movement of the control rods.

Fluoride-salt-cooled High-temperature Reactor (FHR) Annual Report: 2015
MIT, U.C. Berkeley, U. of Wisconsin and U. of New Mexico
For Public Distribution
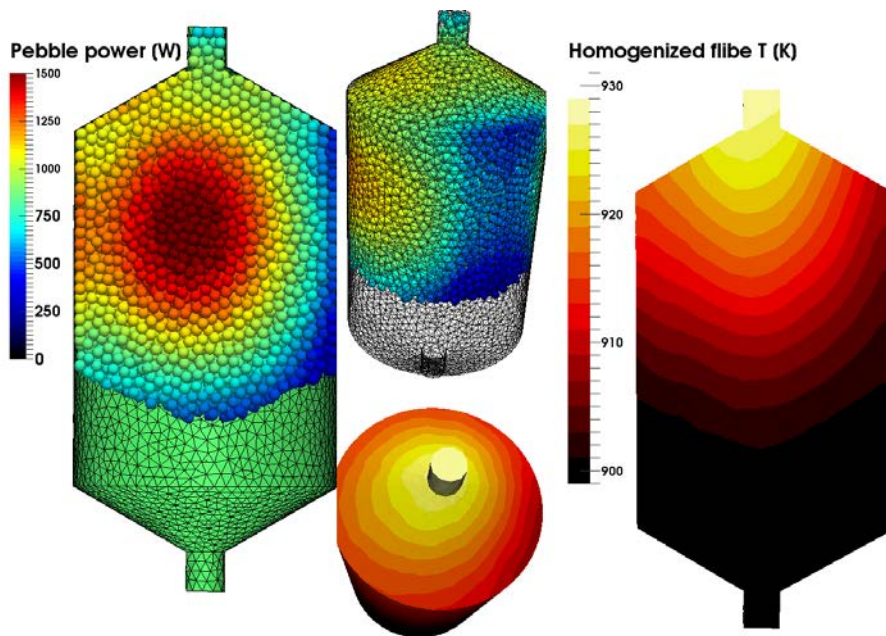

Figure 4.43. Control rod insertion.

Ongoing research involves the study of the impact of cross sections uncertainties on the main reactor parameters. Of particular interest is the coolant expansion reactivity coefficient $\alpha_{coolant}$. The value of $\alpha_{coolant}$ in the TMSR-SF has been calculated adopting several nuclear data libraries, obtaining an approximate estimate around -0.2 *pcm/K*. The results in Figure 4.44 show discrepancies in the order 20% among the commonly adopted libraries.

More accurate analyses are being performed to assess the decomposition of the uncertainty contributions by nuclides and reactions. These research activities involve the adoption of Generalized Perturbation Theory capabilities that have been recently implemented in the Monte Carlo code Serpent, combined with the use of covariance matrices, which are provided within the main nuclear data libraries.
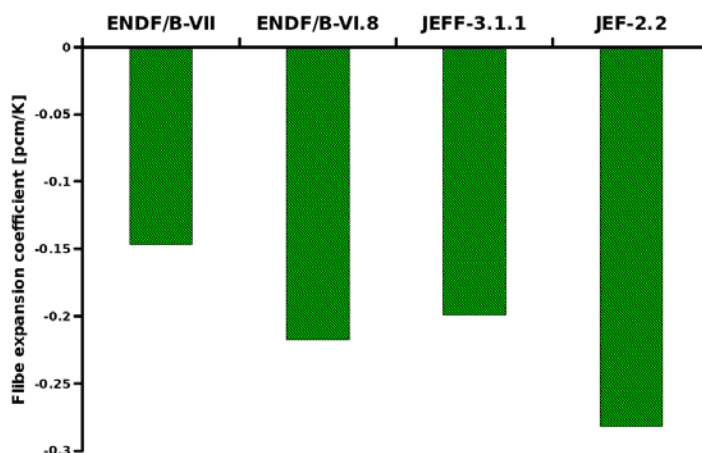

Figure 4.44. Uncertainty in the coolant expansion reactivity coefficient from nuclear data.

Fluoride-salt-cooled High-temperature Reactor (FHR) Annual Report: 2015
MIT, U.C. Berkeley, U. of Wisconsin and U. of New Mexico
For Public Distribution

University of New Mexico

Project work at the University of New Mexico (UNM) made solid progress in the first year of IRP-2 (2015). Several major milestones were met in the first year, involving both experimental and simulation work, which is discussed below. The experimental work centers around two major efforts: reduced-scale heat transfer experiments investigating use of heat exchangers with twisted tubes and mass transfer experiments investigating ultrasonic enhancement of sparging for tritium removal. The simulation work involved redundancy studies for FHR emergency decay heat removal optimization.

Twisted-tube Heat Transfer Experiments

UNM has a reduced-scale heat transfer loop, purpose built to investigate low Reynolds, high Prandtl heat transfer in twisted-tubes, especially under strong buoyancy conditions using the simulant fluid, Dowtherm A. The heat transfer loop was originally supported under an NRC faculty development grant and operated initially in 2014 with a simplified heat exchanger using water as working fluid. The loop has seen substantial renovations in 2015, under support by IRP-2, to accommodate the new heat exchangers (see below) and with the addition of an intermediate loop. Changes to the loop to accommodate the new heat exchangers includes modifying the general dimensions of the loop, designing and fabricating a higher capacity Joule heater, and adding static mixers to provide improved bulk fluid temperature readings. The intermediate loop has been added to allow fine-tuned controlling of secondary side flow rates and temperatures, as well as to allow collection of heat transfer data on the tube side using Dowtherm A. Modifications of the loop are well underway with planned operation using Dowtherm A in Spring 2017.

The loop modifications are taking place to allow data collection from new heat exchangers that were fabricated and shipped to UNM in 2015. Four heat exchangers were procured (Fig. 37):

- Single-wall, bayonet style, plain tube heat exchanger
- Single-wall, bayonet style, twisted tube heat exchanger
- Double-wall, plain outer tube/plain inner tube heat exchanger
- Double-wall, twisted outer tube/plain inner tube heat exchanger

The two single-wall heat exchangers will provide a comparison between twisted and plain tube heat transfer performance under the particular phenomenological conditions present in the FHR. The two double-wall heat exchangers will provide valuable data supporting an effort to investigate the potential use of double-wall heat exchangers in the FHR to manage tritium release. These designs also show promise in coupling an inherently low-pressure primary system to high-pressure power conversions cycles. UNM was recently awarded a 2015 NEUP in conjunction with Sandia National Laboratories to investigate use of double-wall twisted tube heat exchangers in the FHR, especially in regard to coupling FHRs to supercritical carbon dioxide (S-CO2) Brayton power conversion cycles. While this work is independent to IRP-2, there are substantial synergistic research activities which allow leveraging of resources for both activities. Figure 38a shows a picture of the loop with modifications ongoing, and Figure 38b shows a picture of the plain tube heat exchanger being inserted into the shell.

Fluoride-salt-cooled High-temperature Reactor (FHR) Annual Report: 2015
MIT, U.C. Berkeley, U. of Wisconsin and U. of New Mexico
For Public Distribution

(a)   (b)

Figure 37. (a) shows the twisted and plain single-wall, bayonet style heat exchangers. (b) shows the twisted outer/plain inner and plain outer/plain inner double-wall heat exchangers.

Fluoride-salt-cooled High-temperature Reactor (FHR) Annual Report: 2015
MIT, U.C. Berkeley, U. of Wisconsin and U. of New Mexico
For Public Distribution

(a)   (b)

Figure 38. (a) shows modifications being made to the loop and the addition of an intermediate loop. (b) shows insertion of the plain tube bundle into the shell.

Sonoprocessing Mass Transfer Experiments

Tritium is produced in the FHR salt that must be removed. On option for removal is sparging of the salt with an inert gas to remove the tritium. For efficient gas removal, one wants to maximize mass transfer of tritium from the liquid phase to the gas phase. Initial investigations have been performed to study effects of ultrasound for enhancing the diffusion mass transfer of in-line sparging under IRP-2, and preliminary results look to be promising , as illustrated with the results shown in Figure 4.39. The proposed inert gas sparging enhanced by high intensity ultrasonics will cause the stripping bubbles to break into smaller bubbles and increase the convective mass transfer at the liquid gas interface by agitation and increasing gas liquid contact area. The near term goal for this research is to show improvement in sparging using ultrasonics. A set of prototypical ultrasonic flow cells were used to test the theory and some improvement in the degassing was found for a set of given parameters such as gas flowrate, working fluid flowrate, and ultrasonic intensity. Next steps will be to investigate more analogous surrogate fluids such as glycerol and water mixtures in order to match the key mass transfer non-dimensional numbers (Weber, Schmidt, and Sherwood numbers) and look to investigate the scaling arguments for this technology, and scaling arguments in anticipation for potential deployment.

Fluoride-salt-cooled High-temperature Reactor (FHR) Annual Report: 2015
MIT, U.C. Berkeley, U. of Wisconsin and U. of New Mexico
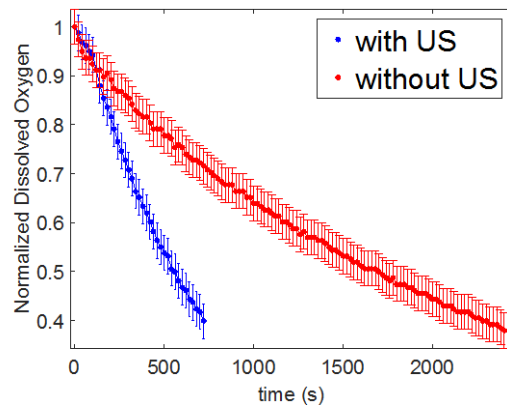For Public Distribution

Figure 4.39. Preliminary results from the prototypical flow cell experiment. This experiment was a prototype small-scale water loop with a volume of 0.8 gallon, inert gas flow of 0.2 sfcm/min, and intensity of 300 W/cm2. This shows a reduction in oxygen removal time by roughly 70%.

The preliminary results indicate that there is potential for success, although it is recognized that before there can be an implementation of this technology there are more challenges to overcome. The bubble production challenge has been investigated extensively. However, the ultrasonic challenges have received less attention. These issues will have to be investigated with a focus on overcoming the effects of tritium migration, high temperatures, potentially high radiation dose, and acoustic coupling. With respect to these challenges, the most advantageous design schemes would be direct coupling or indirect coupling. This would allow the separation of the ultrasonics from the working fluid as well as enable adding temperature control to the ultrasonic system. It will also provide a barrier to prevent the migration of tritium.

RELAP5-3D Simulation Work

During the final quarter of 2015, the heat transfer work at UNM was focused on a simulation study performed in RELAP5-3D investigating redundancy of the DRACS system used in FHRs. The study focused on the performance of emergency decay heat removal during partial blockage scenarios for two different redundancy options: 3 total DRACS with 2 necessary for sufficient cooling, and 6 total DRACS with 3 necessary for sufficient cooling. One of the unique aspects of the FHR is that overheating transients are most likely to be limited by time-dependent creep of metallic components, rather than more convential peak clad or peak fuel temperatures. Peak core outlet temperature (PCOT) was used as a surrogate for peak internal metallic temperature (PIMT). Preliminary results are shown in Figure 4.40, and indicate a generally robust performance of the decay heat removal systems under a wide variety of blockage scenarios, with at least 90% point flow area reductions required to see significant increases in PCOT. The preliminary results also indicate greater sensitivity of PCOT to blockages in the DHX branch(es) compared to blockages in the DRACS loop(s). This is likely due to the lack of access to the additional thermal inertia provided by the DHX branch and heat rejection to DRACS loops, when DHX branches are blocked. This work is helping support the experimental DHX investigations under IRP-2.

109

Fluoride-salt-cooled High-temperature Reactor (FHR) Annual Report: 2015
MIT, U.C. Berkeley, U. of Wisconsin and U. of New Mexico
For Public Distribution
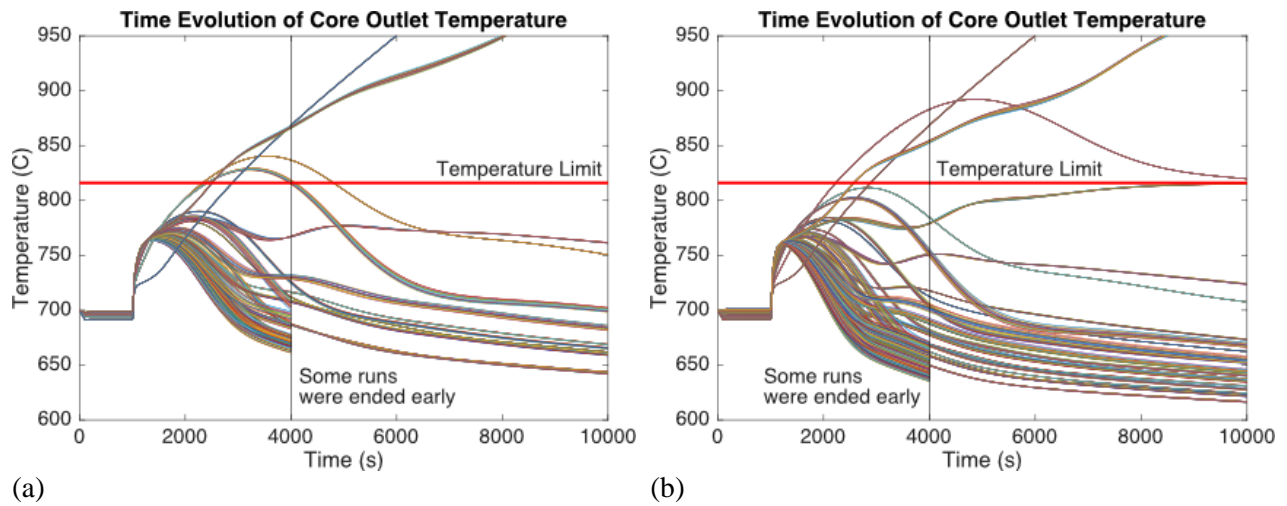
Figure 4.40. "Horsetail" plots illustrating the spread of PCOT results from the various runs. (a) is of the (2/3) option run, with a total of 555 runs presented and (b) is of the (3/6) option runs, with a total of 1095 runs presented.[3]

---

[3] In an effort to limit the computational time required for the runs, only the 95% and 99.99% blockage scenarios were run for a full 10,000 seconds. The rest of the scenarios were limited to 4,000 seconds of simulated problem time.

Fluoride-salt-cooled High-temperature Reactor (FHR) Annual Report: 2015
MIT, U.C. Berkeley, U. of Wisconsin and U. of New Mexico
For Public Distribution

5   Task 4. FHR Evaluation Model Benchmarking and Validation Workshops (UCB)

The objectives of this task are (1) a set of benchmarking activities to validate design tools using the experimental data collected by this IRP and by collaborators and (2) begin the process of developing an international effort to support evaluation model benchmarking for FHR safety and design.

This task involves conducting joint workshops with IRP member universities, advisory committee members, and relevant experts to review current progress, help direct further efforts, and assure that the most critical issues of FHR technology development are addressed by the IRP.

Task 4.1(a): Coordinate 1st IRP-2 Workshop on FHR Phenomenology and Benchmark Exercise Definition

From March 11th to March 13th, UCB organized a workshop including all IRP-2 universities (UCB, MIT, UW and UNM); members from a second FHR IRP (Georgia Institute of Technology, The Ohio State University, and Texas A&M University); national experts from Idaho National Laboratory (INL) and Oak Ridge National Laboratory (ORNL); as well as international experts from the Australian Nuclear Science and Technology Organisation (ANSTO) in Sydney, the Shanghai Institute of Applied Physics (SINAP) in China, and the Ulsan National Institute of Science and Technology (UNIST) in South Korea. In total, roughly 30 experts supported by an equally large group of students from the listed universities discussed the path forward for FHR phenomenology and benchmarking.

The conclusions from this workshop are mainly regarding the structure of the IRP, initial benchmarking efforts, and future workshops. There are three clear technical areas that resulted from the discussions during the workshop: Neutronics, Thermal Hydraulics, and Materials Corrosion, Activation and Mass Transport. Working groups based on these technical areas are being formed and will be led by an IRP member to be determined later, and advised by an advisory group expert on the specific technical area. This breakdown of IRP members into working groups, advised by experts in the different technical areas, should facilitate productive progress on code benchmarking exercises throughout the three years of the IRP. Members of this IRP and the Georgia Tech IRP will collaborate closely on the benchmarking efforts in the three technical areas to maximize the resources dedicated to FHR advancement at the university level.

Initial benchmarking exercises and high-level paths forward were discussed during the workshop for each technical area. The lessons learned from previous benchmarking efforts in the nuclear energy sphere were to begin with simple problems to practice the effort of benchmarking with a large group of participants, then move to more complex and realistic benchmarking exercises as the working groups become familiar with the benchmarking process. Specific initial benchmarking exercises and general paths forward can be found in the associated white paper, which will be completed by the end of August of this year.

The white paper from the previous workshop, titled "Fluoride-Salt-Cooled, High-Temperature Reactor Code Benchmarking White Paper," has been updated, revised, and edited with significant additions from the discussion during the workshop and is available on UC Berkeley's FHR website as UCBTH-15-006 (http://fhr.nuc.berkeley.edu/references/fhr-white-papers/). The primary results are the formation of technical area working groups (neutronics, thermal hydraulics, and materials corrosion, activation, tritium and transport (MATT)), the close collaboration with the second FHR IRP led by the Georgia Institute of Technology, and the establishment of a path forward for the benchmarking campaign including future workshop planning.

Fluoride-salt-cooled High-temperature Reactor (FHR) Annual Report: 2015
MIT, U.C. Berkeley, U. of Wisconsin and U. of New Mexico
For Public Distribution

The three technical areas (neutronics, thermal hydraulics, and materials corrosion, activation, tritium and transport (MATT)) create a clear division of FHR phenomena that encompass the most important phenomena required for FHR commercial development. Based on recommendations from the workshop participants on the division of FHR phenomena into these three technical areas, the IRPs propose to form three working groups to organize future research efforts within the broader FHR benchmarking campaign.

Each working group will consist of students and professors from FHR IRP partner universities with related interests in the technical area of the working group as well as universities and organizations that fall outside the formal IRP organization. Additionally, each working group will have its own advisory committee consisting of professors, national laboratory scientists, and other technical area experts to help guide research efforts. Beyond guiding the efforts within this new IRP, the oversight of an expert advisory committee will help facilitate collaboration and mentorship between established experts within the Nuclear Engineering field and students in Nuclear Engineering, ensuring a high degree of knowledge transfer and continuation of FHR development capability. The flexibility of having the efforts divided among three working groups also allows for more contact and collaboration through video-conferencing and side meetings at conferences related to the working groups' technical area. This will be critical for maintaining communication and progress within working groups in between the larger FHR workshops, which are proposed to meet approximately annually. The IRP partner universities, including the GT-led IRP, are tentatively divided into working groups as follows[4]:

- Neutronics: UCB, GT, MIT
- Thermal Hydraulics: UCB, OSU, UNM, UW
- MATT: UW, MIT

Each working group will identify two lead faculty members who will co-chair the group. The responsibilities of the lead faculty will include: developing a working group charter, communication and coordination within the working group as well as with the other working groups, organization of working group resources, prioritization of benchmarking efforts, coordination and integration of the working group advisory committee, and other managerial duties.

During the beginning of the combined IRP efforts, the working groups will primarily work separately as their technical areas are relatively disparate. However, sharing individual experiences with benchmarking efforts with the other working groups will be critical in further development of benchmarking best practices and creating positive communication practices. Also, as the understanding of FHR phenomena advances during the course of the IRPs, the more complex phenomena will require coupled development between working groups, e.g. thermal hydraulics – neutronics coupling to understand complex FHR transient behaviors that will be important for licensing efforts. Sub-working groups may be necessary to facilitate this cross-working group collaboration, and will be explored further during subsequent workshops as benchmarking efforts advance.

In practice, benchmarking activities within each working group will include participation from organizations outside of the IRP partner universities, both domestically and internationally. Outside collaboration will serve several purposes, primarily: (1) providing additional credibility to benchmarking campaign results as more diverse experimental data, model predictions, and applications of FHR phenomena are contributed by additional benchmarking participants; (2) providing high-quality

---

[4] Texas A&M University has an established and impressive expertise in instrumentation and control, and as such does not readily fall into the proposed working group structure. TAMU's role in this benchmarking campaign has yet to be established, and they may contribute to FHR technology development and understanding in other, equally important ways.

Fluoride-salt-cooled High-temperature Reactor (FHR) Annual Report: 2015
MIT, U.C. Berkeley, U. of Wisconsin and U. of New Mexico
For Public Distribution

experience to students through their collaboration with professionals and experts in the Nuclear Engineering field on a reactor design and development project of significant depth and breadth; and (3) acquiring international attention and interest in the advancement of FHR technology development.

Future IRP workshops are proposed to have two complimentary components: (1) a full IRP discussion component where all participants involved in IRP research efforts and contributing experts can meet to discuss topics pertinent to the IRP at large, and (2) separate breakout sessions consisting of working group members and their respective advisory committees to discuss topics pertinent to only the respective working group in more detail. This workshop structure is a much more efficient use of participants' time while still encouraging collaboration and enthusiasm for FHR research within and outside the IRPs.

The proposed agenda for future combined-IRP workshops is a half-day of welcome activities to allow all participants to arrive, a day dedicated to breakout sessions to discuss more specific topics within the working groups, followed as second day dedicated to general IRP discussion.

The following tentative schedule for combined-IRP workshops is suggested:

- Second FHR Combined-IRP Workshop
    - o Date: April 13-16, 2016
    - o Location: UC Berkeley/San Francisco
- Third FHR Combined-IRP Workshop
    - o Date: February, 2017
    - o Location: TBD
- Fourth FHR Combined-IRP Workshop
    - o Date: October, 2018
    - o Location: TBD

The proposed dates for holding the subsequent three workshops are approximately based on the proposed IRP milestone schedule, but ideally can be coordinated with other large events to facilitate maximum participation. The date and location for the second FHR combined-IRP workshop is chosen to directly precede the ICAPP 2016 conference in San Francisco. SINAP/ORNL combined meetings on the ORNL campus are also ideal for coordinating combined-IRP workshops as many of the key contributors will be present and ORNL has excellent facilities to host an FHR workshop. Each workshop may also consider hosting an ANS 20.1 FHR Safety Standard Meeting the day before the workshop.

Task 4.1(b): Coordinate 2nd IRP-2 Workshop on FHR Benchmark Progress

Planning for the second IRP-2 workshop has begun by establishing the dates and location as April 14-15, 2016, in Berkeley, California. These dates and location were chosen to directly precede the ICAPP conference to be held in San Francisco on April 17-20, 2016.

Fluoride-salt-cooled High-temperature Reactor (FHR) Annual Report: 2015
MIT, U.C. Berkeley, U. of Wisconsin and U. of New Mexico
For Public Distribution

6   Task 5. Using Lessons Learned from FHR R&D to Advance All Generation IV Technologies

The objective of this task is to include in each quarterly report key lessons learned from the IRP activities, and related work elsewhere, that has general importance to facilitating the development of new Generation IV technologies.

Addition A:

The Department of Energy announced a major advanced reactor award to a consortium led by Southern Company and including Terrapower and the Electric Power Research Institute for development of an advanced molten salt reactor. Much of the information being developed by this IRP is applicable to MSRs. In particular, FHRs and MSRs have the same challenges with tritium and thus large incentives for cooperation as discussed in Chapter 2. We will work with this consortium to address common challenges.

Fluoride-salt-cooled High-temperature Reactor (FHR) Annual Report: 2015
MIT, U.C. Berkeley, U. of Wisconsin and U. of New Mexico
For Public Distribution

7. Published Papers and Reports

The primary documentation for the project will be in reports, thesis, conference papers, and journal articles. The following papers were published this quarter. This is the second IRP on FHRs. Some of the results from the first IRP are published after the end date of that work and are included herein. Because this is a combined annual and quarterly report, we have included below some of the papers that were published in earlier quarters. Reports in earlier quarterly reports have an *

Massachusetts Institute of Technology (*Reports, thesis, papers issued this quarter)

1. C. W. Forsberg and P. F. Peterson, "Spent Nuclear Fuel and Graphite Management for Salt-Cooled Reactors: Storage, Safeguards, and Repository Disposal," *Nuclear Technology*, *191*, August 2015.
2. J. Richard, *Design Optimization and Analysis of a Fluoride Salt Cooled High Temperature Test Reactor for Accelerated Fuels and Materials Testing and Nonproliferation and Safeguards Evaluations*, PhD Thesis, February 2016.
3. C. W. Forsberg, *Strategies for a Low-Carbon Electricity Grid with Full Use of Nuclear, Wind and Solar Capacity to Minimize Total Costs*, MIT-ANP-TR-162, Massachusetts Institute of Technology, Cambridge, Massachusetts.
4. D. Carpenter, M. Ames, Y. Ostrovsky, G. Kohse, L.W. Hu, "Status of the Fluoride Salt High-Temperature Reactor Materials Irradiation Tests at the MIT Research Reactor", *European Research Reactor Conference (RRFM-2015*), Bucharest, Romania, April 19-23, 2015
5. J. D. Stempien, *Tritium Transport, Corrosion, and Fuel Performance Modeling in Fluoride Salt-Cooled High-Temperature Reactors*, PhD Thesis, Department of Nuclear Science and Engineering, Massachusetts Institute of Technology, Cambridge, MA. June 2015
6. C. Forsberg et. al., "Development of a Fluoride-Salt-Cooled High-Temperature Reactor (FHR) Using Advanced Gas-Cooled Reactor (AGR) Technology," Paper 13983 *Trans. American Nuclear Society Annual Meeting*, San Antonio, June 7-11, 2015
7. R. R. Romatoski, L.W. Hu, and C. W. Forsberg, "Thermophysical Property Sensitivity Study of $LiF\text{-}BeF_2$ and $NaF\text{-}ZrF_4$ Coolants on Thermal Hydraulic Licensing Limits for a Fluoride Salt-cooled High-Temperature Test Reactor," Paper 15190, *Proc. of the International Congress on Advanced Nuclear Power Plants*, Nice, France, May 3-6, 2015.
8. Y. Xiao, L. W. Hu, S. Qiu, D. Zhang, G. Su, W. Tian, "Development of a Thermal-Hydraulic Analysis Code and Transient Analysis for a Fluoride-salt-cooled High-Temperature Test Reactor", *Nuclear Engineering and Radiation Science* vol. 1 / 011007-1, 2015.
9. *C. Forsberg, Lin-wen Hu, Joshua Richard, Rebecca Romatoski, Benoit Forget, John Stempien, Ron Ballinger, Kaichao Sun, and David Carpenter, "Basis for a Demonstration Fluoride-Salt-Cooled High-Temperature Reactor," *Transactions of the American Nuclear Society*, Washington D.C. November 2015.-
10. *J. Richard, B. Forget, C. Forsberg, and K. Smith, Design Optimization of a Fluoride Salt Cooled High Temperature Test Reactor Capable of Testing Different Salt Coolants. Transactions of the 2015 American Nuclear Society Annual Meeting, Washington D.C., November 2015.
11. *John D. Stempien, Ronald G. Ballinger, and Charles W. Forsberg, "A Model of Tritium Transport and Corrosion in Salt-Cooled Reactors", Paper 15081, Transactions 2015 American Nuclear Society Winter Meeting, Washington D.C., November 8-12, 2015.
12. *Charles Forsberg and Pat McDaniel, "Air-Brayton Systems with Salt, Sodium, and Helium Base-Load Reactors with Variable Electricity, Steam and Hot-Air Output", Paper 15200, *Transactions 2015 American Nuclear Society Annual Meeting*, Washington D.C., November 8-12, 2015.

Fluoride-salt-cooled High-temperature Reactor (FHR) Annual Report: 2015
MIT, U.C. Berkeley, U. of Wisconsin and U. of New Mexico
For Public Distribution

13. *C. Forsberg, J. Stempien and R. Ballinger, "Tritium Removal from Salt-Cooled Reactors Using Carbon", Paper 15199, *Transactions 2015 American Nuclear Society Winter Meeting,* Washington D.C., November 8-12, 2015.

University of Wisconsin (*Reports, thesis, papers issued this quarter)

14. "Corrosion of 316 Stainless Steel in High Temperature Molten Li_2BeF_4 (FLiBe) Salt", G. Zheng, B. Kelleher, G. Cao, M. Anderson, K. Sridharan, T. R. Allen, *Journal of Nuclear Materials*, 2015, Vol. 461, 143-150.
15. "High Temperature Static Corrosion of Hastelloy N in Molten Li_2BeF_4 (FLiBe) Salt", G. Zheng, B. Kelleher, G. Cao, M. Anderson, K. Sridharan, T. R. Allen, *Corrosion*, (accepted for publication, 2015).
16. "Batch Scale Hydrofluorination of Li2BeF4 to Support Molten Salt Reactor Development", B.C. Kelleher, K.P. Dolan, P. Brooks, M.H. Anderson, and K. Sridharan, *Journal of Engineering and Radiation Sciences*, (accepted for publication, 2015).
17. *Corrosion Behavior of Structural Alloys in High Temperature Molten Fluoride Salts*, G. Zheng, Ph.D. Thesis, University of Wisconsin, Madison, April 2015.
18. *Purification and Chemical Control of Molten Li2BeF4 for a Fluoride Salt Cooled Reactor*, B. Kelleher, Ph.D. Thesis, University of Wisconsin, Madison, May 2015.
19. "*Redox Potential Measurement and Control for the Fluoride-Salt-Cooled High-Temperature Reactor*", K. Dolan, Masters Thesis, University of Wisconsin, Madison, August 2015.
20. *"Inter-IRP Meeting on Fluoride Salt-Cooled High Temperature Reactor (FHR): Materialsand Salts*", September 25, 2015, University of Wisconsin-**Madison**

UC Berkeley (*Reports, thesis, papers issued this quarter)

21. C. Andreades, "Nuclear Air-Brayton Combined Cycle Power Conversion Design, Physical Performance Estimation and Economic Assessment," Ph.D. Dissertation, Department of Nuclear Engineering, University of California, Berkeley (2015).

22. Z. Guo *et al.*, "Development of the FHR advanced natural circulation analysis (FANCY) code," presented at NURETH-16, Chicago, IL, 2015.

23. N. Haneklaus *et al.*, "Thermal hydraulic benchmarking exercises to support fluoride-salt-cooled, high-temperature reactor (FHR) licensing," presented at NURETH-16, Chicago, IL, 2015.

24. L. Huddar *et al.*, "Experimental strategy for the determination of heat transfer coefficients in pebble-beds cooled by fluoride salts," presented at NURETH-16, Chicago, IL, 2015.

25. N. Zweibaum, "Experimental Validation of Passive Safety System Models: Application to Design and Optimization of Fluoride-Salt-Cooled, High-Temperature Reactors," Ph.D. Dissertation, Department of Nuclear Engineering, University of California, Berkeley (2015).

26. N. Zweibaum *et al.*, "Design, fabrication and startup testing in the compact integral effects test facility in support of fluoride-salt-cooled, high-temperature reactor technology," presented at NURETH-16, Chicago, IL, 2015.

27. N. Zweibaum *et al.*, "Validation of best estimate models for fluoride-salt-cooled, high-temperature reactors using data from the compact integral effects test (CIET 1.0) facility," presented at NURETH-16, Chicago, IL, 2015.

Fluoride-salt-cooled High-temperature Reactor (FHR) Annual Report: 2015
MIT, U.C. Berkeley, U. of Wisconsin and U. of New Mexico
For Public Distribution

Fluoride-salt-cooled High-temperature Reactor (FHR) Annual Report: 2015
MIT, U.C. Berkeley, U. of Wisconsin and U. of New Mexico
For Public Distribution

+++++++++++++++++++++++++++++++++++